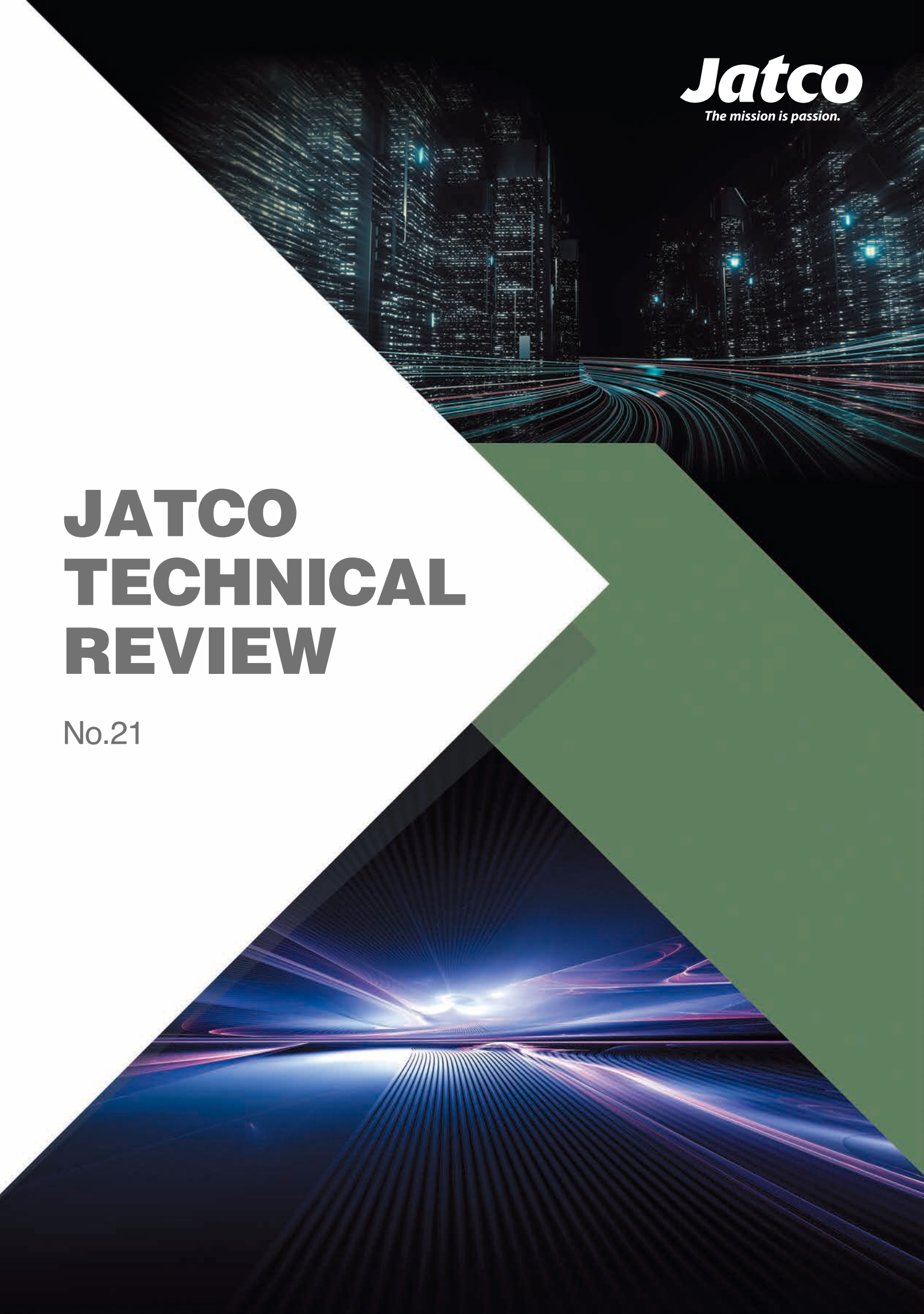

JATCO TECHNICAL REVIEW

No.21

CONTENTS

Preface

Technical Reports

Introduction to Products

Topics

Patents

What Electrification Efforts Mean

Fumitaka NISHIMURA

Senior Vice President

I often hear it said that "the automotive industry is in a once-in-a-hundred-year period of transformation." In simple terms, it is understood that vehicles as a product and their surrounding environment are changing profoundly due to electrification. Naturally, like other companies, JATCO is moving ahead with various measures so that we do not miss this trend and can stay ahead of it.

Public announcements of new products and introductions of new technologies related to electrified powertrains called e-Axles are already increasing with each passing day. I constantly feel this trend is stimulating friendly rivalry that is forming an environment in which even better products can be put on the market. While JATCO's true value as a "monozukuri" company is being questioned, it can also be said on the other hand that this is an excellent opportunity for us to demonstrate the actual capabilities we have accumulated to date.

To say it is a "period of transformation," a key point that must also be considered is that it does not merely signify the use of electric motors to drive vehicles. It will not be surprising that the "use of electricity to power vehicles" will make it possible to easily achieve a wide variety of things that could not be readily attained before. I think we will only be qualified to talk about a "period of transformation" after those things have been incorporated into the business model. Dramatic advancements in convenience can be expected along an axis of so-called connectivity with respect to vehicle performance, quality, customer service and many other aspects. Above all else, it is perfectly clear that customers who use vehicles will have a more discerning eye and that their preferences will continually evolve. Once customers use something that is convenient, they can no longer go back to what they had before. One good example of this is the amazing speed at which music storage media for personal enjoyment have evolved from cassette tapes to CDs to memory devices and then further by riding on the waves of streaming services and digitization. The same is also true for mobile phones and PCs. Examples like these are too numerous to mention. Such evolution creates new business opportunities that can be expected to promote further development of the industries involved. This also applies to the automotive industry in which JATCO operates. I often get the impression when sitting in the driver's seat of one of the various electrified vehicles already released that they are seemingly posing questions to users about product evolution, saying "this is how future vehicles will be," similar to the examples cited above.

Meanwhile, as someone who works in the automotive industry that reportedly is the source of over 20% of all atmospheric emissions, I keenly feel we have an obligation to reduce the global

environmental impact and to minimize emissions, most notably CO_2, as a measure against global warming in view of recent climate changes. Aside from discussions of how electric energy should be generated, the replacement of internal combustion engines with electric motors is a principal measure that engineers should pursue. In parallel with that, developing production methods that do not emit greenhouse gases is another new challenge that should be addressed. Regardless of whether we like or dislike this once-in-a-hundred-year period of transformation, it is absolutely imperative that we also recognize and address these various aspects mentioned here for the continuation and future development of automobile manufacturing.

"Electrification" is the theme before us today, but what we ought to aim for is not just electrification that is imaginable now, as there are many more possibilities. In other words, it is desirable that electrification efforts should embody the pleasure of creating the future as a result of imagining, struggling with and contemplating what might be possible. Moreover, if we can contribute to the formation of a future world and environment that are not yet achievable today, we can feel proud to be a manufacturer. As one individual engaged in the automotive industry, I want to say to everyone: let us definitely make every effort to produce results that will ultimately be satisfying to society, customers and ourselves by working hard to search for and research solutions to today's problems. After all, we are blessed with the good fortune of having an opportunity that comes once in a hundred years.

Compact and high-efficiency 1-axis e-Axle with a planetary gear set

Hiroki UEHARA* Shota OIKAWA* Kazuhiko YOKOYAMA*

Summary

This article describes a compact e-Axle that was developed using a planetary gear set as the gearbox to improve vehicle mountability, expand luggage space, increase degrees of freedom for vehicle styling and reduce aerodynamic drag. The adoption of a stepped planetary gear set configuration and optimization of oil flow inside the unit achieve both excellent transmission efficiency and lubrication performance.

1. Introduction

The automotive industry is moving ahead with electrification of powertrain systems in the form of electric vehicles, hybrid vehicles and other types in order to achieve a sustainable society. Weight reductions, downsizing and improvement of electric powertrain efficiency are necessary and indispensable to promote their widespread diffusion with the aim of markedly reducing greenhouse gas emissions. Companies are developing e-Axles that integrate the motor, inverter and gearbox into a single unit.

This article describes JATCO's new e-Axle with a 1-axis structure that uses a planetary gear set to build a more compact unit with higher efficiency. Special focus is put on explaining the gearbox.

2. Development aims

The following three aims were set for the development of the new 1-axis e-Axle.

(1) To achieve the top benchmark for volume by substantially downsizing the unit in the vehicle's longitudinal and vertical directions.
(2) To aim for top-level transmission efficiency.
(3) To adopt a lubrication system without an oil pump so as to achieve a low-cost, compact unit.

Downsizing the e-Axle provides the following benefits for the vehicle (Fig. 1).

- Mountable regardless of 2WD/4WD.
- Expansion of luggage space.
- Assurance of crumple space for collision safety.
- It allows a lower hood height, increasing the degrees of freedom for vehicle styling and reducing aerodynamic drag.

3. e-Axle specifications

3.1 Major specifications

The major e-Axle specifications are listed in Table 1. The appearance of the new e-Axle is shown in Fig. 2

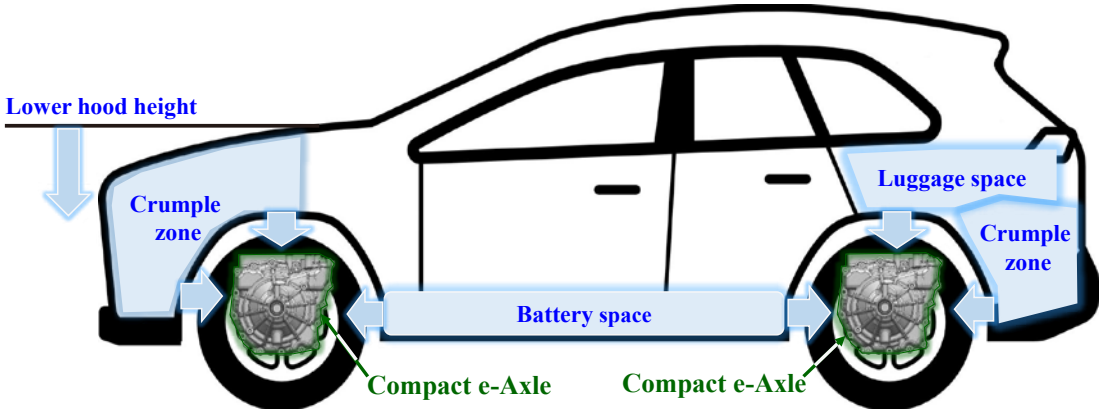

Fig. 1 Benefits for the vehicle of compact e-Axle

* Innovative Technology Development Department

Table 1 e-Axle specifications

Max. electric motor power	150 kW
Max. electric motor torque	320 Nm
Max. electric motor speed	13,000 rpm
Gear ratio	9.692
Unit volume	65 L
Unit size	X:325 mm×Y:540 mm×Z:370 mm

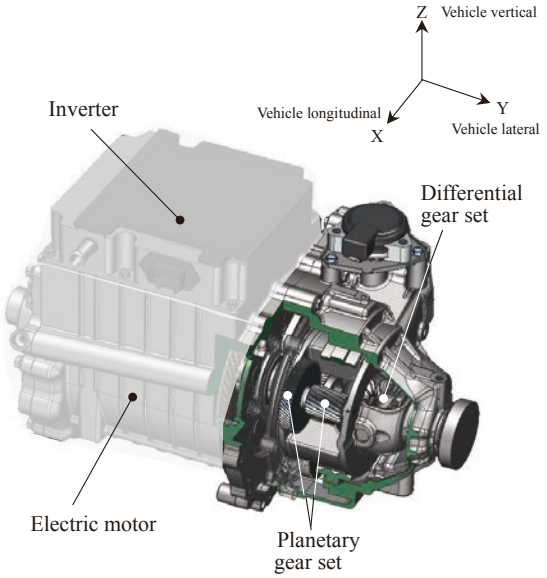

Fig. 2 Appearance of new compact e-Axle

3.2 Aim of downsizing

As illustrated in Fig. 3, the dimension in the vehicle's longitudinal direction was shortened by adopting a single-axis structure.

The e-Axle achieves the top benchmark for torque density as shown in Fig. 4.

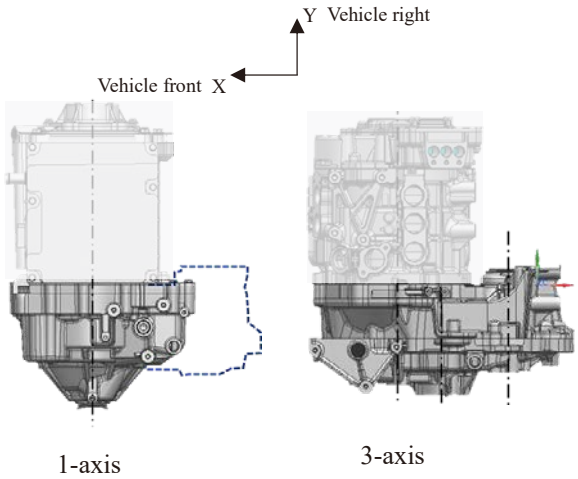

Fig. 3 New compact 1-axis e-Axle

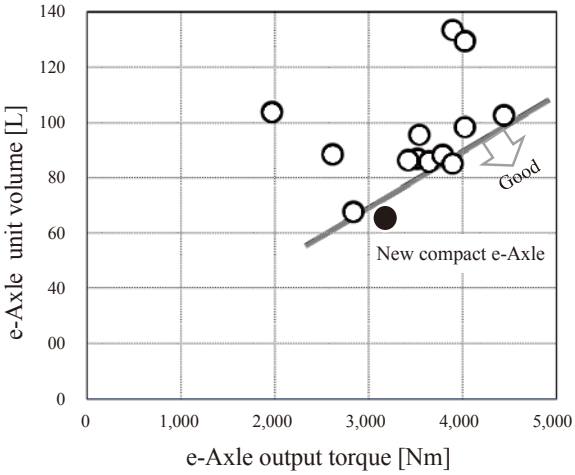

Fig. 4 e-Axle torque density

4. Gearbox

4.1 Gear specifications

As shown in Fig. 5, a stepped planetary gear set was adopted as the gear specifications in consideration of the following requirements (Table 2).

(1) It must allow a gear ratio of 9.4 or higher to be secured in consideration of the required driving force and available motor torque.

Table 2 Planetary skeleton selection

	Single planetary gear set	Stepped planetary gear set	Dual planetary gear set
	Output Input	Output Input	Output Input
Gear ratio	−	+	++
Axial length	++	+	−
Efficiency	+	+	−

− + ++ Good

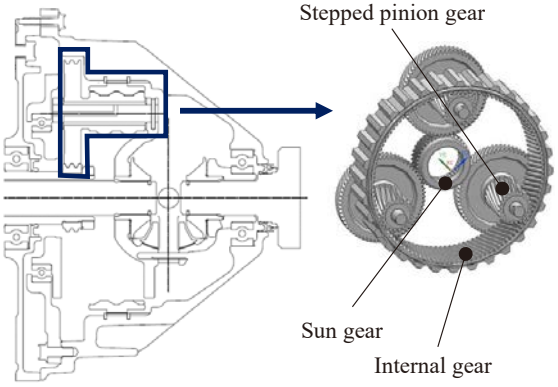

Fig. 5 Stepped pinion planetary gear set

(2) Compact axial length.
(3) Top-level transmission efficiency.

4.2 Gear ratio selection

Increasing the gear ratio reduces motor torque, enabling a smaller motor and inverter. However, increasing the gear ratio enlarges the radial dimension of the planetary gear set.

Motor torque was reduced by increasing the gear ratio of the new e-Axle to 9.692, the maximum dimension that would still allow the unit to be mountable (Fig. 6).

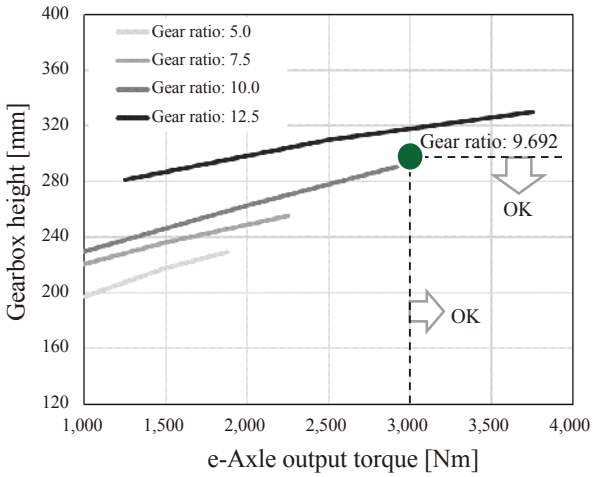

Fig. 6 Gear ratio optimization

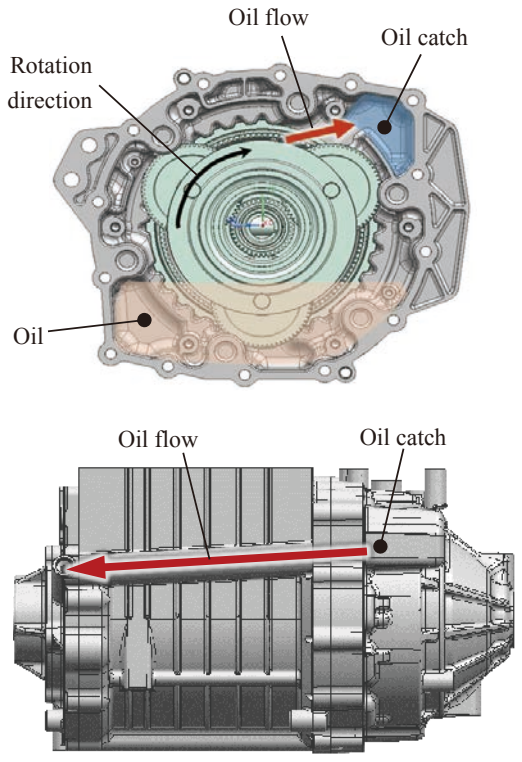

Fig. 7 Oil flow

4.3 Gear lubrication system

A lubrication system was adopted that uses oil churning by the gears to lubricate each part, thus achieving a low-cost, compact system.

4.3.1 Distribution of lubricant

The structure shown in Fig. 7 was adopted to optimize lubrication based on oil churning by the gears. It incorporates improvements regarding oil supply destinations, churning method, flow passages and circulation method.

An oil catch is provided that retains the oil churned by the planetary gears and distributes it to the bearings and seals of the gearbox output shaft positioned on the opposite side from the gearbox.

4.3.2 Results of lubrication simulation

Oil flow inside the unit was simulated using computational fluid dynamics (CFD) simulation software. The results confirmed that lubrication was reliably provided to each part as shown in Fig. 8. It is observed that oil flows into the oil catch and is well distributed to lubricate the planetary gears. In addition, an experiment was conducted to visualize the oil flow. The experimental data validated the simulation results and the validity of the lubrication system.

4.4 Transmission efficiency

The following elements that greatly influence the sensitivity of transmission efficiency were incorporated into the design to reduce loss compared with that of a 3-axis gearbox structure.

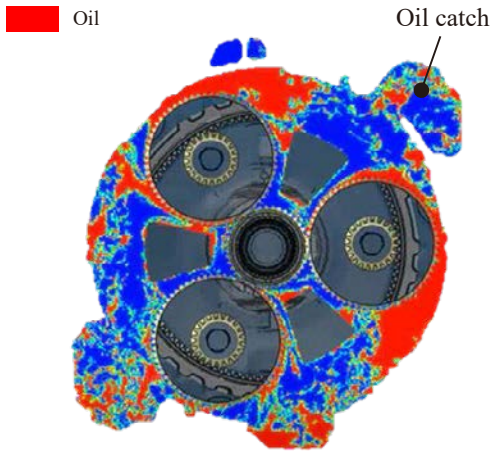

Fig. 8 Oil flow simulation

Gear meshing:
The adoption of the stepped planetary gear set achieved the same number of meshes as that of a 3-axis structure.

Bearings:
The stepped planetary gear set eliminated the tapered roller bearings and reduced the number and load of the ball bearings.

Oil churning:
The oil catch structure reduces churning resistance.

As shown in Fig. 9, these measures reduced the friction loss of the 1-axis unit to nearly one-half that of the 3-axis gearbox to provide top-level transmission efficiency.

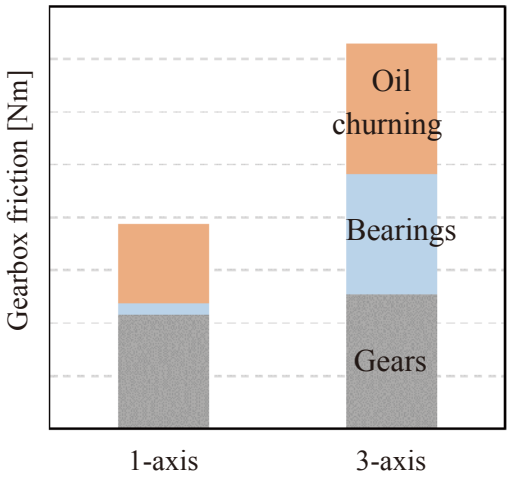

Fig. 9 Gearbox friction reduction

5. Conclusion

A compact e-Axle was newly developed that adopts a planetary gear set as the gearbox, which improves vehicle mountability, expands luggage space, increases the degrees of freedom for vehicle styling and reduces aerodynamic drag.

The adoption of a stepped planetary gear set structure and optimization of oil flow inside the unit achieve both excellent transmission efficiency and lubrication performance.

■ Authors ■


Hiroki UEHARA


Shota OIKAWA


Kazuhiko YOKOYAMA

Improvement of development quality by applying MBD to experiments –Application of a HILS system to AT development–

Shinya KUMAYABU* Tatsuo TAUCHI* Norio SERIZAWA*

Summary

Development costs have tended to increase in recent years owing to longer lead time and greater expenses because of the diversified and higher functionality required of vehicles. The cost burden of experiments using actual vehicles is especially large, and increased efficiency is required in addition to ensuring quality. This article describes the use of a new hardware-in-the-loop simulation (HILS) system that has been improved so as to enable coordinated engine control, making it possible to substitute theoretical experiments for evaluations that previously could only be made with actual vehicles. This improved system achieves solid quality while holding down the cost of developing automatic transmissions by enabling advance evaluations to be conducted efficiently.

1. Introduction

Development lead time and costs have tended to increase enormously in recent years owing to the diversified and higher functionality demanded of vehicles. Issues that occur in actual vehicle evaluations conducted on real-world road surfaces in the later phase of the development period are an especially large cause of rework that puts pressure on development costs.

In order to deal with this issue, JATCO has promoted the use of model-based development (MBD) technology for substituting test bench experiments and theoretical experiments in place of actual vehicle experiments. The following benefits can be expected from this approach.

1) Advance evaluation of conditions simulating real-world road surfaces by using simulation functions.
2) Efficient evaluation of a huge number of conditions by using an automatic experiment system.

This article describes an example of the application of a hardware-in-the-loop simulator (HILS) embodying MBD technology to substitute theoretical experiments for vehicle experiments in developing automatic transmissions (ATs). This approach both reduces development costs and improves quality.

2. Issue

More speed ranges have been added to ATs in recent years to meet demands for better fuel economy among other requirements. Like other companies, JATCO has added more speed ranges to 7-speed ATs to create 9-speed ATs for use on rear-wheel-drive vehicles. As a result, the number of shift patterns has increased 1.6 times as shown in Fig. 1. Moreover, owing to the greater complexity of shift control, conditions with finer throttle valve openings have been added along with various driving environment conditions, including high elevations and road gradients. Automatic transmissions must always provide satisfactory smoothness, response and other shift performance qualities under this vast number of evaluation conditions. However, it is difficult to ensure such performance on the basis of actual vehicle experiments.

As one measure for coping with this issue, for some time now we have been using a HILS-based experiment

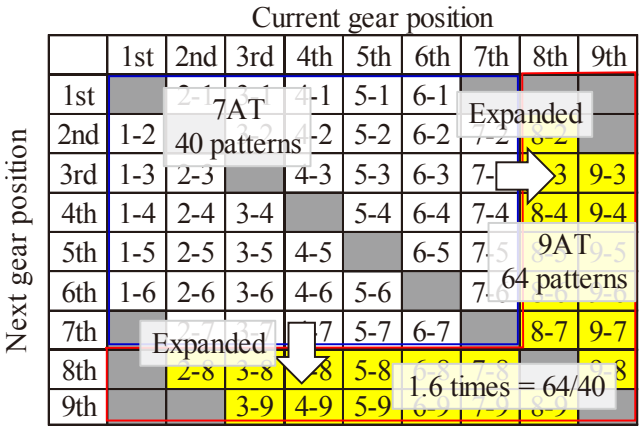

Fig. 1 The number of shift patterns

* Unit System Development Department

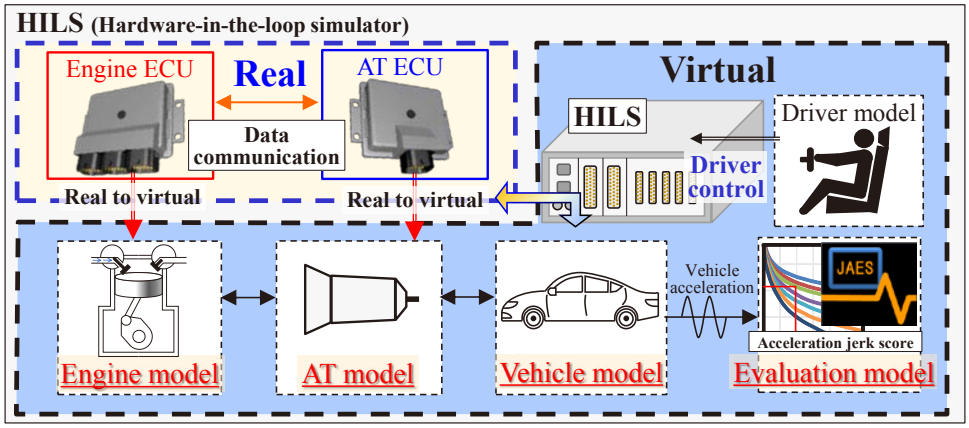

Fig. 2 HILS system with AT ECU + engine ECU

system to confirm the performance of the onboard electronic control unit (ECU) of the AT as a substitute for actual vehicle experiments. However, in order to confirm driveability, it is necessary to reproduce coordinated control for adjusting engine torque. Application of the previous HILS system with only the AT ECU has been limited due to its poor accuracy.

3. Solution to the issue

The following three measures were applied to the previous HILS-based theoretical experiment system to improve its accuracy so as to enable confirmation of driveability.

(1) Development of a HILS system that also operates the engine ECU in addition to the AT ECU in order to enable coordinated engine control.
(2) Enhancement of the accuracy of the AT and vehicle models to enable driveability evaluations.
(3) Implementation of an automatic evaluation system for obtaining higher efficiency.

4. HILS system with engine & AT ECU operation applied to a 9-speed AT

A HILS system with both engine & AT ECU operation was developed for application to a 9-speed AT for rear-wheel-drive vehicles. The system configuration is outlined in Fig. 2. This is a theoretical experiment system that incorporates simulation models other than for the ECUs. An automatic experiment system enables efficient evaluation of a vast number of operating conditions, including driving environment conditions. It is well suited to wide-ranging searches for calibration constants and to narrowing down conditions causing performance problems.

4.1 Improvement of engine model

The intake air volume etc. sent to the sensors must be calculated in order to operate an actual engine ECU. However, implementing a detailed simulation would require an enormous amount of effort and computational complexity, making it difficult to use the HILS system that requires real-time processing. Therefore, a method was adopted for calculating the intake air volume with a simple computational model (Fig. 3). This model uses the mean value of the intake air volume fluctuation among the cylinders, which is found with what is generally known as a mean value engine model (MVEM).

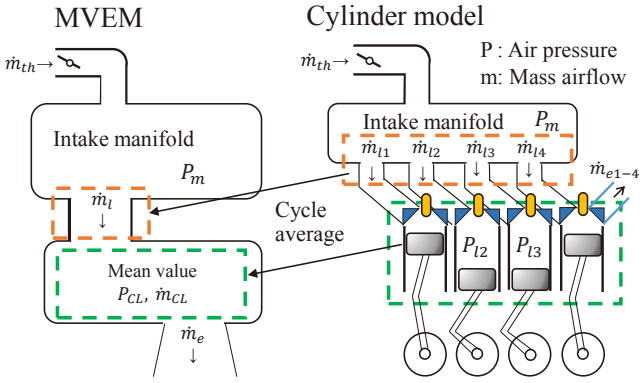

Fig. 3 Mean value engine model (MVEM)

A method of referring to a map of experimental data is used to calculate engine torque and other values.

This method makes it possible to reproduce the coordinated control between the engine ECU and the AT ECU. Figure 4 compares the results obtained with the new HILS system and the previous HILS system that includes only JATCO's standard in-house AT ECU. The data indicate that the new system is capable of reproducing the synchronized control that immediately raises the engine

speed when the coordinated control procedure works to increase engine torque at the time of a downshift.

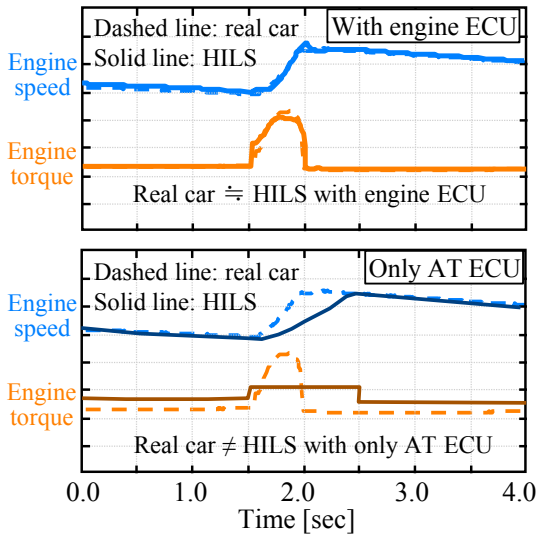

Fig. 4 Comparison of coordinated control for HILS system and real car

4.2 Improvement of AT model

The following improvements were made to the AT model in the new HILS system for the purpose of evaluating driveability during AT shifting.

(1) The equation of motion for the independent inertial moment of each element of the planetary gear set is expressed as a state space representation and calculated.

(2) Drag torque is calculated according to the clearance state of the clutch friction material.

(3) The coefficient of friction of the clutches, which varies depending on the experimental values used for the rotational speed and surface pressure, is calculated in reference to a map.

(4) The elastic modulus of the CVT fluid, which varies according to the hydraulic pressure based on matching with experimental data, is calculated in reference to a map.

These improvements enhance the reproducibility of shift shock, making it possible to evaluate driveability.

4.3 Improvement of vehicle model

A simple mass model was used previously as the vehicle model in performance experiments of an AT unit alone. However, in evaluating vehicle behavior, it is necessary to consider the influence of spring system vibration induced by the suspension and other parts. Therefore, in a cooperative effort with Nissan Motor Co., Ltd., a vehicle model was adopted that can evaluate low-frequency vibration, taking into account a spring element. Figure 5 presents a comparison of vehicle acceleration during an upshift obtained with the improved model, the previous model and a real car. Because the tilting and swaying behavior of the vehicle body induced by acceleration was added to the improved model, it reproduced vehicle acceleration close to the value of the vehicle acceleration sensor.

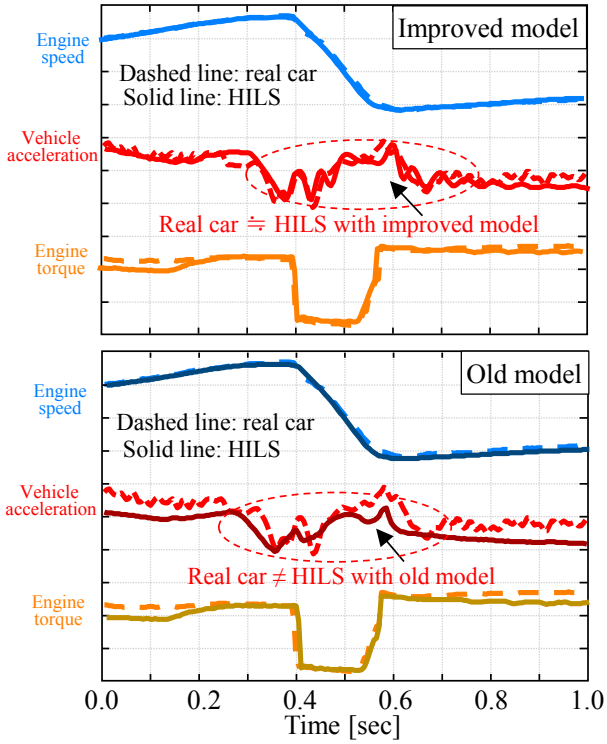

Fig. 5 Comparison with improved vehicle model

4.4 Automatic evaluation system

The Jatco Auto Evaluation System (JAES) developed in-house by JATCO was adopted as the evaluation model. JAES converts the ride quality index, based on the "Evaluation Method for Whole-Body Vibration in ISO2631-1," to JATCO's in-house rating score. This enables automatic operation of the automatic experiment system from the execution of driving operations to the final evaluation of ride comfort.

5. Use of HILS system with both engine and AT ECU operation

This section describes examples of experiments conducted on JATCO's 9-speed AT using the new HILS system that activated the engine and AT ECUs.

5.1 Experiments for varied driving environment conditions

It is now easy to conduct tests on road gradients by

changing the values in the simulation. This capability can be used to examine problems suspected to occur under coordinated engine control only on downhill gradients. It has been helpful in clarifying the mechanism involved and in establishing a corrective control procedure by identifying the conditions causing the phenomenon such as the degree of the downhill gradient and rate of vehicle deceleration.

5.2 Use of automatic capabilities of HILS system

Confirming the standard menu of various shift patterns in actual vehicle experiments takes 7.5 months to check approximately 5,000 patterns, but confirmation can now be completed in seven days with the HILS system because it operates continuously day and night. Based on the results, operating regions where it is suspected performance problems may occur are identified and further narrowed down in detailed experiments conducted with an actual vehicle. In addition, the patterns can be reused to confirm differences when small-scale specification changes or control system changes are made, enabling efficient confirmation of quality.

5.3 Wide-range search for calibration constants

A wide-range search for multiple constants, which is time-consuming with actual hardware, was conducted by taking advantage of the ability to easily change the calibration constants of the ECU in a theoretical experiment. The color-coded regions in Fig. 6 indicate the operating regions where the evaluation model results were poor when calibration constants for the engagement and release pressures of the clutches were varied. As indicated in the figure, the HILS system contributed to constant calibration by finding an acceptable area in the region of high clutch release pressure, which was not found in the test results of the actual vehicle.

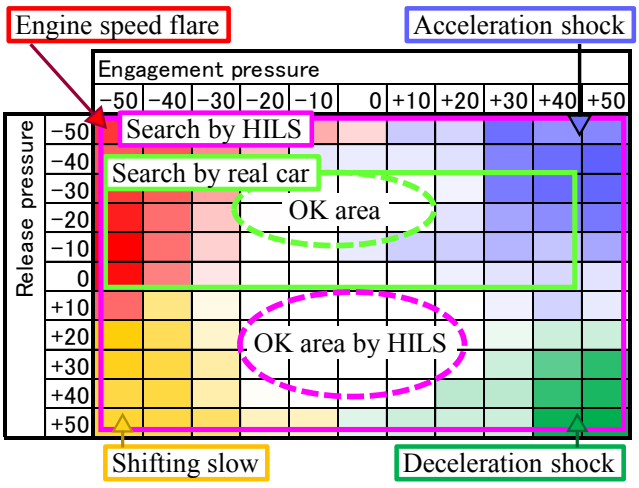

Fig. 6 Calibration constant search by HILS and real car

6. Conclusion

Development costs have been soaring due to the diversified and higher functionality required of vehicles. To address this issue, we included the engine ECU in the new HILS system and made the following improvements in order to expand the operating range that can be confirmed by theoretical experiments. These measures were taken to cope with the explosive increase in experimental conditions especially for the addition of more speed ranges to ATs.

(1) Reproducibility of coordinated engine control was improved by creating the minimum necessary engine model for operating the engine ECU.
(2) Reproducibility of shift shock was improved by further enhancing the AT and vehicle models.
(3) The automatic experiment system now makes it possible to efficiently vary many conditions.

The following results were achieved by using this improved HILS system.

(1) Fine-mesh simulations that included driving environment conditions were conducted at low cost and with high reproducibility, which contributed to the development of the ECU control system.
(2) Potential issues were detected early before in-vehicle testing, wide-range searches were conducted for calibration constants and they were narrowed down.

HILS-based theoretical experiments cannot be substituted for all actual vehicle experiments at the present time because complete accuracy has not yet been obtained. Therefore, we aim to further improve development quality through selective use of the features of each approach. The advantages of the HILS-based automatic experiment system will be utilized to narrow down calibration constants and conditions based on wide-range searches, and experiments will be performed for obtaining highly accurate clarification of the phenomena involved.

■ Authors ■


Shinya KUMAYABU


Tatsuo TAUCHI


Norio SERIZAWA

Improvement of development quality by applying MBD to experiments —Application of a VRS system to CVT development—

Daisuke YAMAGATA*

Summary

Development costs have tended to increase in recent years due to the diversified and higher functionality required of vehicles. The cost of conducting actual vehicle experiments is especially huge, and there is a need for higher efficiency on top of ensuring quality. This article describes the use of a virtual and real simulator (VRS) system to conduct test bench experiments for making evaluations that previously could only be done in actual vehicle experiments. This system selectively uses virtual parts embodying model-based development (MBD) technology and real parts of an actual unit in appropriate places. By enabling advance evaluations to be conducted efficiently, this system supports the creation of solid quality while holding down development costs.

1. Introduction

Development lead time and costs have tended to increase enormously in recent years owing to the diversified and higher functionality required of vehicles. Issues that occur in actual vehicle evaluations conducted on real-world road surfaces in the later phase of the development period are an especially large cause of rework that puts pressure on development costs.

In order to resolve this issue, JATCO has promoted the use of model-based development (MBD) technology to conduct theoretical experiments and test bench experiments in place of actual vehicle experiments. The following benefits can be expected from this approach.

1) Advance evaluation of conditions simulating real-world road surfaces by using simulation functions.
2) Efficient evaluation of a huge number of conditions by using automatic experiment capabilities.

This article presents an example of the use of a virtual and real simulator (VRS) system embodying MBD technology in actual CVT development work to perform test bench experiments in place of actual vehicle experiments. The use of this system builds solid quality while suppressing development costs.

2. Issue

A CVT is built with a variator capable of executing stepless shifting using a belt and pulley system. Precise hydraulic pressure control of each pulley ensures stable shifting and enables torque transmission (Fig. 1).

In addition, the transmission must always ensure shift stability and provide satisfactory vehicle driveability in various driving operations envisioned on a wide range of real-world road surfaces, including those at high elevations and with road gradients.

Numerous actual vehicle experiments on a test course and on real-world road surfaces are necessary in order to confirm such performance. Because of the diversification of requirements and higher functionality needed, it is becoming very difficult to confirm all of the performance requirements using actual vehicles.

As one solution to this situation, JATCO has been

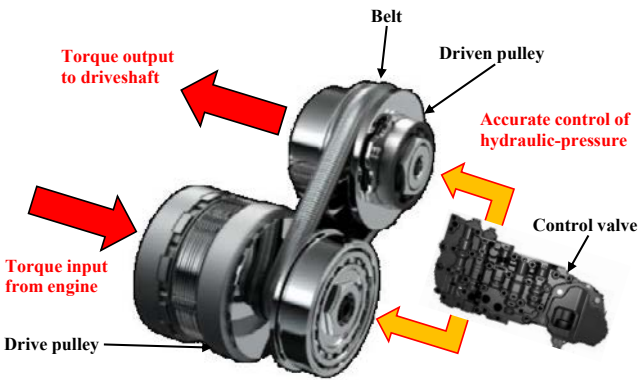

Fig. 1 Variator system of CVT

* Unit System Development Department

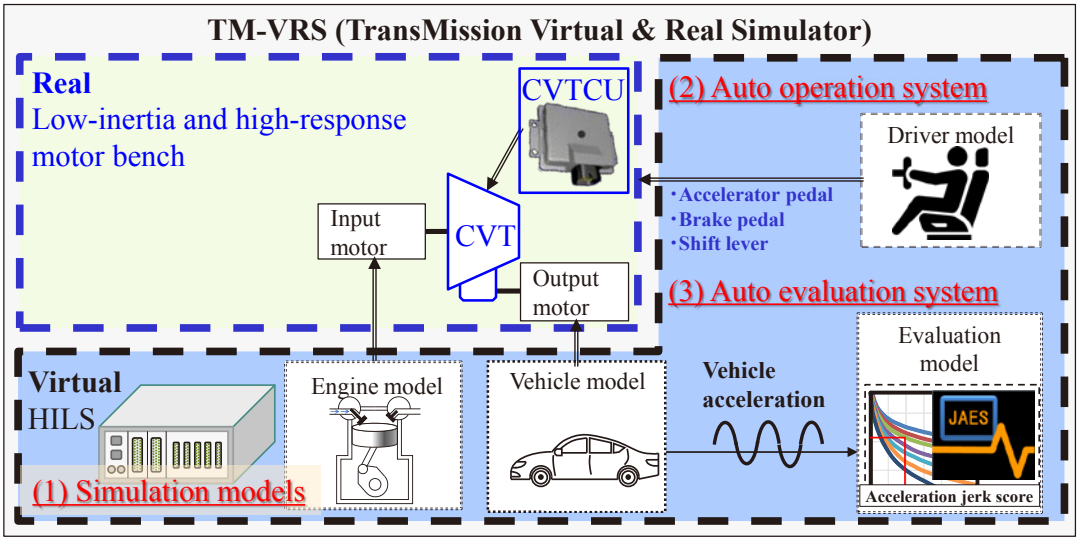

Fig. 2 TM-VRS System

promoting the use of MBD technology to substitute theoretical experiments and test bench experiments for actual vehicle experiments. This approach is aimed at both reducing development costs and ensuring desired quality.

However, a major issue in both theoretical and test bench experiments is to accurately reproduce actual vehicle behavior. In a theoretical experiment, models are substituted for all the vehicle systems including the CVT that is the target of the evaluation. It is desirable to be able to evaluate driveability at a level that includes the variator and hydraulic pressure control system, which are characteristic elements of a CVT. In this case in particular, it is necessary to use highly accurate models that require an extremely long calculation time. One resultant issue is that it becomes very difficult to efficiently evaluate a large number of experimental conditions, which is one of the advantages of theoretical experiments.

3. Solution to the issue

The following practical solution was developed to resolve the issue of the trade-off between accuracy and efficiency. Actual CVT hardware is used for parts that require accuracy and are difficult to model. Simulation models based on MBD technology are substituted for the other parts. In short, an effort was made to replace actual vehicle experiments with test bench experiments by applying the VRS system that selectively uses both real and virtual parts in appropriate places.

JATCO Technical Review No. 17 contained an article entitled "Development of a VRS Test Bench Capable of Validating Transmission Driveability using a Virtual Engine" (referred to hereafter as the previous article). The present article describes an example of the application of the VRS system in the development of an actual CVT.

4. TM-VRS system

The configuration of the TM-VRS system is shown in Fig. 2. It was created by adding hardware-in-the-loop simulation (HILS) models (Fig. 2(1)), an automatic operation system (Fig. 2(2)) and an automatic evaluation system (Fig. 2(3)) to a low-inertia, high-response motor bench.

The high-response motor bench and simulation models serve to reproduce the behavior of an actual vehicle. A large number of conditions can be efficiently evaluated by using the automatic experiment capabilities incorporated in the automatic operation and evaluation systems.

4.1 Engine model

A simple engine model was adopted that reproduces only the narrowed-down characteristics needed for evaluating a CVT. It is not a virtual engine system like that mentioned in the previous article or used for stepped AT evaluation, which employs an actual engine control unit.

This simple engine model was prepared as a measure for addressing an actual operational issue where it is not possible to construct a virtual engine system on a timely basis because the engine is being developed simultaneously or for some other reason. Compared with a stepped AT that requires a coordinated engine control system for switching between clutches of the planetary gear set when shifting, the coordinated engine control for a CVT is limited, making it possible to substitute this simple model.

4.2 Vehicle model

Compared with the simple model that only included running resistance in the previous article, a vehicle model was adopted like that for stepped AT evaluation, which includes the vibration characteristics of the suspension, engine mounts and other parts. This was done in cooperation with Nissan Motor Co., Ltd., and it improved the reproduction accuracy for vehicle acceleration (G), which is critical for evaluating driveability.

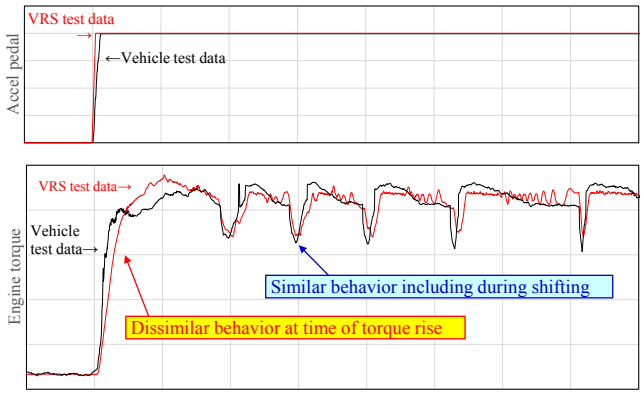

Fig. 3 Engine torque behavior comparison

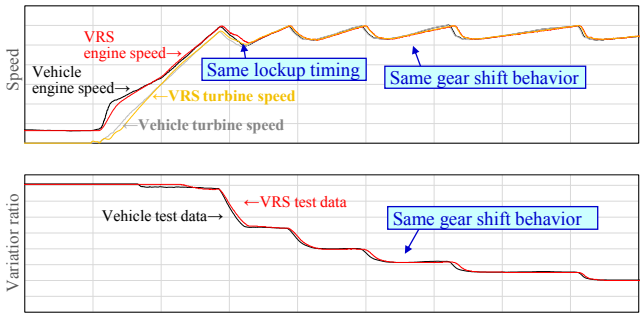

Fig. 4 CVT internal behavior comparison

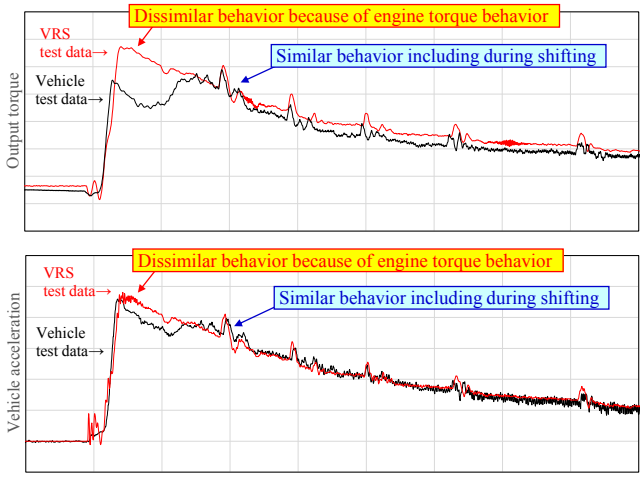

Fig. 5 Vehicle acceleration behavior comparison

4.3 Automatic evaluation system

The automatic evaluation system adopts an evaluation model that is identical to the one mentioned in the previous article and used for stepped AT evaluation. This system enables efficient judgment of the huge volume of data collected by the automatic operation system.

5. Actual vehicle behavior reproduction accuracy of TM-VRS

Figures 3-5 compare the behavior of the time-history data obtained with an actual vehicle and with TM-VRS. Data are shown separately for different parts of the TM-VRS system in order to confirm their reproducibility of actual vehicle behavior.

Figure 3 compares the time-history waveforms for accelerator pedal operation and engine torque that are influenced by the engine model. Except for the start of torque rise, the engine model reproduced engine torque behavior during steady-speed operation and when shifting.

Figure 4 compares the time-history waveforms for the engine speed, turbine speed and variator ratio, which are influenced by the engine model and the actual CVT hardware. It is seen that the TM-VRS system reproduced the same behavior as that of the actual vehicle in each case.

Figure 5 compares the time-history waveforms for output shaft torque, representing the final output, and vehicle acceleration (G). The TM-VRS system reproduced the acceleration behavior of the vehicle, excluding the time when engine torque began to rise.

6. Discovery of development issue and its solution

Figure 6 presents an example of a development issue that was discovered in test bench experiments conducted during the CVT development process before the unit was validated in vehicle testing.

The phenomenon here concerned vehicle vibration that occurred due to variator instability when shifting manually at a low vehicle speed (left-side waveforms in Fig. 6). This issue was discovered for the very reason that the TM-VRS system uses an actual CVT and a high-accuracy vehicle model.

This phenomenon was detected and the issue was resolved before the CVT was validated in vehicle testing (right-side waveforms in Fig. 6).

7. Present issues and benefits of using TM-VRS

One present issue is that test bench experiments cannot fully replace all actual vehicle experiments. However, by

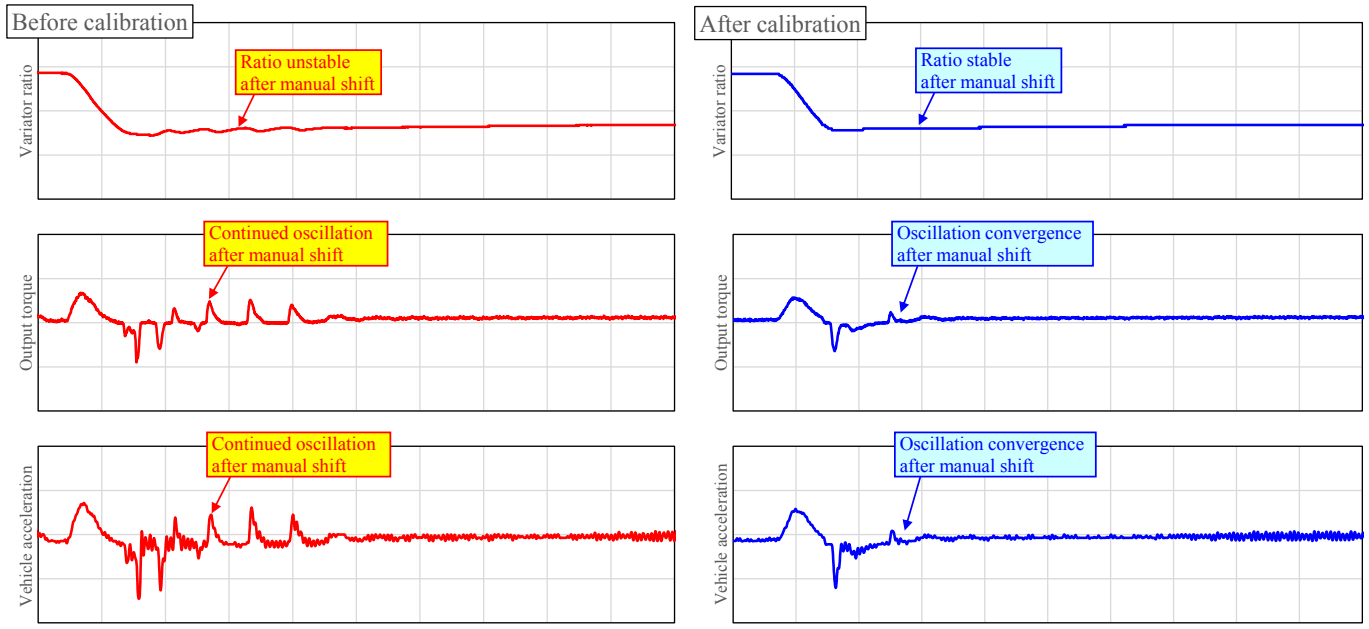

Fig. 6 Problem solution before in-vehicle validation

combining the best features of both approaches as described below, it is possible to both confirm solid quality and ensure efficiency.

Test bench experiments are well suited to a broad examination of many conditions. Specifically, the model-based simulation function enables evaluation of various driving environment conditions simulating real-world road surfaces at an earlier stage than actual vehicle experiments. In addition, the automatic operation and evaluation systems, capable of running day and night including on weekends, enable efficient evaluation of a huge number of conditions. In actuality, vehicle experiments that used to take three months to do on real-world roads can now be completed in one week. As a result, conditions suspected of being development issues can now be identified at an early stage. In addition, by taking advantage of the high reproducibility of driving environment conditions and driving operations, the effects of software changes such as for the control constants or other details and of hardware changes including variability among parts can now be evaluated directly.

Vehicle experiments are well suited to an in-depth examination of a limited number of conditions. Specifically, they can be used selectively to confirm conditions suspected of causing the problems discovered in test bench experiments or when a final judgment must be made by human engineers, among other situations.

8. Conclusion

Development costs have been soaring due to the diversified and higher functionality required of vehicles in recent years. To cope with this issue, JATCO has taken the approach of using a TM-VRS system to substitute test bench experiments for actual vehicle experiments. The following benefits have been obtained by applying this system in actual CVT development activities.

1) Selection of the optimum engine model and improvement of vehicle model accuracy have made it possible to substitute test bench experiments for actual vehicle experiments.
2) An enormous number of conditions can now be evaluated efficiently by using the automatic operation and evaluation systems.
3) Development issues can now be discovered and resolved early by evaluating conditions simulating real-world road surfaces in advance of actual vehicle testing.

In future CVT development activities, we aim to further improve development quality by adopting test bench experiments using the TM-VRS system as a standard process.

■ Author ■

Daisuke YAMAGATA

Development of a torque converter for the Jatco CVT-X mated to engines with fewer cylinders

Kouji OZAKI* Masatsugu ENDO* Satoshi WATANABE* Michinori MATSUO**

Summary

A turbocharged engine with fewer cylinders is effective in improving fuel economy, but idling vibration increases as does the torque difference between the turbocharged and naturally aspirated operating regions. In addition, torque fluctuations increase when accelerating from a low engine speed. Consequently, it was necessary to apply measures to improve the interior noise level obtained with the Jatco CVT-X. This article describes the adoption of a pendulum-type damper for the torque converter of the Jatco CVT-X and the improvements made to hydrodynamic performance characteristics. As a result, the torque converter satisfies both the fuel economy and power performance requirements while resolving noise and vibration issues.

1. Introduction

Turbocharged engines with fewer cylinders have emerged in recent years with the aim of further improving fuel economy. The Jatco CVT-X is our first continuously variable transmission (CVT) to be applied to a 3-cylinder turbocharged engine.

Reducing the number of cylinders causes larger torque fluctuations compared with conventional engines especially in the low vehicle speed range. Locking up the torque converter from the low vehicle speed range is effective in improving fuel economy, but stronger vibration control than before is necessary. Therefore, it was decided to adopt a pendulum-type damper for the torque converter of the Jatco CVT-X in order to resolve this issue.

Applying a pendulum-type damper in an effort to attenuate large torque fluctuations requires more vehicle mounting space. Installing the damper in a narrow space would cause concerns about declines in damping performance and durability. Therefore, it was necessary to consider such concerns when selecting the mass and spring specifications of the pendulum-type damper.

A torque converter serves to amplify engine torque. Large torque amplification is advantageous for improving vehicle launch performance, but there is concern that large engine torque fluctuations during idling would promote vehicle body vibration.

Therefore, the hydraulic performance was tuned to satisfy the requirements for power performance and fuel economy while contributing to the suppression of vehicle body vibration. This article presents examples of the measures that were adopted to resolve these issues.

2. Pendulum-type damper issues and solutions

A 3-cylinder turbocharged engine can produce large torque from a low engine speed, but torque fluctuations also increase (Fig. 1). To suppress interior noise to the previous

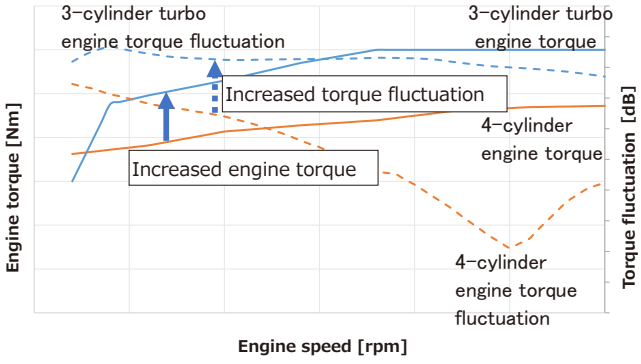

Fig. 1 Engine torque and torque fluctuation

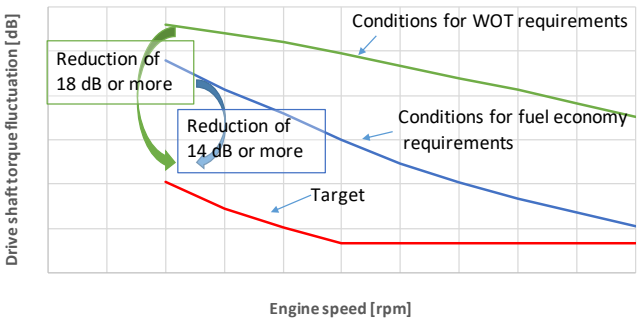

Fig. 2 Targets for reducing drive shaft torque fluctuation

* Hardware System Development Department ** Innovative Technology Development Department

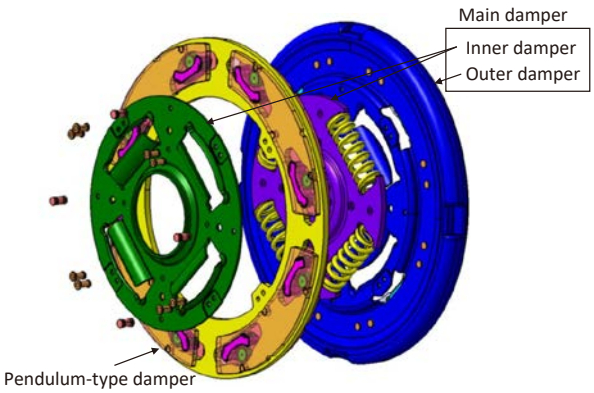

Fig. 3 Structure of pendulum-type damper

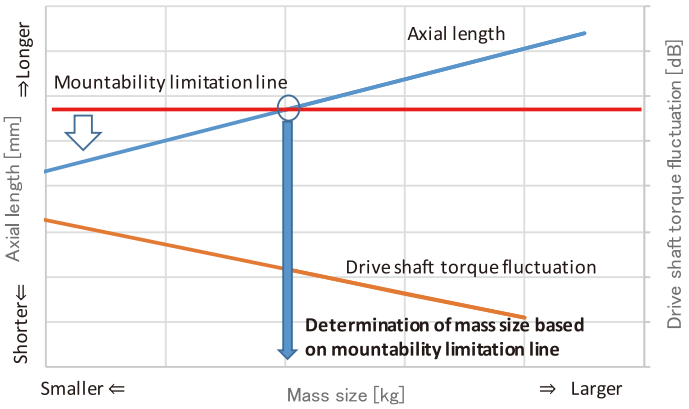

Fig. 5 Sensitivity of axial length and drive shaft torque fluctuation to mass size

level in a locked-up state, drive shaft torque fluctuation must be reduced by 14 dB or more from that obtained with the previous damper under operation that satisfies the fuel economy requirement and by 18 dB or more under wide-open throttle (WOT) operation (Fig. 2). A pendulum-type damper was adopted to attain these reduction targets (Fig. 3).

A pendulum-type damper is built to provide damping force by using the principle of a pendulum to actuate the mass in the opposite phase according to the torque fluctuation frequency. If the pendulum mass moves too much, it will interfere with other parts. This phenomenon is referred to as overshoot.

If pendulum mass overshoot occurs, it gives rise to issues such as noise, vibration and a decline in durability. Therefore, the pendulum mass must be designed so that overshoot does not occur in the region of normal use.

2.1 Study methodology

In general, if the mass stroke is set so that pendulum mass overshoot does not occur in relation to a large torque fluctuation input, a large mass is necessary, which requires sufficient mounting space. However, downsizing is also necessary because of the layout requirements. Accordingly, the torsional stiffness of the damper and the size of the pendulum mass were designed and the specifications were selected so as to achieve a balance between the desired damping effect and the issue of mass overshoot.

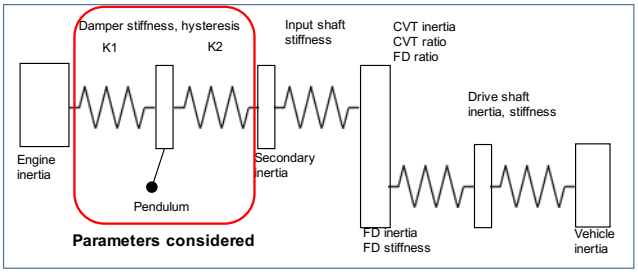

Fig. 4 Analysis model

The model shown in Fig. 4 was used to investigate drive shaft torque fluctuation. A study was made of the feasibility of satisfying the conditions required for fuel economy in relation to the size of the pendulum mass and the spring stiffness of the damper (K1, K2) as parameters. The limits of the mass overshoot region were also simultaneously confirmed.

Increasing the size of the mass has a large effect on reducing torque fluctuation, but the upper size limit is determined by the limitation due to the mountability requirement. Therefore, the value of the mountability limitation was taken as the upper limit of the axial length and the mass size was determined after securing the existing space for the main damper (Fig. 5).

Meanwhile, reducing the spring stiffness of the main damper allows reduction of the engine speed at which pendulum mass overshoot occurs. However, reducing the stiffness more than necessary would require a larger spring size to ensure sufficient strength. That would increase the size of the main damper, making it impossible to satisfy the layout limitation.

Spring stiffness was varied within the existing damper space in order to confirm the drive shaft torque fluctuation level for satisfying the conditions of the fuel economy requirement and the engine speed at which pendulum mass overshoot would occur under the WOT condition. The spring stiffness was then determined so as to satisfy both conditions.

Figure 6 presents the results of an analysis of booming noise when the spring stiffness of the damper was varied. Specification A was for high spring stiffness and specification C was for low stiffness.

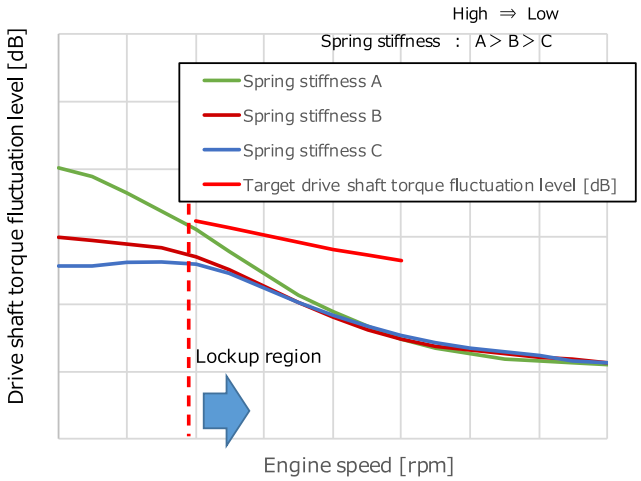

Fig. 6 Booming noise simulation results for various spring stiffness values

The lowest drive shaft torque vibration level was obtained with the low spring stiffness of specification C (blue line), but a drive shaft torque fluctuation value for satisfying the fuel economy target was achievable up to the high spring stiffness of specification A (green line).

Figure 7 presents the results of an analysis of the engine speed for the occurrence of pendulum mass overshoot when the engine torque and resultant drive shaft torque fluctuation were input for each level of damper spring stiffness. The results indicate that lowering the damper spring stiffness makes it possible to reduce the engine speed for the occurrence of pendulum mass overshoot. The spring stiffness of specification C allows an engine speed for satisfying the driveability requirement.

Within the limited space available, a spring stiffness specification was determined for satisfying both the booming noise level relative to the fuel economy requirement and overshoot under the WOT condition.

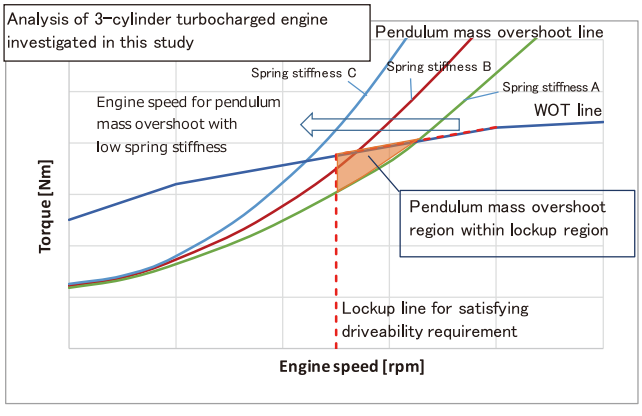

Fig. 7 Engine speed for occurrence of mass overshoot at each stiffness level

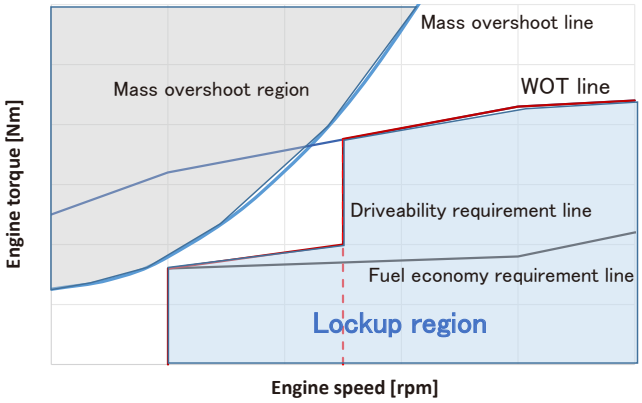

Fig. 8 Lockup region and mass overshoot region

2.2 Level of achievement

Figure 8 is a map of the region where lockup operation is possible in relation to engine speed and engine torque. A lockup region was defined so as to satisfy the fuel economy requirement in the D-range relative to a balance among the pendulum mass size, damper spring stiffness and layout.

The region was also defined so that lockup operation would be possible up to the driveability requirement line without any occurrence of overshoot under the WOT condition that emphasizes power output.

In this way, the lockup region was defined so as to contribute to both power performance and practical fuel economy.

3. Hydrodynamic performance issue and solution

This section presents examples of the improvement of hydrodynamic performance for satisfying the desired fuel economy and power performance while avoiding vibration issues during D-range idling.

Large torque fluctuation occurs during idling of a 3-cylinder turbocharged engine so there is concern that it might promote vehicle body vibration. As a measure against vibration, improvement can be expected by reducing the torque input to the drive shaft. One conceivable approach here is to reduce the output torque of the torque converter.

The output torque of the torque converter (To) is expressed by the following equation in relation to the torque capacity coefficient (τ), engine speed (Ne) and torque ratio (t).

$To = \tau \times Ne^2 \times t$

Accordingly, reducing the torque capacity coefficient and the torque ratio can be expected to lower the output torque.

However, reducing the torque capacity coefficient of the torque converter overall would cause driveability and

fuel economy to deteriorate during acceleration because of engine speed flare. For that reason, it is necessary to keep the torque capacity coefficient at a high level on the high speed ratio side.

Therefore, an effort was made to improve hydrodynamic performance for satisfying fuel economy and power performance requirements while avoiding vibration during idling. That was done by reducing the torque capacity coefficient at the low speed ratio used during idling, including the stall phase, and the torque ratio.

The target for improving hydrodynamic performance so as to achieve the requirements mentioned here was to reduce the torque capacity coefficient and torque ratio relative to the base performance at a low speed ratio below 0.4 and to maintain the same respective values in the region of a speed ratio of 0.4 or higher. Figure 9 shows the improvement targets defined for hydrodynamic performance.

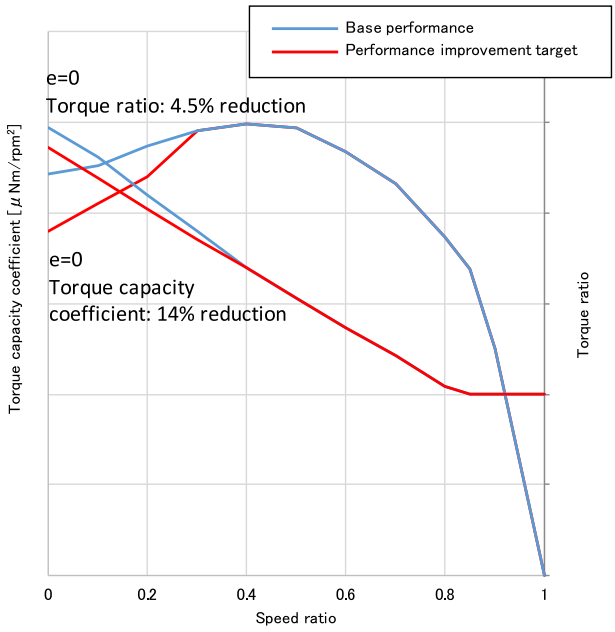

Fig. 9 Targets for improving hydrodynamic performance

3.1 Method for examining hydrodynamic performance

Using the stator blade geometry to increase the amount of flow separation is an effective way to reduce the torque capacity coefficient and torque ratio at low speed ratios. Therefore, hydrodynamic performance was tuned by varying the stator tip geometry so as to ascertain the sensitivity of hydrodynamic performance to the variation.

Figure 10 shows a flow velocity distribution around the stator obtained by simulation at the time of stall. At stall, transmission fluid flows in from the direction of the arrow, striking the stator blade, and the flow branches to the ventral and dorsal sides of the blade. The area of separation at that time is determined by the stator tip geometry. The torque capacity coefficient and torque ratio can be reduced by increasing the amount of flow separation.

Ways of increasing the amount of separation that can be cited include changing the amount of chamfering at the stator blade tip on the inflow side and adjusting the blade thickness at the blade inlet.

The blade geometry was determined by ascertaining the sensitivity of hydrodynamic performance to adjustments made to the amount of stator tip chamfering and blade thickness in relation to the base stator geometry (Fig. 11).

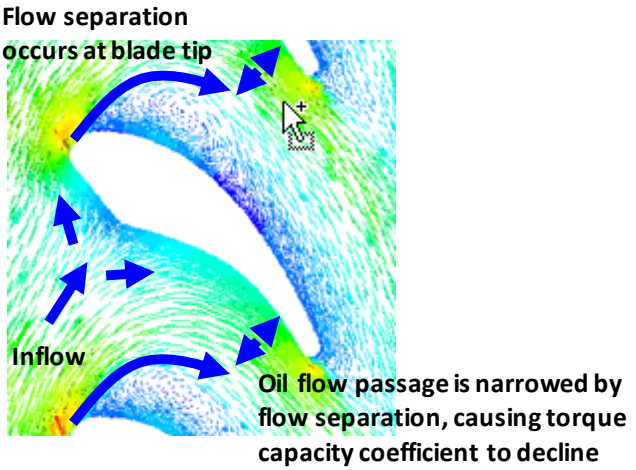

Fig. 10 Flow velocity distribution around the stator

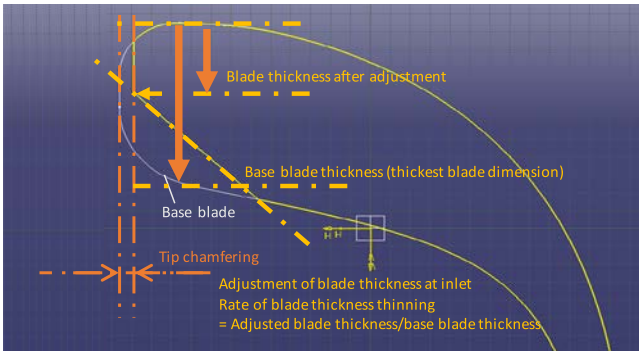

Fig. 11 Cross-sectional view of stator blade: Schematic diagram of tip chamfering

3.2 Performance sensitivity results and level of accomplishment

Figure 12 is a graph showing the rate of change in hydrodynamic performance of the torque capacity coefficient as a function of the amount of stator tip chamfering. The sensitivity of the torque capacity

coefficient to the amount of tip chamfering was found experimentally. As a result, it was confirmed that there was a large reduction effect in relation to the amount of chamfering (red line).

However, considering practical productivity, it would be necessary to apply a round shape to the blade tip edge (Fig. 13). Performance sensitivity was obtained taking that factor into account. As a result, it was found that the effect on reducing performance became smaller. The reduction effect decreased from 11% to around 7% for the same amount of chamfering.

The sensitivity of performance to the adjustment of the blade thickness was then investigated (Fig. 14). The results confirmed that thinning the blade thickness was effective in reducing the stall torque capacity coefficient and the torque ratio.

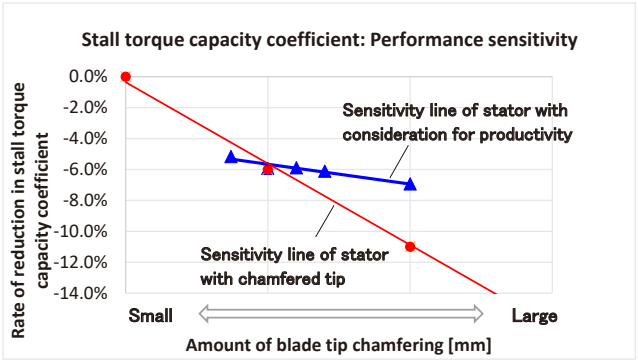

Fig. 12 Stall performance sensitivity to blade tip chamfering

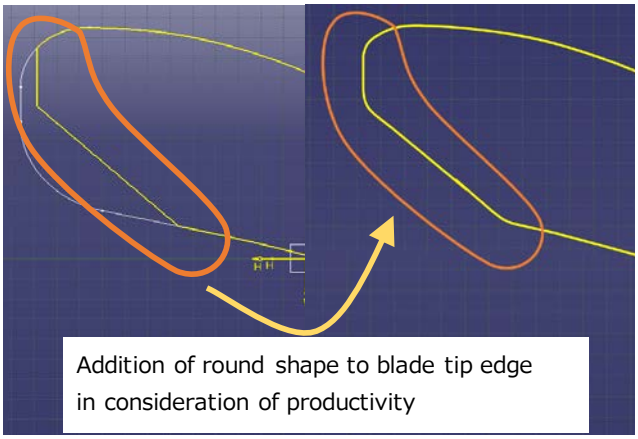

Fig. 13 Stator geometry considering productivity

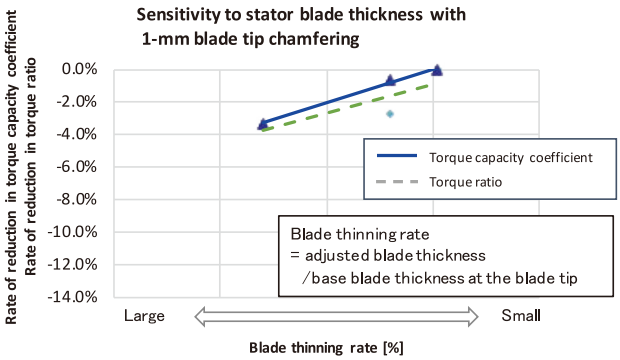

Fig. 14 Sensitivity of torque capacity integer to blade thickness

Stator tip chamfering and blade thickness thinning also reduce the torque capacity coefficient at medium to high speed ratios in addition to low speed ratios (Fig. 15). Therefore, the specifications were determined taking into account the contribution against idling vibration and the effect on power output and fuel economy due to the reduced hydrodynamic performance at medium to high speed ratios.

In terms of the level of accomplishment, the stall torque capacity coefficient was reduced by 8.3% compared with a target of 14% and the torque ratio was reduced by 4.5% compared with a target of 4.5% (Fig. 16).

At speed ratios of 0.6 or higher, both the torque capacity coefficient and torque ratio were maintained at the base performance levels, thereby suppressing the effect on power output and fuel economy.

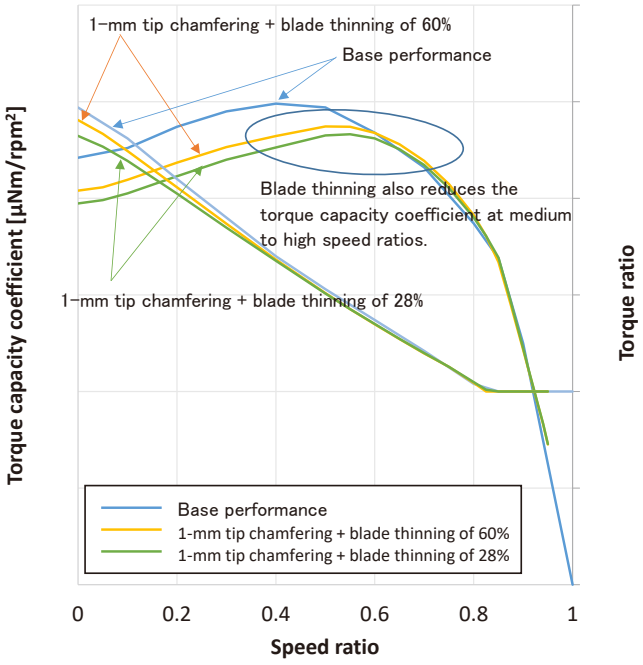

Fig. 15 Overall performance results for blade geometry variation

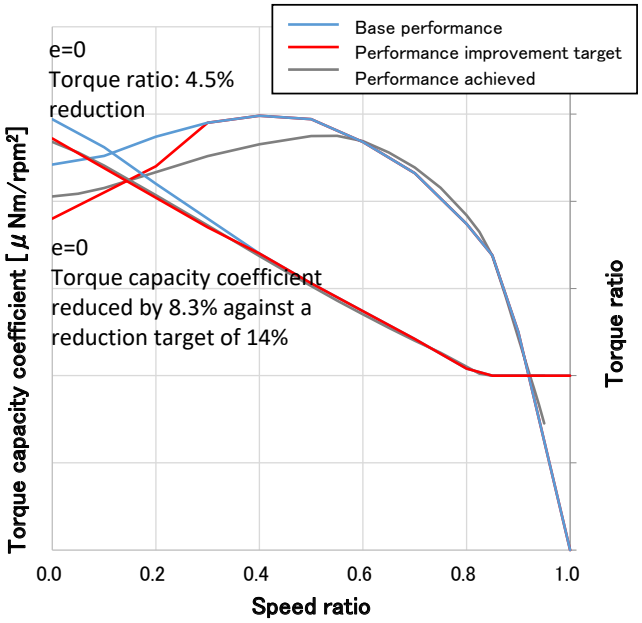

Fig. 16 Level of hydrodynamic performance achieved

4. Conclusion

This article has described the determination of torque converter specifications for JATCO's first application to a 3-cylinder turbocharged engine. Within the limited space allowed, the pendulum mass overshoot issue of the pendulum-type damper and the issue of idling vibration were both satisfactorily resolved.

1) A lockup region was achieved that satisfies the fuel economy requirement and also allows lockup operation for satisfactory driveability without any pendulum mass overshoot as a result of adjusting the damper spring stiffness.
2) Torque converter performance was tuned as a measure against idling vibration. The torque capacity coefficient was reduced by 8.3% and the torque ratio by 4.5%. This tuning provides hydrodynamic performance that satisfies power output and fuel economy requirements while contributing to the suppression of vibration.

■ Authors ■


Kouji OZAKI


Masatsugu ENDO


Satoshi WATANABE


Michinori MATSUO

Clarification of the mechanism reducing torque capacity due to differences between the ideal and actual CVT chain path

Kyohei WATANABE* Jumpei HAYAKAWA* Atsushi IKEDA* Kouhei TOYOHARA* Kazuhiro HAYAKAWA*

Summary

A phenomenon occurred where the torque transmission capacity of a CVT chain did not increase linearly with pulley clamping force. It was confirmed by dynamic analyses and experimental measurements that the deviation of the running radius of the chain from the ideal path caused this phenomenon. Path deviation originated from pulley sheave stiffness. This finding now enables prediction of torque capacity and also supports execution of a suitable pulley stiffness design.

1. Introduction

The variator that provides the shifting capability of a continuously variable transmission (CVT) consists of a pulley assembly and a chain as shown in Fig. 1.

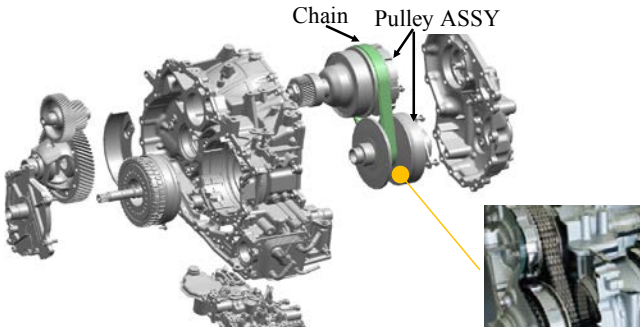

Fig. 1 Structural parts of CVT

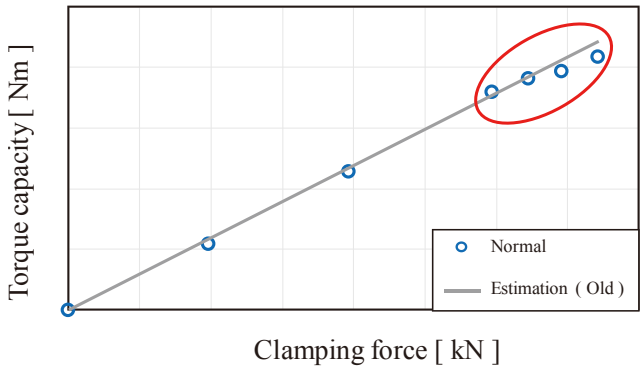

Fig. 2 Torque capacity measurement result

Pulley clamping force is produced by applying hydraulic pressure to the pulley hydraulic chamber. That clamping force generates frictional force between the pulleys and the chain to transmit torque. In general, the torque transmission capacity of a chain is thought to be proportional to pulley clamping force.

During the development of a new variator with high torque capacity, a phenomenon was observed where the torque transmission capacity was not linear relative to pulley clamping force in the region of high pulley clamping force and high torque as shown in Fig. 2. This article presents the results of an investigation undertaken to clarify the mechanism causing this phenomenon, focusing on changes in the running radius of the chain.

2. Investigation of the cause of torque capacity decline

2.1 Calculation equation for torque capacity

Torque capacity due to friction transmission can be expressed as shown in Eq. (1) below.

$$T = F \times R = \Sigma(\mu \times N \times r) \quad (1)$$

T: torque capacity
F: frictional force between chain and pulleys
R: chain average running radius
μ: coefficient of friction of each chain pin
N: clamping force applied to each individual pin
r: running radius of each pin

It was assumed that changes in μ, N and r accompanying an increase in clamping force and torque were the reasons why the torque transmission capacity was not linear

* Hardware System Development Department

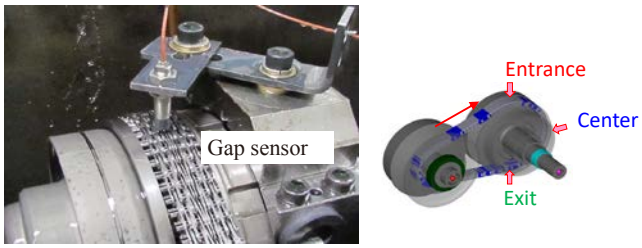

Fig. 3 Gap sensor installation position

relative to pulley clamping force in the region of high pulley clamping force and torque. The amount of change confirmed in each of these parameters is described in the following subsections beginning from 2.2.

2.2 Change in running radius

Changes in the running radius relative to torque were measured under a condition of constant pulley clamping force. As shown in Fig. 3, gap sensors were placed at the entrance, center and exit positions of the chain where it wrapped around the secondary pulley in order to confirm the running radius at each point. The variator test bench shown in Fig. 4 was used to conduct measurement experiments.

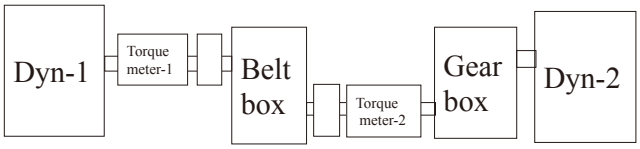

Fig. 4 Variator test bench overview

Table 1 lists the measurement conditions. Figure 5 presents the measured results for the change in the running radius on the secondary pulley in relation to a radius difference of 0 mm when the input torque was 0 Nm. As is also described in Ref. (2), the results show that the running radius of the chain on the entrance side did not change with increasing input torque, but the values at the center and exit on the inside diameter side changed. Figure 6 is a schematic diagram of this radius shift.

As the results in Fig. 5 illustrate, the running radius of the chain changed from the entrance side toward the exit side as input torque increased, which was accompanied by an increase in chain tension on the tension side. As a result, the chain followed a path closer to the inside diameter side at the exit position close to the tension side, which influenced the change in the running radius.

Table 1 Measurement condition

Ratio	-	Low
Input speed	Ni	3,000 rpm
Input torque	T	0→390 Nm
Sec. pulley clamping force	Fs	70 kN

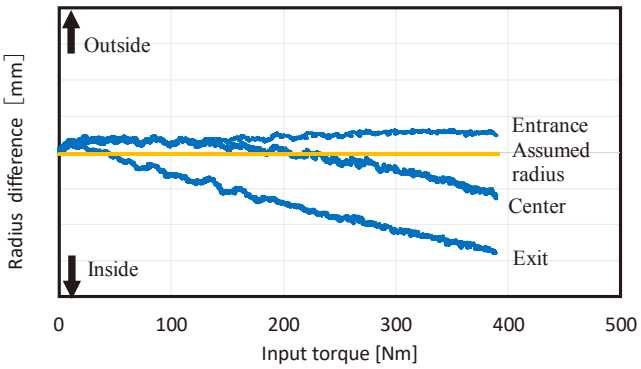

Fig. 5 Radius shift test result

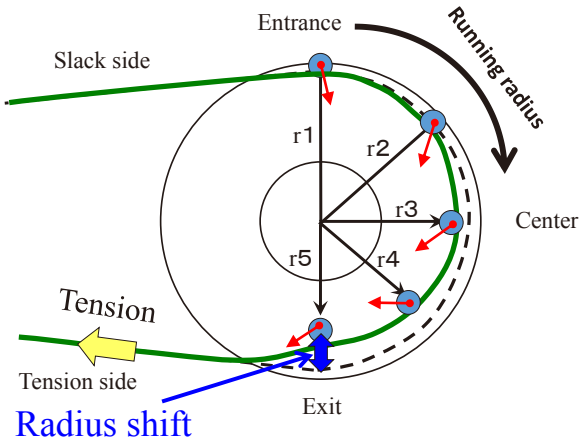

Fig. 6 Radius shift overview

2.3 Change in clamping force applied to each individual pin

Strain gauges were then attached to individual rocker pins in the chain as shown in Fig. 7 to confirm the change in the clamping force applied to each individual pin. The measured strain results from the entrance side to the exit side of the secondary pulley are plotted in Fig. 8 for the measurement conditions listed in Table 2.

The measured strain was proportional to the clamping force of the secondary pulley, and it increased from the entrance side to the exit side where the chain wrapped around the secondary pulley.

The following reason was assumed for the sharp increase in strain toward the exit side as seen in the results in Fig. 8. As described in subsection 2.2, the path traced by the chain near the exit on the tension side was closer to

the inside diameter side. As a result, the pins were further compressed in the section on the inside diameter side, causing the pins themselves to generate large reaction force that increased the amount of strain toward the exit.

With the traditional design method, the running radius between the pins wrapped around the pulley and the sheave face as well as the generated load were treated as being constant values in the design calculations. However, as indicated by the results in Figs. 5 and 8, the running radius between the pins and the sheave face and the generated load constantly change toward the exit owing to the displacement of the pins to the inside diameter side of the pulley. Accordingly, it was reasoned that the running radius r and clamping force N had to be applied to Eq. (1) according to the actual state of each individual pin wrapped around the pulley and thus incorporated into the design calculations.

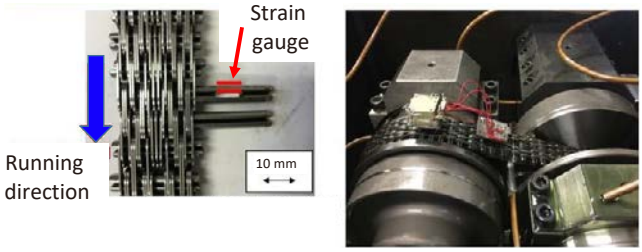

Fig. 7 Locations of strain gauges set on surfaces of pin

Table 2 Measurement condition

Ratio	-	Low
Input speed	Ni	500 rpm
Input torque	T	100 Nm
Sec. pulley clamping force	Fs	30, 50, 70, 80 kN

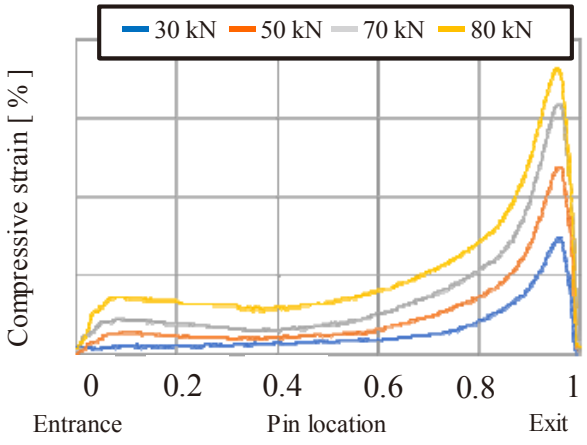

Fig. 8 Measurement of strain gauges set on surfaces of pin

2.4 Estimation of coefficient of friction μ

In general, the coefficient of friction changes according to the sliding velocity and vertical load, and it decreases with increasing oil film thickness h in the boundary lubrication to mixed lubrication regime as indicated by a Stribeck curve.[3] As was made clear in subsection 2.3, the radius between the pulley and the pin end faces changes, so it is assumed that the sliding velocity also varies accompanying such radius changes. In this explication of the mechanism of interest, it was necessary to estimate the coefficient of friction using the sliding velocity and load at the position of each individual pin where the chain wrapped around the pulley. Accordingly, line contact was assumed for the contact between the pulley and the chain; the oil film thickness h under the condition of line contact was calculated using the Dowson-Higgison formula in Eq. (2).

$$\frac{h_{min}}{R}=2.65\left(\frac{\eta_0\bar{u}}{ER}\right)^{0.7}(\alpha E)^{0.54}\left(\frac{W}{ERL}\right)^{-0.13} \quad (2)$$

hmin: minimum oil film thickness
ηo : kinematic viscosity
ū : sliding velocity
E : Young's modulus
A : coefficient of pressure-viscosity
W : load
R : equivalent radius of curvature

Letting the Young's modulus and other parameters in Eq. (2) be constants, it is assumed that the coefficient of friction has a negative first-order correlation with the oil film thickness. Equation (2) can then be replaced by Eqs. (2-1) and (2-2). This assumption was confirmed to be valid on the basis of experimental measurements.

$$\mathrm{hmin} = \mathrm{a}\cdot\bar{u}^{0.7}\cdot W^{-0.13} \quad (2\text{-}1)$$

$$\mu \propto 1/\mathrm{hmin} \quad (2\text{-}2)$$

a: constant

Here, it is necessary to calculate the coefficient of friction μ in relation to the load W and the sliding velocity u. However, because it would be difficult to measure the coefficient of friction for one pin during the operation of the chain, μ was measured in a single part test using a pin-on-disk method as shown in Fig. 9.

Figure 10 presents the coefficient of friction results that were measured when the sliding velocity was varied in a load range of 500-1,600 N/pin. Using the measured results in Fig. 10, the vertical axis in Fig. 11 shows the coefficient of friction μ that was obtained in relation to the calculated product of the sliding velocity and load ($\bar{u}^{0.7}\cdot W^{-0.13}$) on the horizontal axis. The results show that the coefficient of

friction has a negative first-order correlation with the oil film thickness. This indicates that the coefficient of friction μ can be predicted using Eqs. (2-1) and (2-2) that were assumed above.

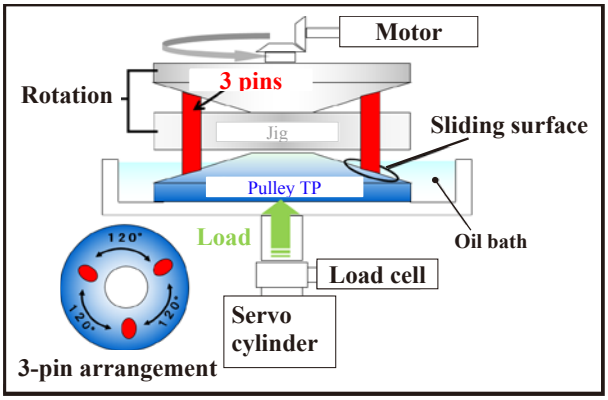

Fig. 9 Pin-on-disk overview

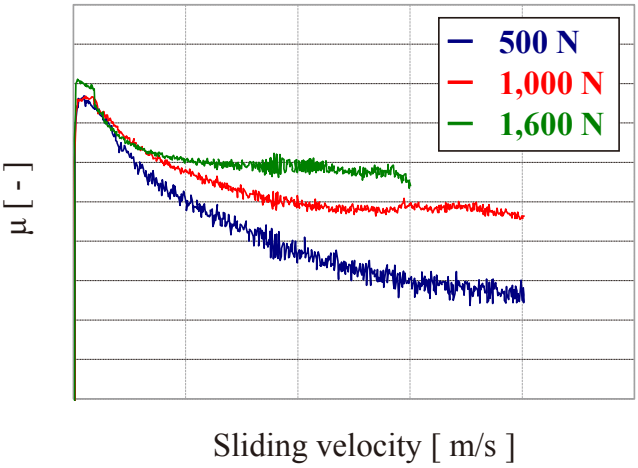

Fig. 10 μ measurement result

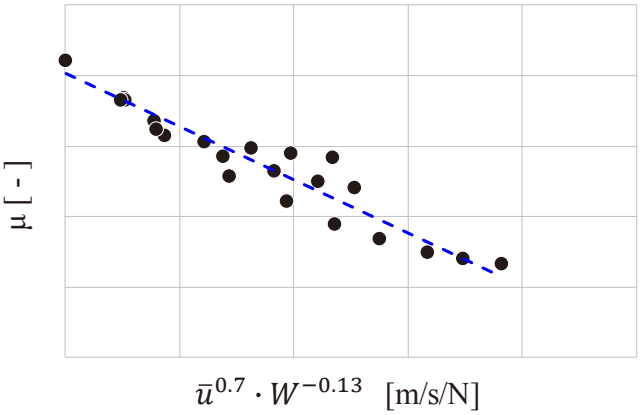

Fig. 11 Friction coefficient result

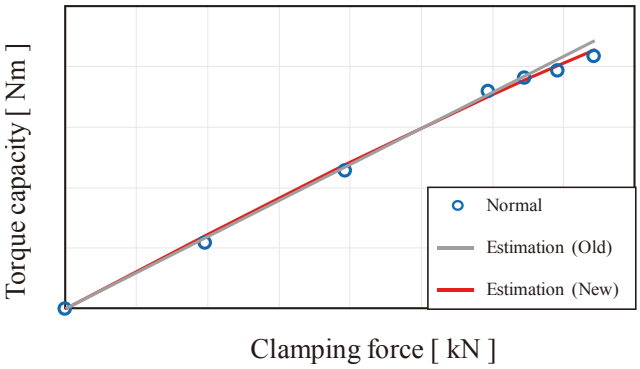

Fig. 12 Comparison of torque capacity between estimation and experimental value

2.5 Torque capacity calculation reflecting the measured results

The measured and calculated μ, N and r values were applied to Eq. (1) to calculate the torque capacity and the results are shown in Fig. 12. As seen in the figure, the values estimated with the new method are closer to the experimental results than those previously estimated.

3. Explanation of mechanism causing non-proportional torque capacity relative to pulley clamping force

3.1 Mechanism causing non-proportional torque capacity

It was shown in section 2 that the torque capacity can be calculated accurately. Therefore, an investigation was made of the mechanism causing the torque transmission capacity to be non-proportional relative to pulley clamping force.

The results in section 2 made it clear that the value of Σr in the torque capacity calculation formula of $\Sigma(\mu \times N \times r)$ in Eq. (1) was smaller than the theoretical calculation.
When Σr becomes smaller, in addition to a decline in torque transmission capacity, the shift toward the inside diameter side becomes larger, thus also increasing the sliding velocity. Because μ has the characteristic that it becomes smaller as the sliding velocity increases, $\Sigma(\mu \times r)$ declines in the region of high pulley clamping force and high torque. This was assumed to be the mechanism causing the torque transmission capacity to become non-proportional.

3.2 Investigation of torque capacity sensitivity to differences in pulley deflection stiffness

It was reasoned that pulley deflection stiffness was the parameter influencing the decline in r and μ. Measurements were made to verify if torque capacity would decline when deflection stiffness was intentionally reduced by shaving

the back side of the pulley, i.e., the portion of the parking lock indicated in the red circle in Fig. 13.

The results presented in Fig. 14 show a tendency for torque capacity to decline further for a pulley with lower deflection stiffness. This indicated that pulley stiffness had to be improved in order to reduce the decline in torque capacity under a high clamping force condition.

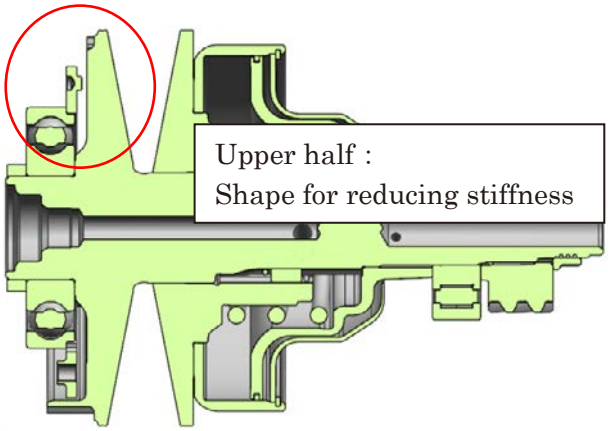

Fig. 13 Overview of pulley stiffness change

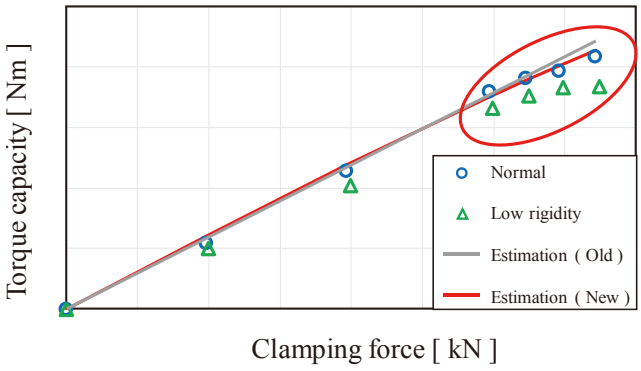

Fig. 14 Torque capacity result between low rigidity pulley and normal pulley

4. Conclusion

- The running radius, clamping force and coefficient of friction of individual chain pins were confirmed on the basis of measured and calculated values. The results were used to calculate the torque capacity, enabling reproduction of the phenomenon where the torque transmission capacity was not proportional to pulley clamping force. The mechanism causing this phenomenon was thus clarified.
- It was found that pulley deflection stiffness must be improved to mitigate reduction of the torque capacity under a high clamping force condition.

5. References

(1) Lubrication Handbook, Yokendo Co., Ltd., p. 265 (1974) (in Japanese).
(2) Nilabh Srivastava, Imtiaz Haque: A review on belt and chain continuously variable transmissions (CVT): Dynamics and control, Mechanism and Machine Theory 44 (2009)
(3) Introduction to Tribology, Yokendo Co., Ltd. (1999) (in Japanese).

■ Authors ■


Kyohei WATANABE


Jumpei HAYAKAWA


Atsushi IKEDA


Kouhei TOYOHARA


Kazuhiro HAYAKAWA

Memo

Development of a method for suppressing CVT chain noise

Minyong LEE* Kazuhiro HAYAKAWA** Jongyun CHOI*
Fumikazu NAGAOKA** Satoru UEDA*** Masanori SANO***

Summary

A chain has been increasingly adopted for CVTs in recent years, making the reduction of chain noise a critical issue. A method has been newly developed for suppressing chain noise without changing the CVT hardware. This was accomplished by clarifying that the balance between chain stiffness and pulley clamping force correlates with chain noise.

1. Introduction

The variator that provides the shifting capability of a continuously variable transmission (CVT) consists of a pulley assembly and a belt. There are two kinds of belts; one is more aptly called a pull chain (i.e., chain) and the other is a push belt (i.e., belt). A chain is mainly used on vehicles requiring high-torque capacity (Fig. 1). One advantage of a chain over a belt is lower friction, but chain noise is an issue, which has been addressed by reducing the pitch width or applying noise insulation materials, among other measures.

In recent years, it has become necessary to downsize transmissions even for high-torque vehicles in order to meet the requirements of the automotive industry. Consequently, that has made it necessary to apply large clamping force to pulleys that are now smaller than before. The application of larger clamping force than in the past has caused an issue of chain noise due to microslipping, which is different from previous chain noise. This article describes a newly developed method that can suppress chain noise without changing the CVT hardware.

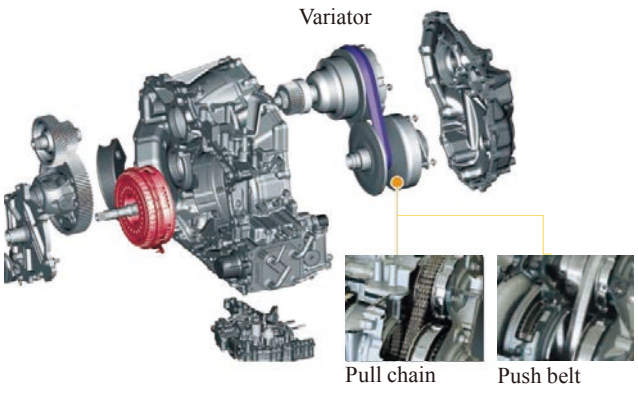

Fig. 1 Structural parts of CVT

2. Chain structure and noise

2.1 Chain structure

Figure 2 shows the structural parts of a chain and the motion that occurs when it curves around a pulley. A chain consists of two types of parts: pins and linkage plates. Two pins combined back-to-back constitute a pair that connects multiple linkage plates to form the chain structure. The adopted structure allows rolling contact between the pins

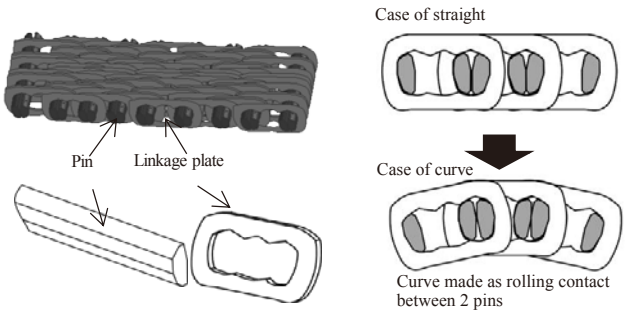

Fig. 2 Structural parts of chain

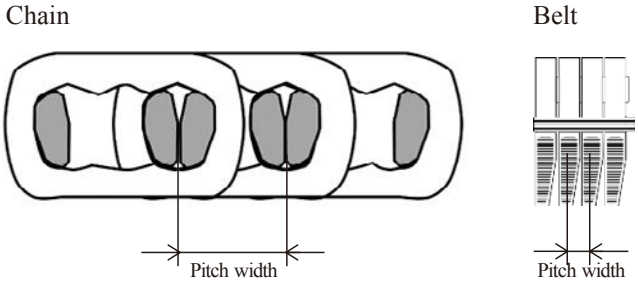

Fig. 3 Comparison of pitch width

* Hardware System Development Office, JATCO Korea Engineering Corporation
** Hardware System Development Department
*** Unit System Development Department

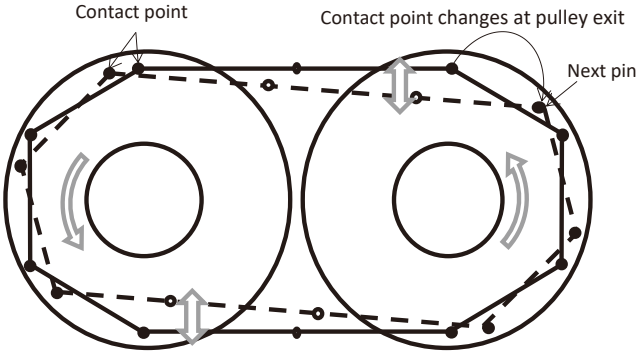

Fig. 4 String vibration due to polygonal motion

when the chain curves, which has the advantage of low friction because frictional losses can be reduced.

Figure 3 compares the pitch width of a chain and a belt. A chain features larger pitch width than a belt. With large pitch width, the chain pins undergo polygonal winding motion as they wrap around the pulley. After a pin in a polygonal winding state exits the pulley, the next pin just behind it supports the chain tension. The repetition of this motion produces string vibration in the chain's straight section, thereby inducing noise (Fig. 4). For that reason, it is known that a chain has a disadvantage regarding noise compared with a belt.

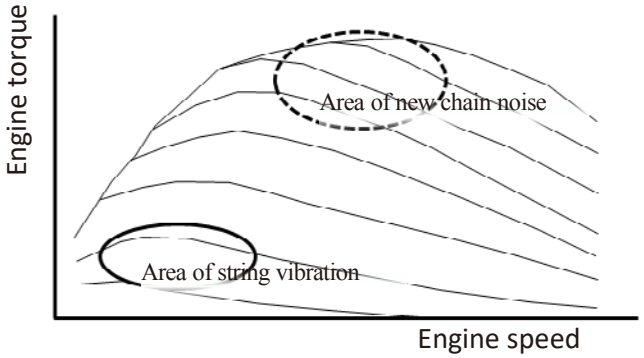

Fig. 5 Areas of chain noise occurring on an engine map

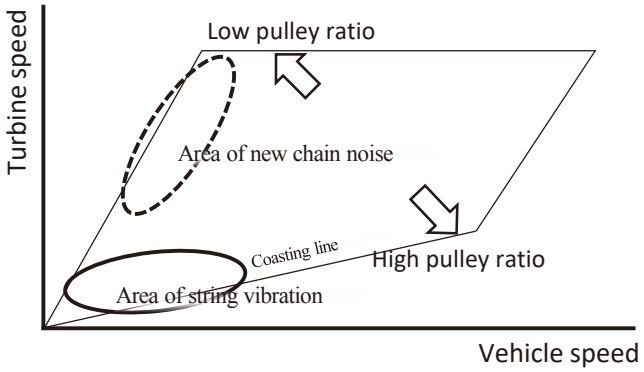

Fig. 6 Areas of chain noise occurring on a shift schedule

2.2 Chain noise

The engine performance map in Fig. 5 shows the areas in which chain noise occurs. The area within the solid line is the region where chain noise has traditionally occurred due to string vibration originating from the pitch width. This chain noise occurs while a vehicle is coasting or gradually accelerating (area within the solid line in Figs. 5 and 6). The reason for that is because string vibration is apt to occur when chain tension decreases in the case of a low torque input.

The new chain noise observed in this development project occurred in a rapid acceleration situation where a low pulley ratio is used (area within the dashed line in Figs. 5 and 6). Because high torque is input to the variator during rapid acceleration, the clamping force is raised to avoid chain slippage. However, applying high clamping force causes microslipping owing to elastic deformation of the chain pins in the pulley radial direction. Because of the chain structure, such microslipping is a phenomenon that has also occurred with previous CVTs. However, it became apparent as a new chain noise in this project because microslipping increased accompanying the reduction of the chain's running radius due to the downsizing of the pulleys. Figure 7 illustrates the force applied to a pin when clamping force is input to the chain and the resultant elastic deformation of the pin. The contact surface of the pulley with the chain pin is called the sheave face. Because the sheave face and the pin come in contact at an angle of 0 deg., the application of clamping force gives rise to f_a and f_b as reaction forces of the clamping force and chain tension. The effect of these forces deforms the pin in the radial direction of the pulley, producing microslipping V between the sheave face and the pin. The contact point between the pulley and the pin at that moment also moves in the radial direction of the pulley, causing axial

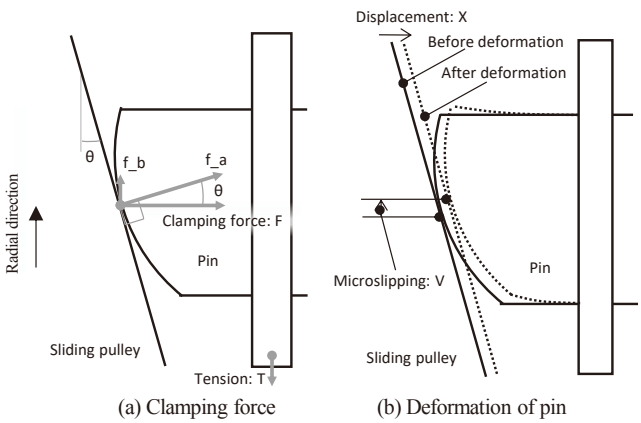

(a) Clamping force (b) Deformation of pin

Fig. 7 Pin deformation under clamping force

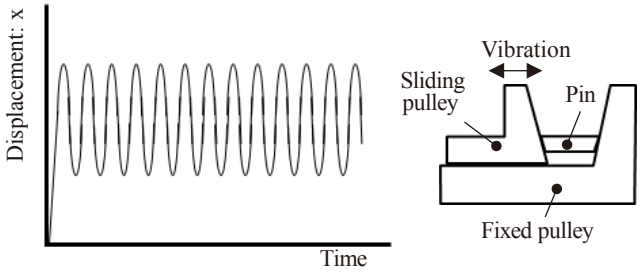

Fig. 8 Vibration of sliding pulley

displacement X of the sliding pulley. Because contact between the chain pins and the sheave face is continuously repeated as the pulley rotates, the axial displacement X of the sliding pulley also repeatedly fluctuates, causing it to vibrate.

The minimum running radius of the chain was reduced in this project accompanying the downsizing of the pulleys. A smaller minimum running radius also reduced the number of pins in contact with the pulley sheave face. For that reason, the clamping force applied to individual pins increased compared with that of previous chains. As a result, it was assumed that axial vibration of the sliding pulley would become larger as illustrated in Fig. 8, thereby leading to the occurrence of chain noise.

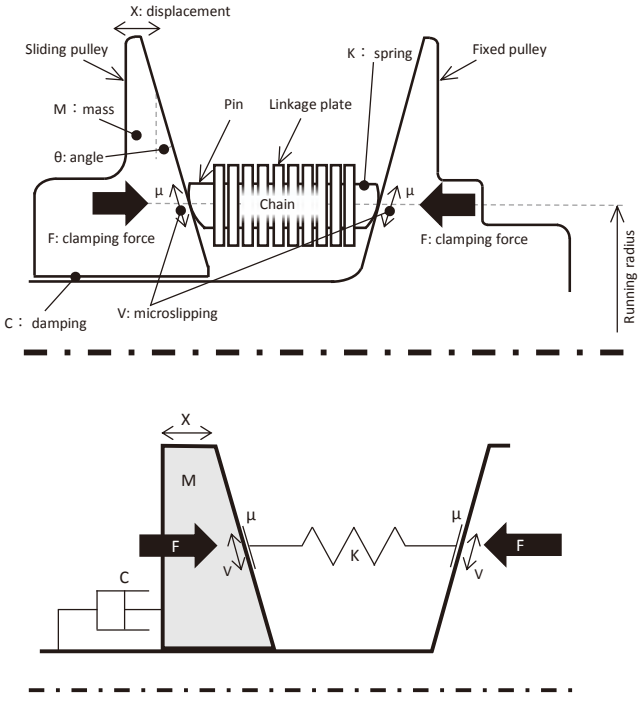

Fig. 9 Modeling of CVT variator

3. Selection of parameters related to chain noise

As described in foregoing subsection 2.2, the new chain noise that became apparent in this project originated from microslipping and was induced by larger vibration of the sliding pulley. In view of this mechanism, it was reasoned that this chain noise could be suppressed by reducing microslipping. The variator was then modeled in order to identify the parameters related to microslipping.

3.1 Modeling of variator

As diagrammed in Fig. 9, the variator was modeled as a damped vibration system for the purpose of identifying the parameters involved in microslipping. The sliding pulley that vibrates was defined as the mass M, the spring constant of the total stiffness of the pins wrapped around the pulley as K, the sliding resistance accompanying movement of the sliding pulley as the damper C, the coefficient of friction between the sliding pulley and pins as μ, the clamping force as F, and the displacement of the sliding pulley due to microslipping at that moment as X.

3.2 Selection of parameters

It was assumed that the new chain noise due to microslipping occurred in the operating region indicated in Fig. 6. Accordingly, it was necessary to suppress microslipping by envisioning various driving situations that occur in this region. In the variator model shown in Fig. 9, the total pin stiffness K that varies according to the running radius and the clamping force F at that moment were selected as parameters that can be controlled during vehicle operation.

• Clamping force F: The clamping force between the pins and the pulley control the torque capacity when the variator transmits torque. Lowering the clamping force

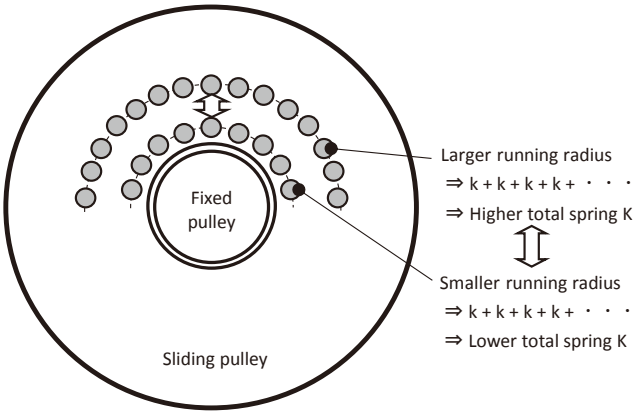

Fig. 10 Total spring K according to running radius

results in insufficient torque transmission capacity. Raising the clamping force excessively, on the other hand, also increases the vibration X of the sliding pulley due to greater microslipping, as explained in subsection 2.2 (Fig. 8). Therefore, it is necessary to set the clamping force suitably so as to both ensure torque transmission capacity and suppress microslipping.

• Total pin stiffness K: In situations where the pulley ratio changes owing to the driving conditions, if the running radius of the chain becomes larger, as shown in Fig. 10, the number of pins wrapped around the pulley also increases. Letting k represent the stiffness of one pin, a parallel spring can be substituted for the pins wrapped around the pulley. The total stiffness K of the pins comprising the parallel spring increases as the running radius becomes larger. The higher the total pin stiffness K is, the more the displacement X of the sliding pulley is suppressed.

4. Confirmation of sensitivity to selected parameters

4.1 Sensitivity of vibration level to clamping force F

An experiment was conducted to ascertain the sensitivity of the vibration level to the clamping force under certain given driving conditions. The vibration level was measured by attaching an acceleration sensor to the side cover of the CVT unit. The experimental results confirmed that a positive first-order correlation existed between the clamping force F and the vibration level (Fig. 11).

4.2 Sensitivity of vibration level to total pin stiffness K

An experiment was conducted to ascertain the sensitivity of the vibration level to the running radius under certain given driving conditions. A larger running radius increased the number of pins wrapped around the pulley, as described in subsection 3.2, which also increased the total pin stiffness K. The experimental results confirmed that a negative first-order correlation existed between the total pin stiffness K and the vibration level (Fig. 12).

5. Proposal and validation of a judgement formula

The sensitivity of chain noise to the clamping force F and the total pin stiffness K was respectively confirmed as explained above. However, these two parameters are interlinked and controlled under actual vehicle operating conditions. Therefore, a judgment formula is proposed here in which the Stribeck equation expressing the relationship between the coefficient of friction and the clamping force is

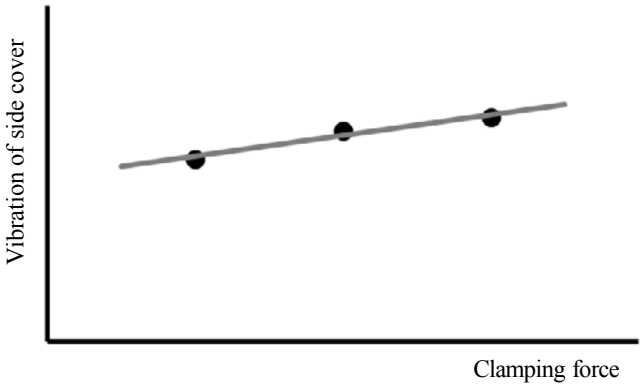

Fig. 11 Clamping force vs. vibration of side cover

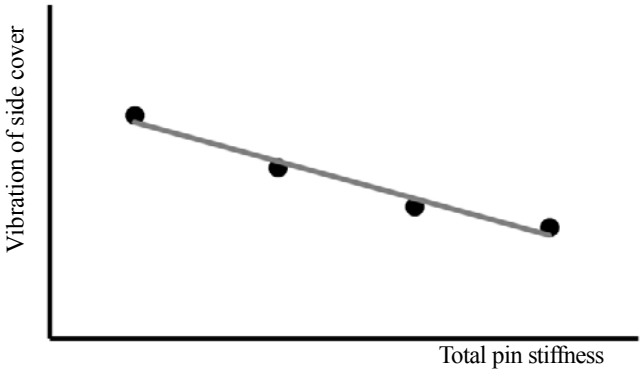

Fig. 12 Total pin stiffness vs vibration of side cover

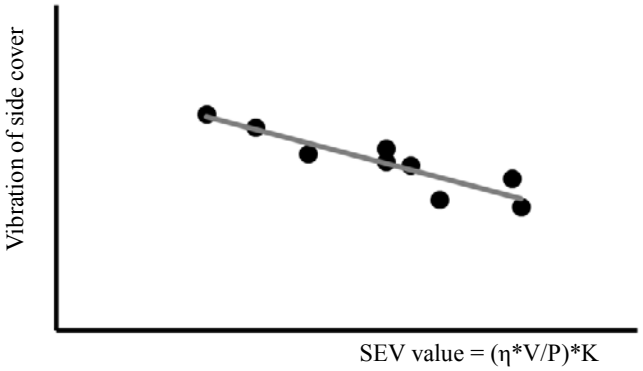

Fig. 13 Validation results for SEV value

multiplied by the total pin stiffness so as to enable judgment on the basis of a single function. The value thus obtained is referred to as self-excited vibration (SEV).

$$\text{SEV value} = (\eta^{*}V/F)\ ^{*}K$$

where η is the viscosity of the CVT fluid between the pins and the pulley sheave. Figure 13 shows the sensitivity of the side cover vibration to the proposed SEV value when the latter was varied. The experimental results confirmed that increasing the SEV value lowered the vibration level of the side cover. This result indicated that using the SEV

value makes it possible to suppress the vibration level in various driving situations envisioned in the area shown in Fig. 6.

6. Conclusion

The minimum running radius of the chain was made smaller than before as a result of downsizing the pulleys in this project. That gave rise to a new chain noise issue caused by microslipping, which differed from previous chain noise. The method developed for suppressing this chain noise without changing the CVT hardware is summarized below.

(1) Downsizing the pulleys increased the clamping force applied to individual pins. It was estimated that this would result in larger axial vibration of the sliding pulley, which would lead to the occurrence of the new chain noise.

(2) It was confirmed experimentally that the vibration level of the side cover had a positive first-order correlation with the clamping force F and a negative first-order correlation with the total pin stiffness K.

(3) Based on the results in (2), the SEV value was proposed as the single criterion of a judgment formula. It was confirmed that the SEV value had a high correlation with the vibration level of the side cover.

The results of this project have been applied to actual vehicles. Using the SEV value as a judgment criterion to suitably control the clamping force and the total pin stiffness has made it possible to suppress chain noise caused by microslipping.

7. References

(1) "Introduction to Tribology," Saiwai Shobo Publishing Co., Ltd., Tokyo, 2014 (in Japanese).

(2) "Tribology," Rikogakusha Publishing Co., Ltd., Tokyo, 2003 (in Japanese).

(3) "Introduction to the Continuously Variable Transmission—CVT," Grand Prix Book Publishing Co., Ltd., Tokyo, 2004 (in Japanese).

Authors


Minyong LEE


Kazuhiro HAYAKAWA


Jongyun CHOI


Fumikazu NAGAOKA


Satoru UEDA


Masanori SANO

Memo

Clarification of parameters and development of a method for estimating loading forces acting on the spool valve of a hydraulically controlled automotive transmission

Daisuke YANAGAWA* Masahiro KOUYA* Sho TOZUKA*
Masaru SHIMADA** Idris TENGKU*** Naoki UEZONO****

Summary

The control valve used in hydraulically controlled automotive transmissions contains a spool valve that drains the excess portion of the fluid flow rate while regulating the pressure. The complex flow around the spool valve exerts various loading forces on the valve. These forces can delay valve response owing to increased sliding resistance and also press the valve against the control valve body, giving rise to concern about valve body wear. Although the forces acting on the valve can be calculated by fluid simulations, it has not been known whether the simulation results are correct. Therefore, in this study a load cell was used to measure the loading forces directly. The results confirmed that the tendencies of the calculated results obtained by fluid simulations agreed well with those of the experimental data, thereby verifying the validity of the simulation results.

1. Introduction

An automotive transmission uses a control valve to supply fluid to multiple hydraulic circuits and to regulate the pressure. Located inside the control valve is a spool valve that drains the excess portion of the fluid flow rate while adjusting the pressure. Loading forces induced by the fluid flow act on the spool valve during the draining process and exert various effects on the valve.

However, heretofore it has been difficult to measure the loading forces acting on the spool valve, although they have been calculated by fluid simulations. Consequently, it has not been known whether the simulation results have been correct. For that reason, judgments about the feasibility of changing transmission specifications have to be based on experimental evaluations of response, wear and other performance parameters. Because specification changes require judgments based on experimentation, a lot of trial and error is involved, which can affect the product development period.

In this work, an experimental setup was built that can directly measure the loading forces acting on the spool valve. This paper presents the results measured with this setup, which confirm the validity of fluid simulations.

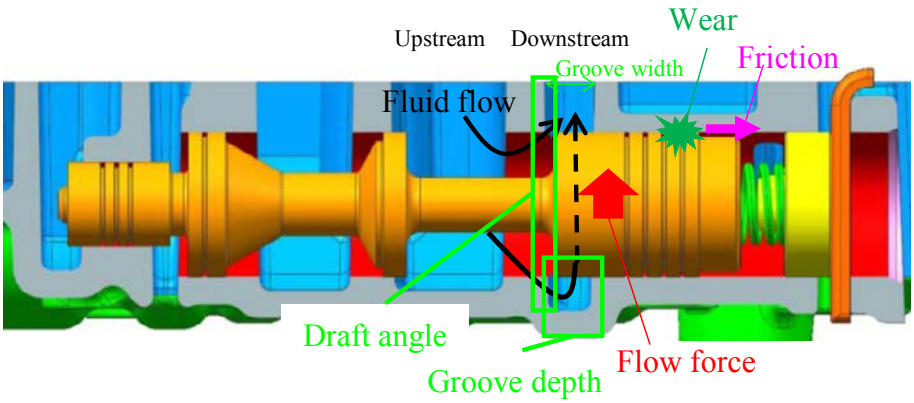

Fig. 1 Loading forces acting on the spool valve and their effects

* Hardware System Development Department
** Hardware System Development Department, JATCO Engineering Ltd
*** Production Administration Department
**** Experiment Department, JATCO Engineering Ltd

2. Spool valve structure and confirmation of dimensional effects

Figure 1 shows the structure of the spool valve for which experimental measurements were made in this study. As fluid flows from upstream to downstream, the loading forces produced by the fluid act on the valve to increase friction. That can cause a delay in responsiveness, which is a key characteristic for transmission control. In addition, the loading forces press the spool valve against the control valve body in which it is housed, giving rise to concern about valve body wear.

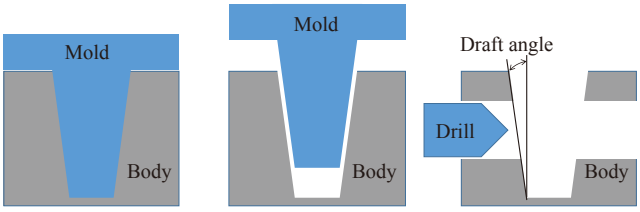

Fig. 2 Definition of draft angle

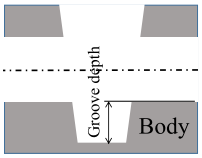

Fig. 3 Definition of groove depth

The experiments measured the effects of two dimensions, the draft angle and the groove depth. It was inferred from fluid simulation results that these two dimensions affect the loading forces.

The draft angle refers to the angle of inclination of the valve body wall and is defined as shown in Fig. 2. This inclination is provided to enable easy removal of the mold in the casting process, and the angle is retained by the valve body. The groove depth is defined as shown in Fig. 3.

3. Experimental setup

It would be difficult to directly measure the loading force that the spool valve inside the control valve applies to the latter valve body. However, the experimental setup was designed so that the force applied by the spool valve can be measured by a load cell via a rod used as a probe. The position of the rod was determined from simulation results and by confirming the point from wear marks where the spool valve pressed against an actual valve body. A hole was then drilled at that position for installing the rod.

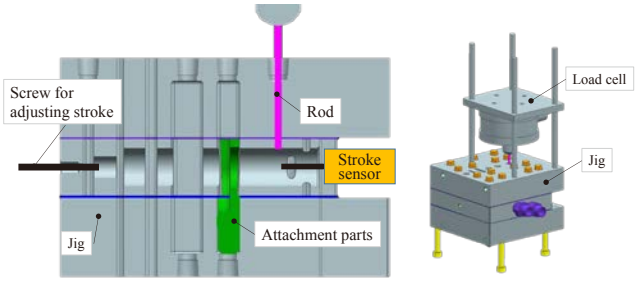

Fig. 4 Structure of jig, attachment parts and rod

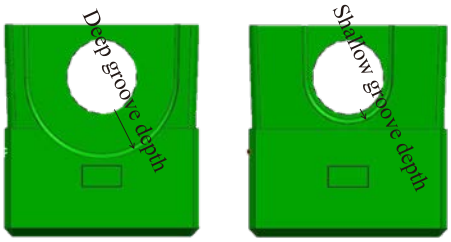

Fig. 5 Attachment parts

The rod passed through a jig to come in contact with the load cell installed above. This structure made it possible to measure the loading forces acting on the spool valve using the load cell via the rod.

The structure of the experimental setup is shown in Fig. 4. The shape of the area around the spool valve in an actual control valve was cut out in the jig, and the attachment parts shown in Fig. 5 enabled the dimensions around the spool valve to be varied. This setup made it possible to determine how the loading forces were affected by the dimensions around the spool valve.

In addition, a screw was provided in the jig at the end of the spool valve for adjusting the amount of stroke from outside the jig so that the pressure would apply force to the rod at the proper stroke position during the experiment.

Figure 6 shows the measured output of the load cell, representing the loading force applied to it when the upstream pressure was varied using the experimental setup described here. The specifications used in the experiment were a draft angle of 2.0 deg. and a groove depth of 11.5 mm. The vertical axes show the pressure and the loading force applied to the load cell in relation to time on the horizontal axis. The red line is the upstream pressure and the black line is the loading force.

The measured results show that the loading force rose along with the increase in the upstream pressure, indicating that the loading force followed the change in pressure. Presumably, this means that the flow rate increased owing to the differential pressure between upstream and downstream, thereby increasing the loading force

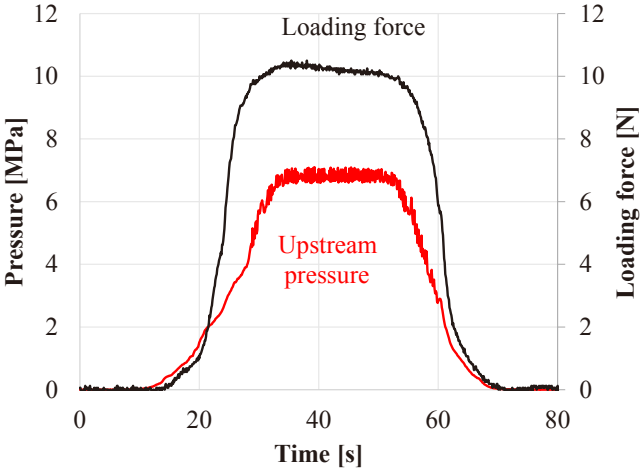

Fig. 6 Output of load cell related pressure

produced by the fluid flow. These results confirmed that the experimental setup was capable of measuring the loading force.

4. Simulation model

A 3D model was created of the jig, attachment parts and spool valve described above and used to conduct a fluid simulation of the loading force that was produced by the hydrodynamic force and acted on the position of the rod.

An example of the simulation model is shown in Fig. 7. The loading force simulated in this study acts in the annular clearance between the spool valve and the control valve body as illustrated in Fig. 8. Accordingly, computational accuracy was improved by modeling the annular clearance with a finer mesh.

The simulation conditions were aligned with those of the experiment. In both cases, the upstream pressure was 5.7 MPa, the downstream pressure was 0.7 MPa, the fluid temperature was 50 ˚C, and the specification of the spool valve diameter was 17 mm.

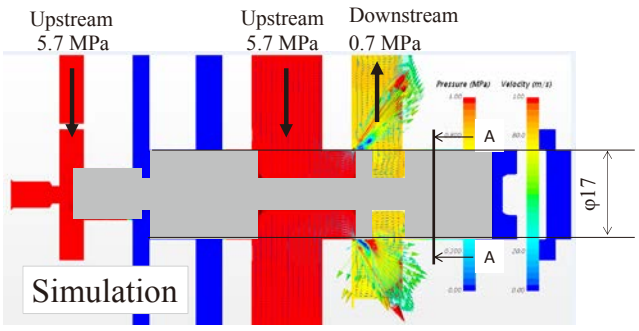

Fig. 7 Simulation model

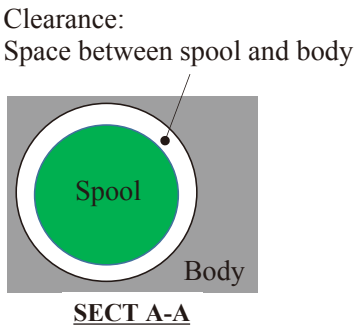

Fig. 8 Definition of clearance

5. Comparison of experimental and simulation results

The results obtained for the effect of the draft angle are shown in Fig. 9. The graph plots the loading force on the vertical axis as a function of the draft angle on the horizontal axis. The blue line is the experimental result and the red line is the simulation result. A loading force of 6.3 N was measured under a condition of a draft angle of 0 deg. It is seen that the loading force increased with a larger draft angle, and a value of 19.3 N was measured at an angle of 2.0 deg. The results of the fluid simulation conducted under the same conditions show a loading force of 14.8 N under a condition of a draft angle of 0 deg. and a value of 24.6 N at an angle of 2.0 deg.

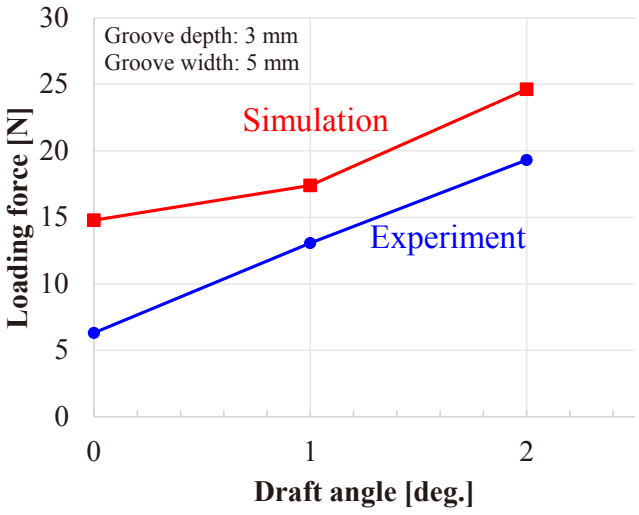

Fig. 9 Loading force as a function of draft angle

Although there is some discrepancy in absolute values between the experimental and simulation results, both sets of data show the same tendencies and effects on the loading force, thus confirming the validity of the simulation.

It is assumed that the reason for the effect of the draft angle on the loading force is that it produces a pressure unbalance between the circuit side and the back side, thereby applying force to the circuit side.

As the draft angle increases, a difference occurs in the size of the valve opening between the circuit side and the back side, with the opening becoming larger on the circuit side (Fig. 10). As a result, because the flow rate on the circuit side increases, the flow velocity becomes faster than on the back side. The pressure on the circuit side thus decreases, resulting in a differential pressure. The pressure around the spool valve on the circuit side declines locally to produce the pressure unbalance shown in Fig. 11.

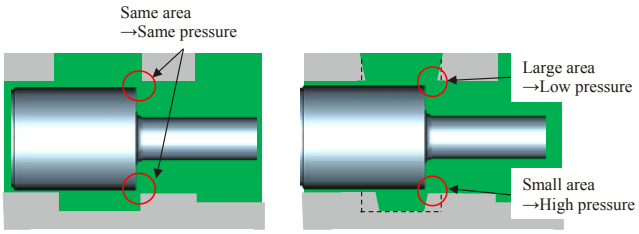

Fig. 10 Effect of draft angle

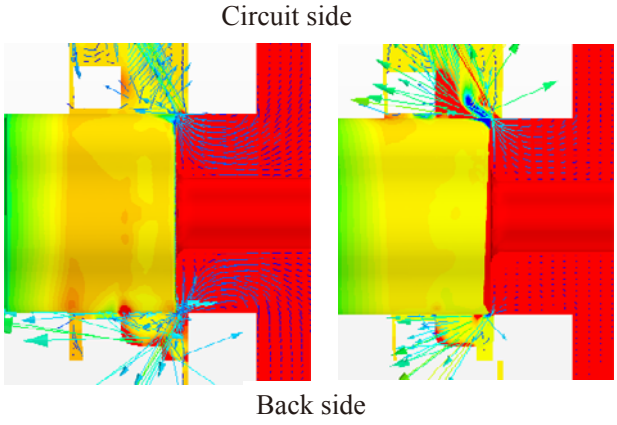

Fig. 11 Simulation results for draft angle

Figure 12 shows the results obtained for the effect of the groove depth. The loading force is plotted on the vertical axis as a function of the groove depth on the horizontal axis. The blue line is the experimental result and the red line is the simulation result. A loading force of 11.2 N was measured at a groove depth of 3.0 mm. The loading force decreased as the groove depth was increased, declining to 3.3 N at a groove depth of 11.5 mm. The simulation results show a loading force of 9.1 N at a groove depth of 3.0 mm and a value of 3.8 N at a groove depth of 11.5 mm.

Although there is some discrepancy between the experimental and simulation results, both sets of data show the same tendencies, as was seen for the draft angle.

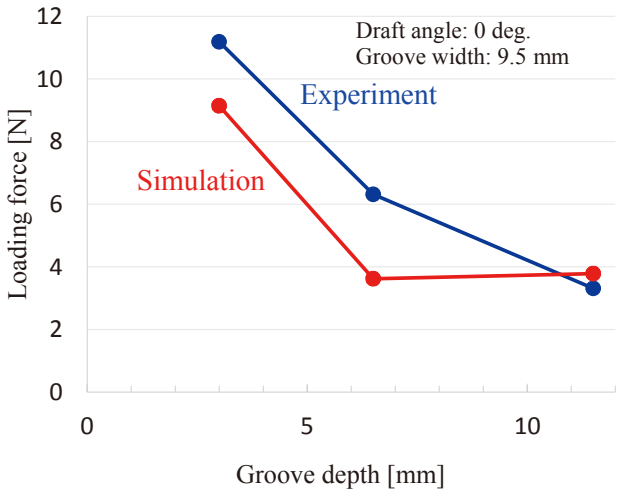

Fig. 12 Loading force as a function of groove depth

The action of the following two factors can be considered to explain the reason for the effect of the groove depth on the loading force.

(1) The pressure rise induced by the collision of the fluid with the spool valve applies force to the circuit side.

(2) The pressure gradient between the back side and the circuit side raises the pressure on the back side, thereby applying pressure to the circuit side.

As shown in Fig. 13, the first factor concerning the collision of the fluid with the spool valve occurs as the fluid in the grooves on the back side flows toward the circuit side (Fig. 14). In the case of a deep groove depth, the flow spreads out before the collision occurs so the effect of the collision is smaller. In contrast, in the case of a shallow groove depth, the effect of the collision is larger so a pressure rise is observed.

As shown in Fig. 15, the second factor concerning the pressure gradient occurs in the direction of the flow of the fluid between the spool valve and the valve body when the fluid in the grooves on the back side flows toward the circuit side. This is more pronounced for a shallow groove depth because the flow passage is narrower. The influence is small in the case of a deep groove depth (Fig. 16). As a result, the pressure on the back side rises compared with that on the circuit side, thus increasing the loading force.

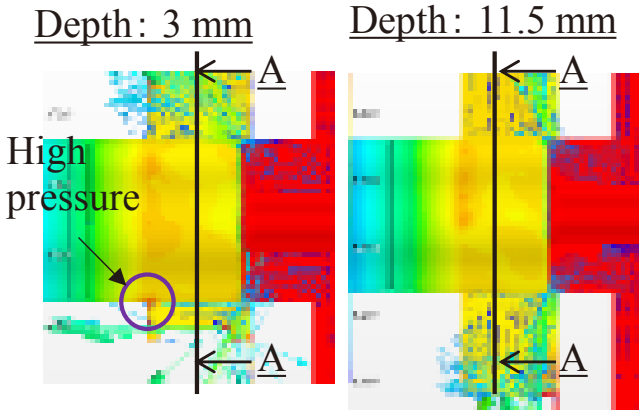

Fig. 13 Simulation results for groove depth

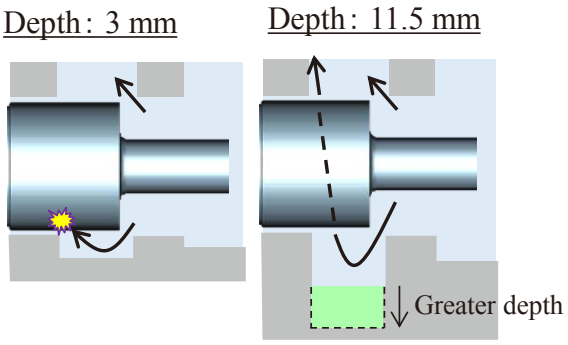

Fig. 14 Effect of groove depth

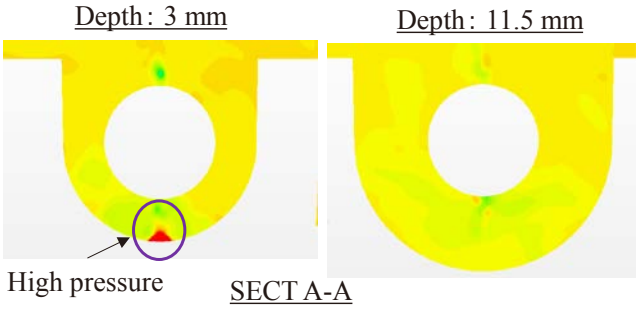

Fig. 15 Simulation results for groove depth in sect A-A

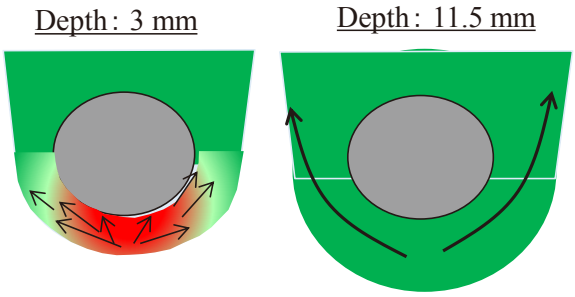

Fig. 16 Effect of pressure drop

6. Conclusion

(1) Using a jig cut out in the shape of the area around the spool valve, a rod as a probe and a load cell, the loading forces acting on the valve were measured directly, which has been difficult to do heretofore.

(2) A comparison of the experimental and simulation results revealed that there was some discrepancy in the absolute values, but both sets of data agreed well regarding the tendencies of the dimensional effects on the loading forces. This confirmed the validity of the simulation results.

(3) This has now made it possible to make design judgments of transmission specifications at the development stage before conducting physical tests.

7. References

This paper was presented at the 11th JFPS International Conference in October 2021.

(1) Kenji Sakakibara, "Development of a hydraulic control system for a new JATCO wide-range CVT," 10th International CTI Symposium USA. Automotive Transmissions, HEV and EV Drives, USA, 2016, B2_ Sakakibara_Jatco_paper, pp. 5-6.

(2) Masaru Shimada, "Application of CFD to develop a control valve spool featuring reduced fluid force," 2017 JSAE Congress (Autumn), No. 20176045

■ Authors ■


Daisuke YANAGAWA


Masahiro KOUYA


Sho TOZUKA


Masaru SHIMADA


Idris TENGKU


Naoki UEZONO

Memo

A study on a bolt fastening structure of a plastic valve body for CVTs

Jongho PARK* Jongyun CHOI* Daewon KIM** Cheolsoon KIM* Kenji KOJIMA***

Summary

It is becoming increasingly important to reduce the weight of automotive parts in order to improve the energy efficiency of vehicles. Lighter weight is also required for the control valve that serves as the mechanism for supplying hydraulic pressure in continuously variable transmissions (CVTs). One weight reduction approach is to apply plastic materials. The control valve body is fastened with bolts, and it is necessary to prevent fluid leakage while suppressing bore deformation. However, because plastic has low stiffness, the design method used for aluminum materials cannot be applied to a plastic control valve body. This article presents a study in which a simple finite element method model was used to confirm the influence of certain variables on bolt tightening force. It was verified experimentally that a plastic control valve body can satisfy the required hydraulic pressure performance while suppressing deformation.

1. Introduction

The automotive industry is facing strict environmental regulations in every country around the world, and vehicle exhaust emission and fuel economy standards are continually being tightened. In order to cope with this situation, technologies for reducing the vehicle weight are becoming increasingly important. Studies are being conducted on ways of reducing the weight of the components of the automatic transmission that is a key vehicle part.

The control valve, one of the internal parts of an automatic transmission, optimally controls the pressure and flow rate of the hydraulic flow produced by the oil pump for supply to the working elements. It has been increasingly desired to reduce the weight of the control valve because it accounts for approximately 10% of the total weight of the internal parts, excluding the housing. Except for the high-pressure hydraulic circuit and the bore hole into which the valve is inserted, research is already underway to change the material of the valve body, which secures electric and other components, from aluminum to plastic.

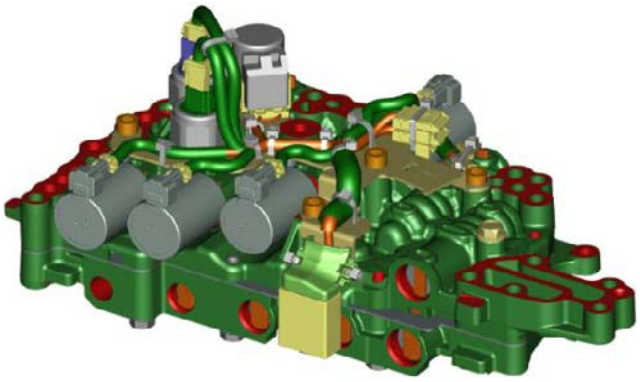

Fig. 1 Structure of control valve

In order to manufacture the bore of plastic, it is necessary to satisfy the performance required of the transmission fluid while suppressing any deformation from external forces such as the bolt tightening force. Because plastic has less stiffness than aluminum, it is difficult to use the same design method as that applied to the aluminum valve body geometry.

In this study, a method was extensively examined for simulating and predicting deformation of a plastic control valve body induced by the bolt fastening structure. A prototype control valve body was manufactured and tested to verify that it satisfied the required hydraulic performance.

2. Structure of control valve body and issues involved in applying plastic

The configuration of the control valve is shown in Fig. 1, and the functions of its component parts are explained below.

1) Valve body: It consists of passages that supply hydraulic pressure and the bore that regulates the pressure together with the spool valve. It serves as the body for assembling the valve parts.
2) Spool valve: It moves reciprocally under the input hydraulic pressure and spring force to regulate the

* Hardware System Development Office, JATCO Korea Engineering Corporation
** System Development Office, JATCO Korea Engineering Corporation
*** Hardware System Development Department

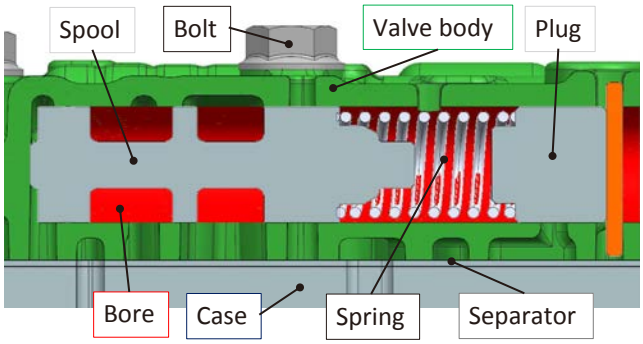

Fig. 2 Structure of spool valve

pressure according to the opening/closing of the passages.

3) Separator plate: It connects the fluid passages between multiple valve bodies and also provides a sealing function between parts to prevent fluid leakage.
4) Electric components (solenoids, sensors, distribution board, etc.): These parts actuate the control valve using electric signals and detect the operating conditions.
5) Bolts and nuts: They fasten together the component parts of the control valve and fasten the control valve to the case.

The parts to be made of plastic in this study included the valve body and spool valve, as shown in Fig. 2. The functions that would be influenced are described below.

1) Hydraulic pressure control and distribution: The reciprocal motion of the spool valve in the axial direction generates and distributes hydraulic pressure passing through the opening and closing of the entry/exit ports of the passages and supplies transmission fluid to parts requiring it.
2) Assurance of flow rate: The sealing force between parts must be maintained to prevent fluid leakage.

2.1 Vulnerability and issues of a plastic control valve

In general, plastic has only 6% of the stiffness of aluminum, so it is susceptible to deformation caused by input loads. Accordingly, the following two concerns must be carefully considered when designing a plastic control valve.

1) Excessive valve body deformation induced by bolt tightening force: The tightening force of the bolts used to fasten the control valve can induce deformation in the valve body when the bolts are tightened. The bore with its hollow structure especially undergoes relatively large deformation. Excessive bore deformation makes it impossible to ensure the necessary minimum space for the sliding of the spool valve. That inhibits movement of the spool valve, which can cause pressure adjustment failure or abnormal pressure distribution.
2) Insufficient sealing performance due to inadequate bolt tightening force: Bolts not only serve to fasten valve parts, they also have the function of ensuring sealability between parts by using the surface pressure produced between them at the time of tightening. Insufficient bolt tightening force can result in large gaps between the valve body and the case and the separator plate. Transmission fluid can leak through such gaps, causing the required flow rate to parts to be insufficient.

Abnormal hydraulic pressure and insufficient flow rate are serious problems that can affect the entire functionality of an automatic transmission, so it is essential to ascertain the relationship between the bolt fastening structure and tightening force.

3. Simulation study of valve body deformation

3.1 Range of influence of axial force

The axial force produced by bolt tightening torque is one cause of valve body deformation. The range of influence of bolt axial force on valve body deformation can be calculated with a method for determining the spring constant between the fastening bolt and the fastened valve body. With Shigley's method, the spring constant of the fastened body can be calculated with Eq. (1) in the manner illustrated in Fig. 3. This calculation is based on the range of influence of axial force on the stiffness of the fastened body at the time of fastening.

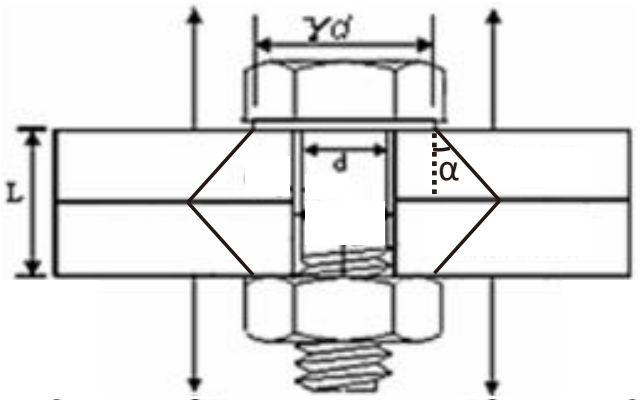

Fig. 3 Shigley's method for tightening structure

$$k_f = \frac{\pi d E \tan(\alpha)}{2\ln\left(\frac{(L\tan(\alpha)+\gamma d-d)(\gamma d+d)}{(L\tan(\alpha)+\gamma d+d)(\gamma d-d)}\right)} \quad (1)$$

where k_f in the equation is the spring constant of the fastened body, γd is the diameter of the bolt seating surface, d is the diameter of the bolt shank, L is the valve body

Table 1 Condition of simulation model

Part	Material	Mesh
Body	Plastic/Aluminum	3D/Tet
Separator	Steel	3D/Tet
Case	Aluminum	3D/Tet
Bolt/Nut	Steel	1D

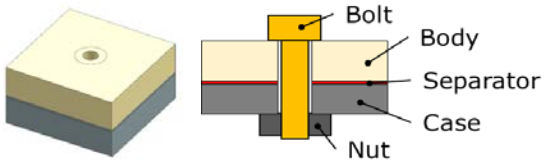

Fig. 4 Simple model for simulating tightening

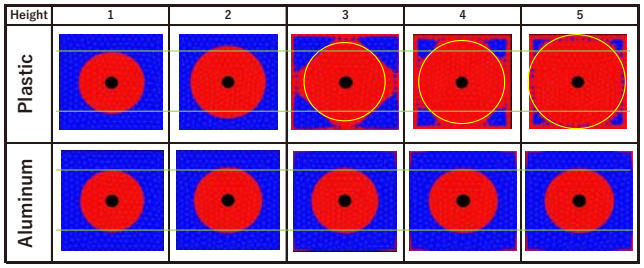

Fig. 5 Comparison of surface pressure of simple models

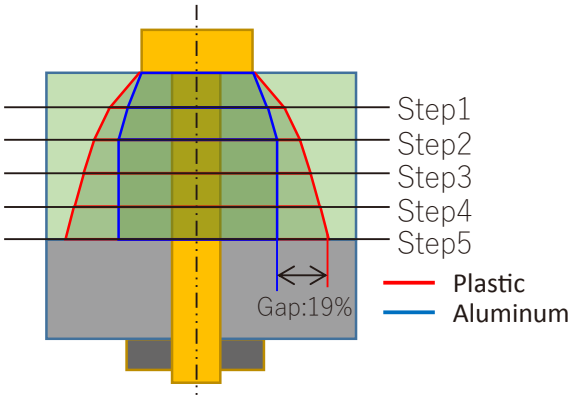

Fig. 6 Surface pressure range for different materials

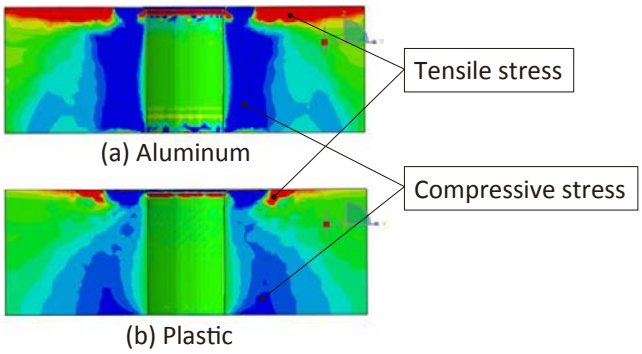

Fig. 7 Comparison of stress distribution

thickness and α is the range of influence on the stiffness of the fastened body at the time of fastening. E is Young's modulus.

In general, it is assumed that 30° represents the value of the spring constant α of the fastened body. However, if the fastened body is thick and has a complicated shape, it is difficult to apply the formula above to the calculation.

3.2 Simulation of range of influence of axial force using a simple model

A parametric simulation was conducted to ascertain the relationship between the bolt fastening structure and valve body deformation. First, a comparison was made of the range of influence of axial force for different valve body materials. That was done using a simple rectangular model consisting of the body, separator plate and the case, as shown in Fig. 4.

In order to investigate the surface pressure distribution corresponding to the body thickness, five levels of thickness were defined for a regular hexahedron model having an ample area. The shapes of the other parts were defined in the same way. A simulation was performed for plastic and aluminum valve bodies having five levels of height. Table 1 lists the materials and meshes of the simulation model.

As shown in Fig. 5, the simulation results confirmed that the area influenced by the bolt tightening force became increasingly larger as the body thickness increased.

Figure 6 presents a cross-sectional view of the simulation results for the surface pressure distribution of the model having varied heights. It is seen that above a certain body thickness the surface pressure region expanded in the shape of a second-order curve, which differed from the linear distribution indicated by Shigley's method. For the thickest model, the surface pressure area of the plastic material was 19% larger than that of the aluminum material.

It will be noted that the stress distribution of both materials also displayed a second-order curve as shown in Fig. 7. Although the stress values generated in the two different materials differed, it was confirmed that the compressive stress distribution of the plastic material increased over a wider area than that of the aluminum material.

Surface pressure is a parameter showing the contact pressure produced by the compressive deformation of two fastened members. The above-mentioned range of influence can be seen as the deformation distribution of

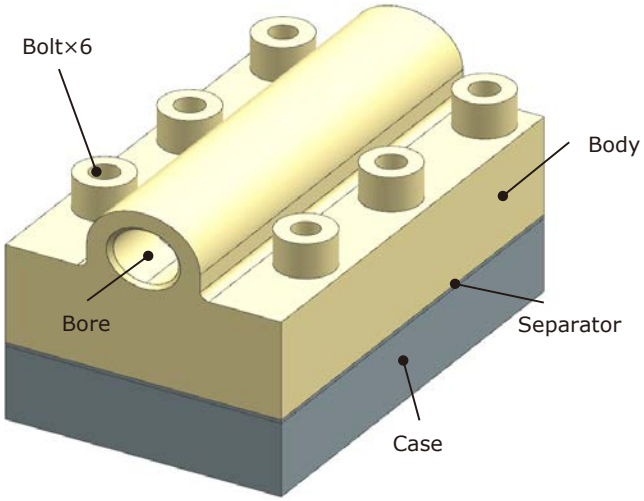

Fig. 8 Simulation model with shape of bore

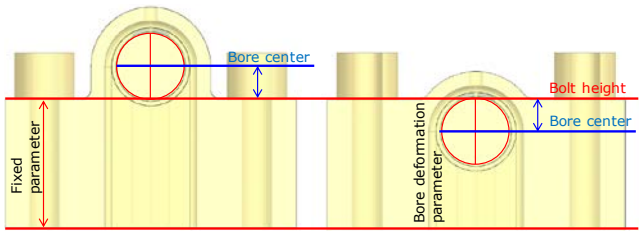

Fig. 9 Bore deformation parameter

the fastened valve body induced by the bolt axial force. By comparing the results for the surface pressure and the stress distribution, it is possible to predict the range of influence of the bolt tightening force on valve body deformation. Deformation of the bore can influence the movement of the spool valve. Defining the position of the bore away from this range of influence is one way of reducing the amount of bore deformation.

3.3 Simulation of range of influence of axial force using a bore model

A parametric simulation was conducted to ascertain the bolt fastening structure for creating the necessary surface pressure between parts while suppressing bore deformation. That was done by using a simple bore model to predict the range of influence of axial force on bore deformation when the bolts were tightened.

1) Simulation model and methodology

As shown in Fig. 8, the simulation model replicated the valve body by taking into account a single hollow bore and the bolt fastening structure. The number of bolts, the body length and the distance between bolts were defined using

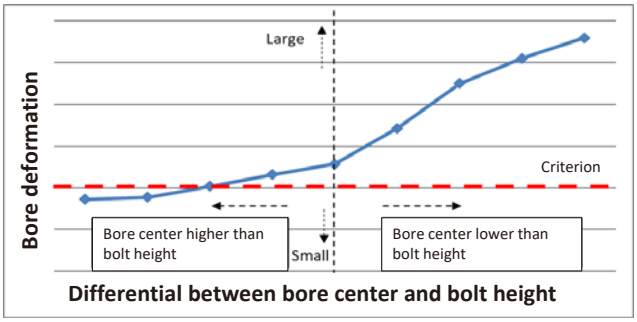

Fig. 10 Simulation results for bore deformation

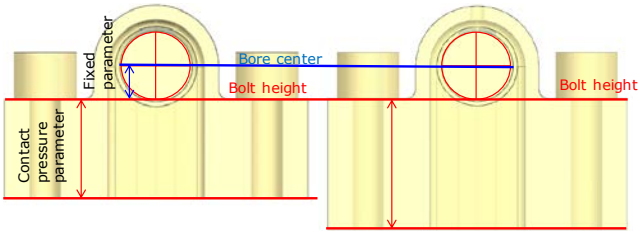

Fig. 11 Contact pressure parameter

simulation results obtained with the simple model and considering the influence of fastening on sealability.

Plastic material was specified only for the valve body containing the bore, and other parts were defined in the same way as in the simple model.

The amount of bore deformation and the contact pressure produced between two fastened members were confirmed while varying two parameters of the simulation model as indicated in Figs. 9 and 11.

Bore deformation parameter: The amount of bore deformation was confirmed by varying the relationship between the bore center position and the bolt height for a fixed body thickness (Fig. 9).

The simulation results for the bore deformation parameter are presented in Fig. 10. It is seen that bore deformation increased sharply when the bolt height was higher than the bore center position and that it was reduced when the bolt height was lower than the bore center.

Contact pressure parameter: The radius of the contact pressure range relative to changes in the valve body thickness was confirmed for a fixed relationship between the bore center position and the bolt boss height (Fig. 11).

The simulation results for the contact pressure parameter are presented in Fig. 12. It is seen that the range

of effective contact pressure increased with a thicker valve body.

The sensitivity graphs in Figs. 10 and 12 confirmed the sensitivity of bore deformation and the radius of the effective contact pressure range. That made it possible to determine a bolt fastening structure for satisfying both of these required characteristics.

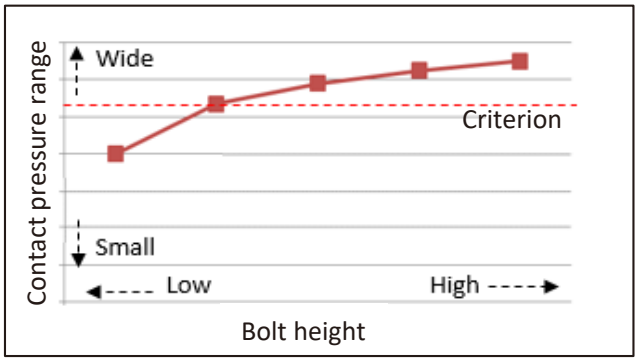

Fig. 12 Simulation results for contact pressure range

4. Experimental validation

The simulation results revealed that bore deformation decreased with a higher bore center position and that the range of effective contact pressure widened with a thicker valve body. However, the weight also increased, so a simulation model for comparison with experimental data was created using specifications from among the results that satisfied both criteria and reduced the weight the most. This model was used to simulate bore deformation for making a comparison with the experimental results.

4.1 Comparison of simulation and experimental results for bore deformation

Using a plastic valve body having the same geometry, bore deformation was measured for various levels of bolt tightening torque. The experimental and simulation results are compared in Fig. 13. Although the simulated bore deformation differed from the experimental results by 61.7% and 63.4% under low and high tightening torque conditions respectively, the results confirmed that both sets of data show the same tendencies.

4.2 Validation of plastic control valve hydraulic pressure performance

An experiment was conducted with the same model to validate the hydraulic pressure performance. As the first step, the indicated current and hydraulic pressure were

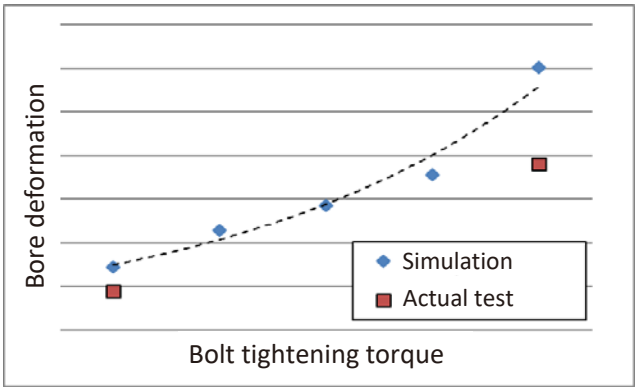

Fig. 13 Comparison between simulation and experiment

measured in relation to time. As confirmed by the results in Fig. 14, the hydraulic pressure reached the necessary level within the target time following the issuance of the current command.

Hydraulic hysteresis was also measured under the application of a pressure change at a certain level. The results in Fig. 15 confirm that the pressure fluctuation was below the target level.

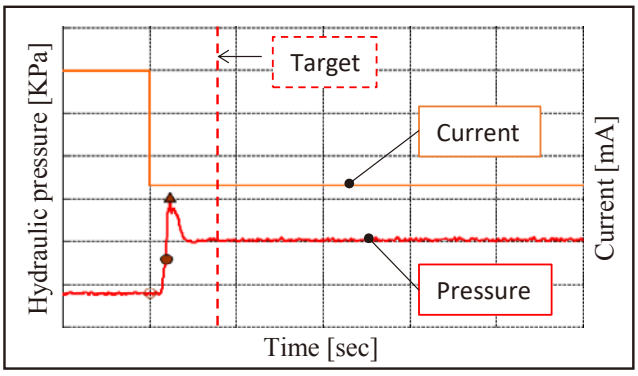

Fig. 14 Hydraulic response

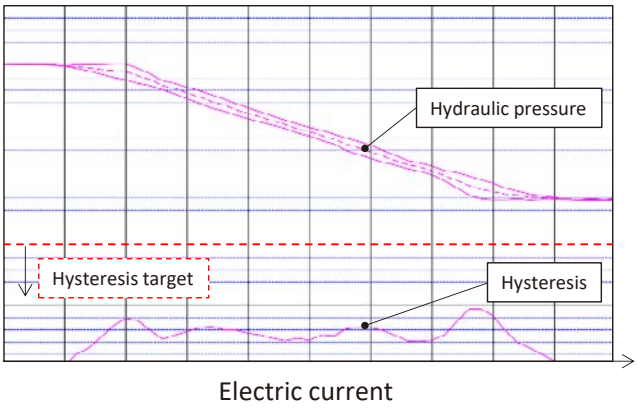

Fig. 15 Hydraulic sweep characteristic

5. Conclusion

This study analyzed the bolt fastening structure in conjunction with the application of plastic to the control valve body. The following conclusions were drawn from the results.

1) It was confirmed that the transmission range of bolt axial force varied with the material of the fastened valve body and that it can be predicted by simulation.
2) It was found that bore deformation of a plastic valve body can be predicted, confirming that even the sliding part of the spool valve can be made of plastic, in addition to component parts that are simply fastened.
3) Based on parametric simulations of a plastic valve body, a bolt fastening structure was proposed that satisfies the criteria for bore deformation suppression and hydraulic pressure performance.

6. References

(1) Takahiro Yamamori, Takashi Shibayama, Izumi Amemiya: Automatic Transmission for Automobiles, September 2005.
(2) Nawras Haidar, Salwan Obeed and Mohamed Jawad: Mathematical representation of bolted-joint stiffness: A new suggested model, Journal of Mechanical Science and Technology 2011.
(3) Jian Wang, Qimin Li, Changwei Yang, Yidan Huang, Caizhi Zhou: A Simple Model for Elastic-Plastic Contact of Granular Geomaterials, Hindawi 2018.
(4) Shigley's Mechanical Engineering Design, McGraw-Hill Series in Mechanical Engineering, 2014.

Source: Japanese translation of a paper originally published in Korean with an English title: Jongho PARK, "A Study on a Bolt Fastening Structure for a Plastic Valve Body of CVTs," Transactions of KSAE, p. 88-93, 2020.

■ Authors ■

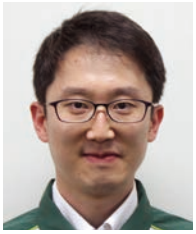
Jongho PARK


Jongyun CHOI


Daewon KIM


Cheolsoon KIM


Kenji KOJIMA

Implementation of an AI-based forging equipment failure diagnosis system

Masakazu MURANO* Toshio HIRAKU* Toru ENDO* Gen TAKAHASHI*

Summary

Forging equipment has advanced in recent years to support fully automated production, making control systems more complicated. This has required more time for identifying the causes of equipment failures when they occur. Therefore, artificial intelligence (AI) was used to develop an equipment failure diagnosis system that converts the tacit knowledge possessed by veteran maintenance personnel into explicit knowledge. This article describes the system that has been implemented to reduce the time needed for diagnosing the causes of failures.

1. Introduction

Progress has been made in recent years in fully automating the transport devices of forging equipment to achieve high-efficiency production. For that reason, control systems have become more complicated than those of previous equipment, making it more difficult to pinpoint the true cause of a failure when one occurs. The failure diagnosis procedures used by maintenance personnel to repair failures and their failure diagnosis time vary depending on the knowledge and skills of each individual.

This article describes an equipment failure diagnosis system that has recently been created in which artificial intelligence (AI) was used to incorporate the tacit knowledge, i.e., skills, know-how and experience, of veteran maintenance personnel. This system has proved to be effective in shortening the mean time to repair (MTTR).

2. Present status

2.1 Present status of forging equipment

Figure 1 shows MTTR data for assembly, casting, machining and forging equipment. It takes more time to repair and restore forging equipment compared with assembly, casting and machining equipment.

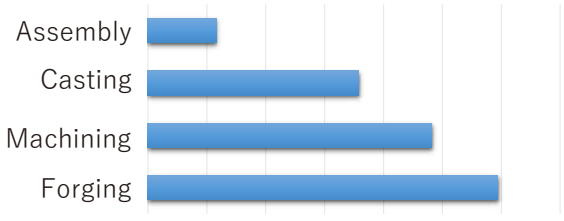

Fig. 1 Analysis of mean time to repair (MTTR)

Figure 2 shows a percentage breakdown by task of the MTTR for forging equipment. The percentages indicate that diagnosis time is the next longest task after recovery time.

Progress was made in automating assembly equipment beginning from the 1990s. The equipment composition was established, and accumulated data and skills have been reliably handed down to support short diagnosis times.

In contrast, automation of forging equipment has advanced rapidly in the past decade or so. Existing large-scale forging machines were automated and connected by transport devices to form the forging line. Along with the increased complexity of the control system, the causes of failure also vary widely. Consequently, one factor causing longer MTTR for forging equipment is that differences in the skill levels of maintenance personnel are clearly reflected in their diagnosis time.

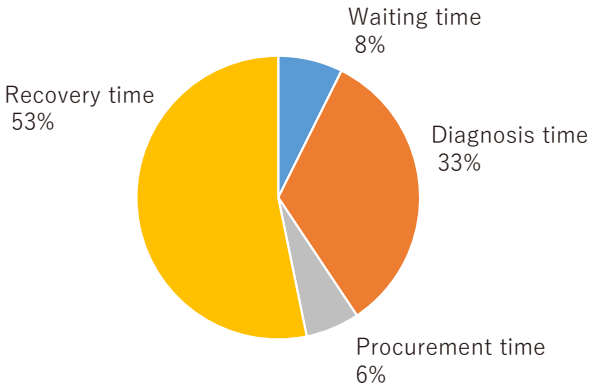

Fig. 2 Percentage breakdown by task of MTTR for forging equipment

* Production Administration Department

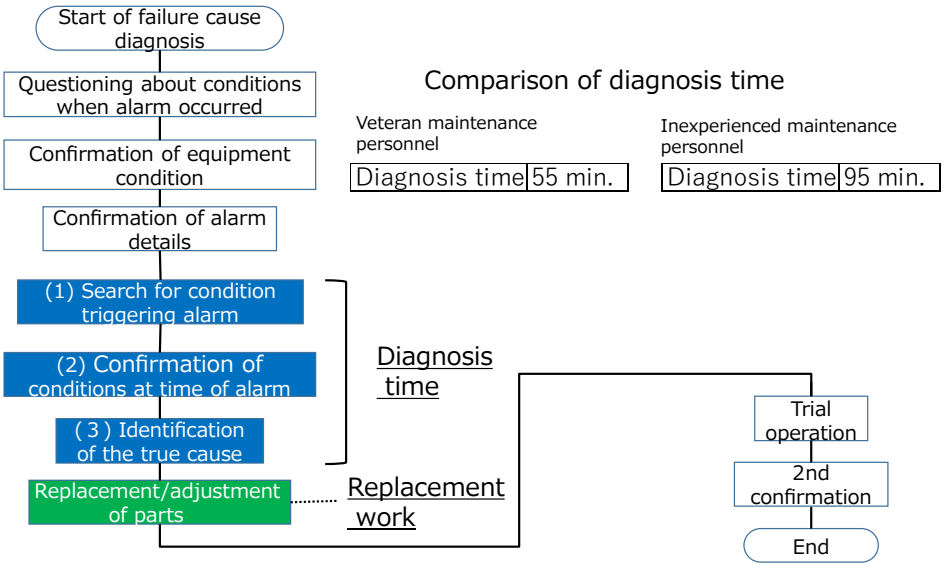

Fig. 3 Flow of failure recovery

2.2 Failure recovery method

Figure 3 outlines the flow of the failure recovery method used by maintenance personnel. The results of an analysis of the failure recovery time of veteran and inexperienced maintenance personnel revealed that their diagnosis time differed by 40 minutes.

A survey was conducted to clarify the reasons for the difference in diagnosis time between veteran and inexperienced maintenance personnel. Veteran maintenance personnel were interviewed concerning their failure diagnosis procedures, and a comparison was made with inexperienced maintenance personnel regarding the following three perspectives to clarify what was different between the two groups.

(1) Search for the condition triggering an alarm

When veteran maintenance personnel arrive at the site of a problem, they check the condition of the equipment and alarm details and consider whether a similar situation occurred in the past. On that basis, they propose candidates as possible causes of the failure. It was found that the number of their candidates differed from that of the inexperienced maintenance personnel.

(2) Confirmation of conditions when an alarm occurs

Veteran maintenance personnel carefully observe and remember the normal operating conditions of equipment on a regular basis. In diagnosing a failure, they operate the equipment and reproduce the conditions at the time an alarm occurred. By comparing the operation and signals with the normal conditions, they narrow down the candidates for the possible cause of the failure. The time taken to narrow down the candidates differed from that of the inexperienced maintenance personnel.

(3) Identifying the cause of a failure

It was found that veteran maintenance personnel perform a mental why-why analysis in the process of using the methods in (1) and (2) above and quickly identify the cause of a failure based on rules and principles. Their accuracy in identifying the causes of failures also differed from that of the inexperienced maintenance personnel.

Therefore, in order to close the gap in diagnosis time due to the skill levels of maintenance personnel, it was decided to build a model line and develop an equipment failure diagnosis system.

3. Development of an equipment failure diagnosis system

3.1 Development aim

The purpose of this equipment failure diagnosis system is to enable anyone to perform a failure diagnosis equal to that of veteran maintenance personnel in a short period of time. Accordingly, anyone who uses this system can efficiently acquire the knowledge and skills possessed by veteran maintenance personnel.

3.2 System configuration

The system uses AI to learn the normal equipment operating conditions so that it can automatically identify the cause of a failure when an alarm occurs.

Figure 4 shows the system configuration, which can be

broadly divided into two sections. One is a data acquisition/ storage device group consisting of a Supervisory Control and Data Acquisition (SCADA) system for collecting operating condition data in real time, mainly by means of sensors attached to the equipment and push buttons, and a file server for storing the data. The other is a PC equipped with an AI program for performing a failure analysis using the data stored in the server. The PC performs the data exchanges, learning and analysis.

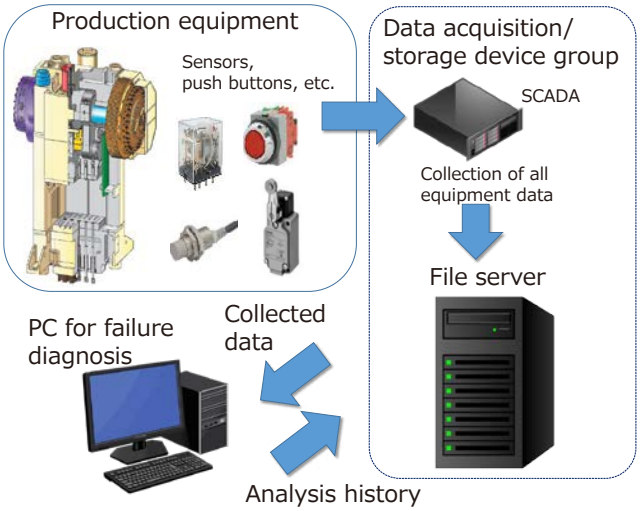

SCADA (Supervisory Control and Data Acquisition)
This computer system provides remote centralized monitoring and control at one location of various production machines at the plant and elsewhere. It collects and centrally records data from sensors and other devices.

Fig. 4 System configuration

3.3 Method of learning normal operating data

In order for the system to learn the normal equipment conditions, the AI-equipped PC for failure analysis reads operating data from the file server when no alarms have been issued.

Calculating and learning large volumes of device data every time would put an enormous load on the CPU of the PC for failure analysis. To avoid that, Welford's method was used to perform mean and variance calculations. This calculation method repeats a procedure whereby the difference from the previous data is calculated and reflected in a cycle diagram as the standard deviation. An example of a learned cycle diagram is shown in Fig. 5. In one cycle of a cycle diagram, the system learns the data from all the acquisition devices that number approximately 8,000 in total, including sensors, push buttons and others. The system learns the time-history data and timing and records the standard deviation and the current data as waveforms.

As one example, the equation for calculating the mean with Welford's method is shown below.

$$\mu_n = \frac{1}{n}\sum_{i=1}^{n} x_i$$

The recurrence relation of the equation above is expressed as:

$$\mu_{n+1} = \frac{1}{n+1}(x_{n+1} - \mu_n) + \mu_n$$

μ_{n+1}: updated mean
μ_n: mean calculated the previous time
x_{n+1}: newly obtained collected data
n: number of collected data

3.4 Database of individual causes of failure

In order to quickly and accurately identity failure causes, it is essential to create in advance a database containing the causes of failures that have occurred previously. A failure history list was made, and a database of individual failure causes was created that summarizes the time when alarms occurred, the device causing each failure and other details.

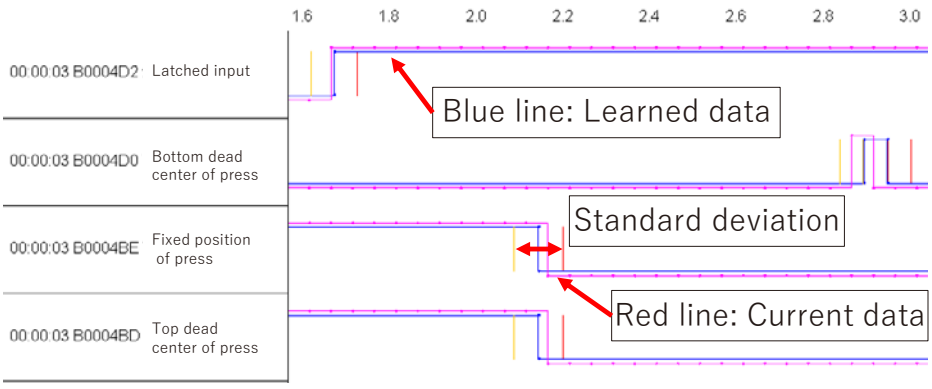

Fig. 5 Learning screen of a cycle diagram

3.5 System for failure diagnosis

The instant an equipment alarm occurs the present cycle diagram is cut into sections and a comparison is made of the sectioned current cycle diagram and the previously learned cycle diagram. Devices showing a mean exceeding $\pm 3\sigma$ among all the device data are narrowed down as failure cause candidates.

The narrowed down candidates are cross-checked with data in the database for individual failure causes, and a matching device is identified as the cause of the failure. If multiple matching devices are found, the time when the alarm occurred is cross-checked with the database and a matching device is identified as the failure cause.

3.6 Effectiveness of AI-based failure diagnosis system

It has become possible to narrow down failure cause candidates by teaching the system the normal operating conditions of the equipment and making a comparison with the cycle diagram when an alarm occurs.[1] In addition, the accuracy of judgments for identifying failure causes has been improved by drawing upon the knowledge of veteran maintenance personnel.

The implemented system can search for the cause of a failure in the shortest diagnosis time possible without being influenced by the skill levels of maintenance personnel. Figure 6 shows the effect of the system on reducing diagnosis time following its implementation.

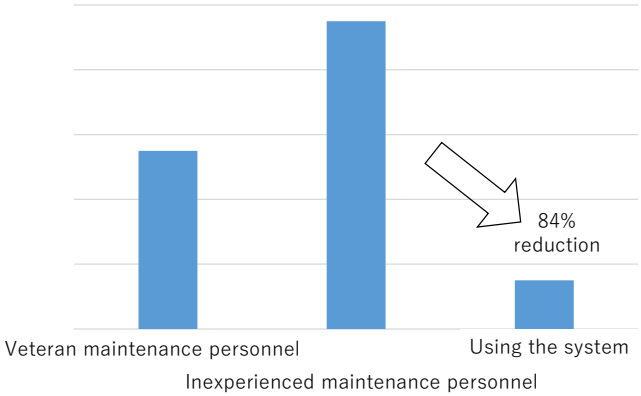

Fig. 6 Effect on improving diagnosis time

The newly developed system uses AI to automate the skills that veteran maintenance personnel possess for narrowing down candidate failure causes. This capability markedly shortens the time needed for identifying the cause of a failure by eliminating the need to operate the equipment and to reproduce the conditions present when an alarm occurs.

As a result, using this AI-based failure diagnosis system has reduced failure diagnosis time by 84%.

4. Future issues

An analysis of the methods used by veteran maintenance personnel to diagnose failures revealed the logic that maintenance personnel have traditionally applied in diagnosing the causes of failures. That made it possible to convert the tacit knowledge of veteran maintenance personnel into explicit knowledge.

It is planned to deploy this system horizontally on other production lines in the future and also to use it to improve maintenance personnel educational methods that have been practiced heretofore.

5. Reference

(1) Yoshi Sano, Optimization of Rolling Conditions by Microsecond Analysis using ICT, Plant Engineer, Japan Institute of Plant Maintenance, Vol. 53, No. 12 (in Japanese).

■ Authors ■


Masakazu MURANO


Toshio HIRAKU


Toru ENDO


Gen TAKAHASHI

Stabilization of gear machining accuracy by controlling gear honing machine vibration

Hideaki MATSUISHI* Toshirou SHIMOSAKA* Yuya NAKATANI*

Summary

Ghost noise originating from gear accuracy is one issue concerning automotive transmission quality. In this study, it was determined that abnormal gear honing machine vibration, which can suddenly occur during machining, is transferred to the gear tooth surface and gives rise to ghost noise. Therefore, a method was established for monitoring and detecting abnormal machine vibration so as to prevent the release of defective gears.

1. Introduction

Ghost noise originating from abnormal tooth surface geometry is an issue related to the noise and vibration produced by the transmission. This study focused on the gear honing method that is the cause of such abnormal tooth surface geometry. As a result of investigating the cause, it was found that abnormal tooth surface geometry originates from unusual gear honing machine vibration. Because such vibration can be detected based on the level of its magnitude, stable manufacturing quality has been ensured by monitoring the vibration level for all gears produced on the honing machine. This paper describes the details of the investigation.

2. Ghost noise

2.1 Explanation of ghost noise

Among the types of noise stemming from the transmission, gear noise originates from gear meshing, striking sounds are caused by gear nicks, and rattles are produced by backlash. Gear noise originating from gear meshing includes an order component (referred to here as the first order of gear meshing) matching the number of meshing gear teeth, order components that are integral multiples of the meshing order, and ghost noise having an order component other than the integral multiples. It is necessary to eliminate this ghost noise because it is heard as an annoying abnormal noise in the cabin.

2.2 Example of ghost noise analysis and its cause

Figure 1 presents an analysis of cabin noise data at the time ghost noise was detected for a transmission. The horizontal axis shows the noise orders per axle rotation, the vertical axis is the driving time with acceleration/deceleration events, and the different colors indicate the cabin noise level. The data show that the 0.8th-order component that deviated from the first-order component of gear meshing was higher compared with other order components.

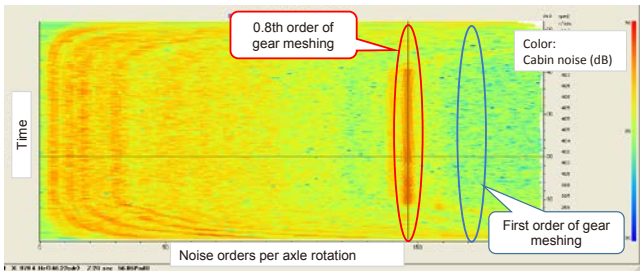

Fig. 1 Cabin noise data at the time of ghost noise detection

Fig. 2 Gear data measured at the time of ghost noise detection: Measurement of tooth trace of all teeth

* Parts Process Engineering Department

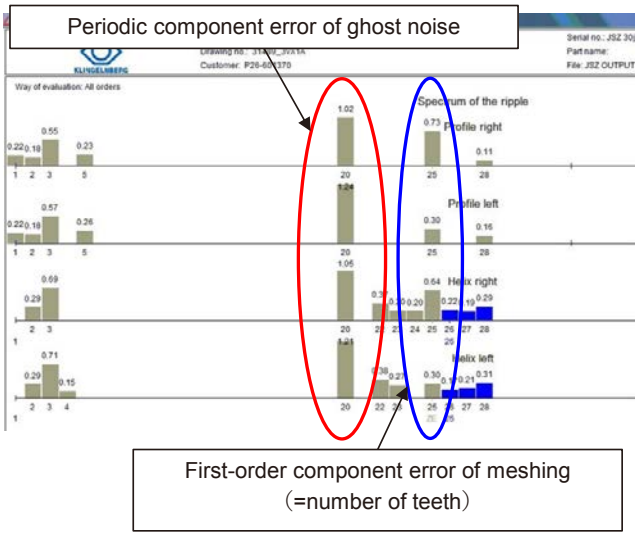

Fig. 3 Gear data measured at the time of ghost noise detection: Measurement of periodic component error

The gear causing this higher order component was then identified by conducting tests in which the parts of the transmission were replaced in turn, and the accuracy of the identified gear was investigated. The measured gear surface data in Fig. 2 show the presence of abnormal undulation geometry. In addition, a spectrum analysis was performed on the measured gear surface data. High values were found for the spectrum corresponding to the 0.8th-order component detected in the cabin noise, and the order coincided with ghost noise. Figure 3 presents the results of a spectrum analysis performed on the measured tooth trace data.

The foregoing results revealed that the true cause of the ghost noise examined in this study was the undulation geometry of the gear tooth surface. This indicated that the cause of ghost noise could be identified by analyzing the tooth surface geometry in detail.

3. Explanation of gear honing

3.1 Gear manufacturing processes

The sequence of processes in gear manufacturing is shown in Fig. 4. Following hobbing and gear shaving, carburizing and quenching are performed. Heat treatment strain occurs during quenching, causing deformation of the tooth profile and tooth trace geometry. Gear honing is then performed to correct that deformation, and the tooth surface geometry is smoothed to suppress the occurrence of gear noise.

3.2 Gear honing process

Gear tooth surfaces are finished to high accuracy in the honing process performed on a gear honing machine. A honing wheel with internal gear geometry is engaged with the workpiece gear to execute tiny cuts and tooth surface smoothing as the rotating wheel is pressed against the workpiece. The configuration of the gear honing machine is shown in Fig. 5.

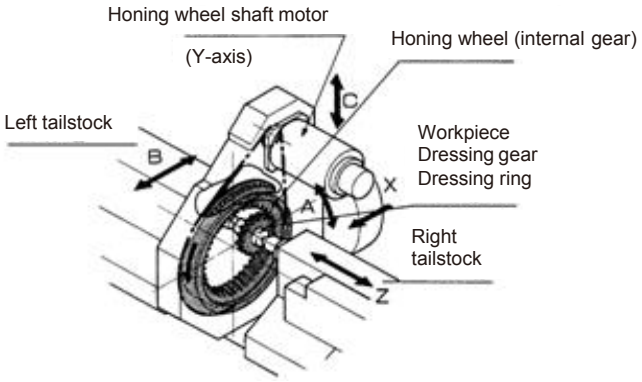

Fig. 5 Configuration of gear honing machine

Tooth surfaces of the internal-gear honing wheel are dressed with an electrodeposited diamond dressing wheel to the accuracy desired of the finished gear. Dressing forms the tooth surfaces of the honing wheel to high accuracy. The honing wheel is then used to finish-machine the gear tooth surfaces. In this process, the accuracy of the honing wheel is transferred to the workpiece to obtain high-accuracy gear tooth surfaces (Fig. 6).

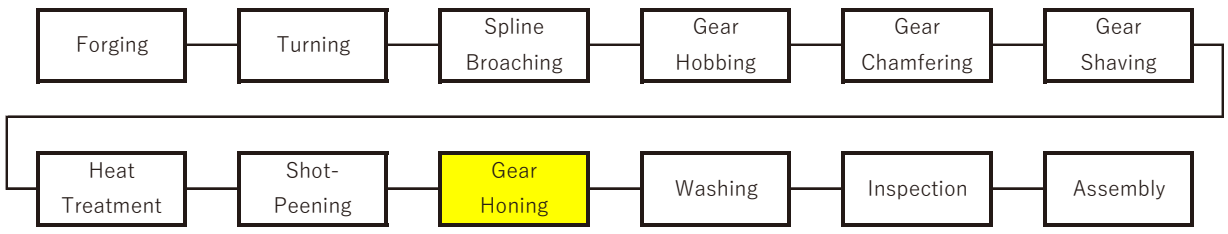

Fig. 4 Outline of gear manufacturing processes

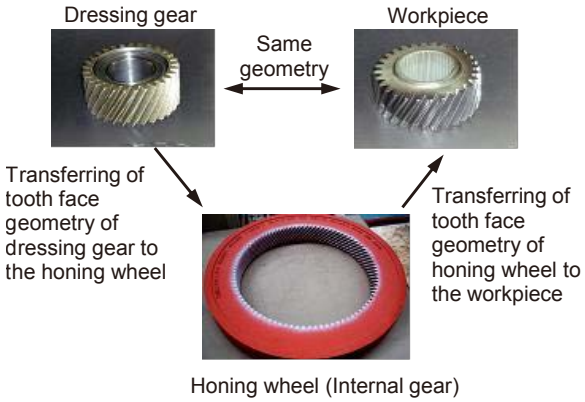

Fig. 6 Honing wheel, dressing gear and workpiece

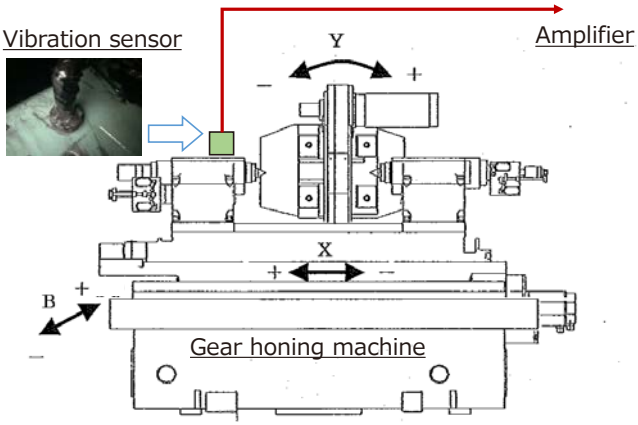

Fig. 7 Vibration measurement on gear honing machine

Because this honing method transfers the honing wheel accuracy to the gear tooth surfaces, the occurrence of rotational speed fluctuation or center distance fluctuation can change the contact condition between the honing wheel and the tooth surfaces, thereby affecting accuracy. Consequently, if vibration that causes center distance fluctuation occurs during machining, undulation geometry is apt to occur on the machined tooth surfaces. Because gear honing is the process that determines the final tooth surface geometry, the tooth trace undulation geometry found on the gears examined in this study was assumed to have occurred in the honing process.

4. Measurement of gear honing machine vibration

4.1 Vibration measurement positions on gear honing machine

A method of monitoring the state of the gear honing machine during the honing operation was examined in order to investigate whether the tooth surface undulation geometry that was the focus of interest in this study actually occurred in the gear honing process. It was decided to measure the vibration of the tailstocks supporting the meshing reaction forces between the honing wheel and the workpiece.

4.2 Method of measuring machine vibration

Measurements were made by attaching an acceleration sensor and an amplifier to the gear honing machine. These devices are generally used to measure machine vibration. The configuration of this vibration measurement system is shown in Fig. 7.

4.3 Explanation of frequency of measured machine vibration

In evaluating the measured data of gear honing machine vibration, an investigation was made of the vibration frequency leading to ghost noise. The spectrum of the gear that produced ghost noise showed a 0.8th-order component (= periodic component error). Assuming that this order component was influenced by vibration that occurred during gear honing, the vibration frequency can be calculated from the workpiece shaft rotational speed. In this study, the workpiece shaft rotational speed was 3,052 rpm and the 0.8th order occurred per workpiece rotation. Accordingly, the vibration frequency can be calculated as follows:

vibration frequency (Hz) = rotational speed (rpm) x
number of teeth (25 teeth) x
0.8/60 ≒ 1,017 Hz

Therefore, it was assumed that this order component was influenced by vibration of approximately 1 kHz. The workpiece was clamped in the tailstocks by means of a jig. The excitation point response function of the workpiece was measured at the place where impact excitation was applied. It was confirmed that the response function displayed an eigenvalue at the above-mentioned frequency of approximately 1 kHz. The frequency response function data at the excitation point are shown in Fig. 8. Accordingly, it was decided to evaluate the vibration level focusing on vibration in the vicinity of 1 kHz.

4.4 Relationship between spectrum analysis values for tooth surface geometry and gear honing machine vibration values

Figure 9 presents the results of an investigation of the correlation between the vibration acceleration peak value of the gear honing machine near 1 kHz and the spectrum quantity (0.8th-order component) of the tooth surface

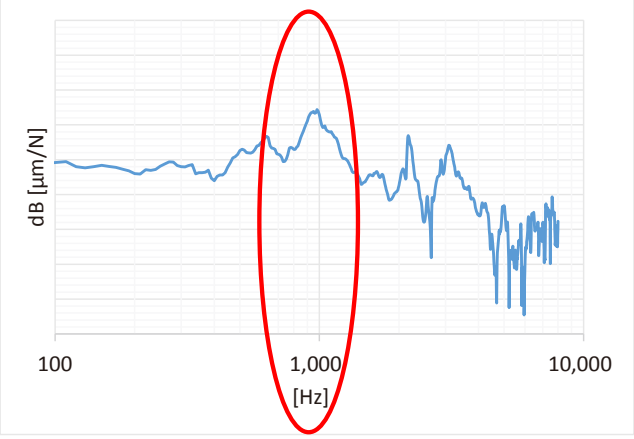

Fig. 8 Frequency response function data

geometry. The figure shows a high correlation between the two values. This means that an evaluation of the vibration level of the gear honing machine can be substituted for a spectrum evaluation of the tooth surface geometry.

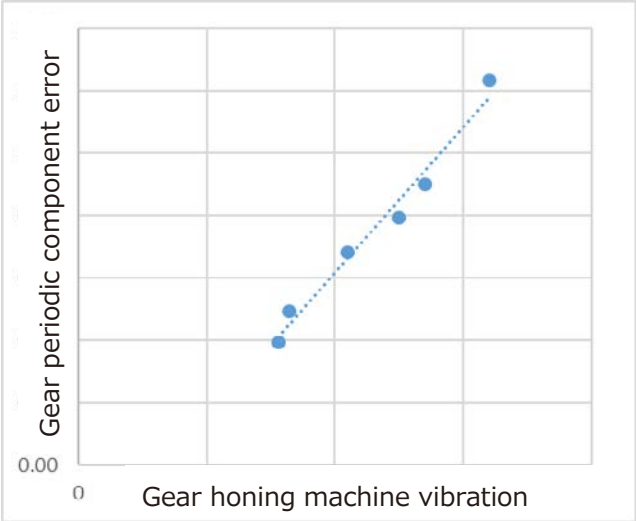

Fig. 9 Graph of gear periodic component error vs. vibration values

5. System for monitoring gear honing machine vibration

As explained here, a high correlation is seen between vibration acceleration at a specified frequency and the spectrum quantity of the tooth surface geometry. This implies that monitoring the vibration level can enable the detection of defective gears. Moreover, if honing machine vibration can be suppressed to a certain specified level, the spectrum quantity of the gear tooth surface geometry can be kept to a low level. Therefore, this can be expected to lead to stabilization of manufacturing quality. Figure 10 shows an example of the vibration monitoring data obtained daily on the mass production line.

As shown in Fig. 10, a judgement criterion (red line) has been defined in relation to the measured vibration data, making it possible to prevent the release of unacceptable products. This has now made it possible to ensure the quality of all manufactured gears.

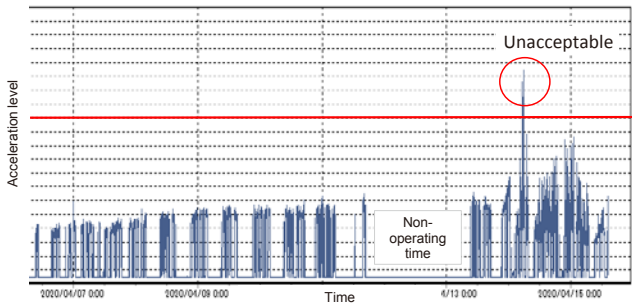

Fig. 10 Vibration monitoring data on gear honing machine

6. Conclusion

This study investigated the cause of ghost noise that originates from abnormal tooth surface geometry and is one issue of the noise and vibration produced by an automotive transmission.

(1) It was found that ghost noise is caused by periodic component error originating from the tooth surface undulation geometry.

(2) It was shown that evaluating the vibration level of the gear honing machine can be substituted for an evaluation of the periodic component error.

Based on these results, the release of defective gears can be prevented by monitoring the vibration level of the gear honing machine.

■ Authors ■

Hideaki MATSUISHI

Toshirou SHIMOSAKA

Yuya NAKATANI

Supply chain resilience through monozukuri engineering support

Takayuki KURATA*

Summary

This article describes purchasing engineering activities carried out by the Purchasing Division to support efforts to improve the competitiveness of our parts suppliers. It also includes examples of activities for Business Continuity Management and digital transformation that we have been emphasizing in recent years. JATCO aims to further strengthen the resilience of our supply chain through support for suppliers' monozukuri reforms.

1. Introduction

In 2003, JATCO launched a monozukuri improvement program as a collaborative activity with our suppliers.[(1)] Initially, emphasis was put on reducing costs (C), but quality improvement (Q) based on quality checkups was added later.[(2)-(3)]

After the Chuetsu earthquake in Niigata prefecture in 2004, a business continuity management (BCM) activity was also started together with suppliers. Through the implementation of measures to disperse production centers and to ensure stocks of parts, among other things, certain results have been obtained for ensuring delivery (D) even in the event of subsequent earthquakes, floods or other natural disasters. Moreover, in more recent years a fire at a semiconductor factory, an infectious disease pandemic and other concerns have occurred that have wide-ranging and long-lasting effects. Accordingly, there is growing interest in further strengthening the resilience of the supply chain and in methods of collaboration in this age of the new normal.

This article describes the current status and envisioned future of support for supplier monozukuri engineering. It presents specific examples of supplier BCM support following recent natural disasters, and remote improvement activities through the use of information and communications technology (ICT) under the current COVID-19 pandemic.

2. Activities of the Purchasing Monozukuri Support Department

Suppliers, too, have their own production engineering and process engineering functions, but their systems and actual capabilities vary depending on the size of the company and its policies. Sometimes they cannot respond to JATCO's QDC management system requirement immediately. Resolving QDC issues that straddle suppliers and JATCO is also within the scope of the activities of the Purchasing Monozukuri Support Department as part of its production engineering function (Table 1).

Table 1 Activities of Purchasing Monozukuri Support Department

Objective	New products	Existing products
Q Quality	– Support for production preparation ・Simultaneous engineering ・4M interviews/ design reviews ・PPAP (Production Parts Approval process)	– Quality checkup score improvement ・Process improvements, GK (workplace management) ・Failure analysis and recurrence prevention
D Delivery	– Project schedule management	– BCM ・Serious failure support
C Cost	– Production design – Investment reduction proposals – Planned JEPS (Jatco Excellent Production System)	– Improvements based on IE (industrial engineering) methods – Tooling improvements/ logistics improvements – Introduction of in-house process improvements
M Management	– Employee education support ・Information on JATCO in-house training programs ・QC circle activities ・Monozukuri exchange meetings	

* Purchasing Monozukuri Support Department

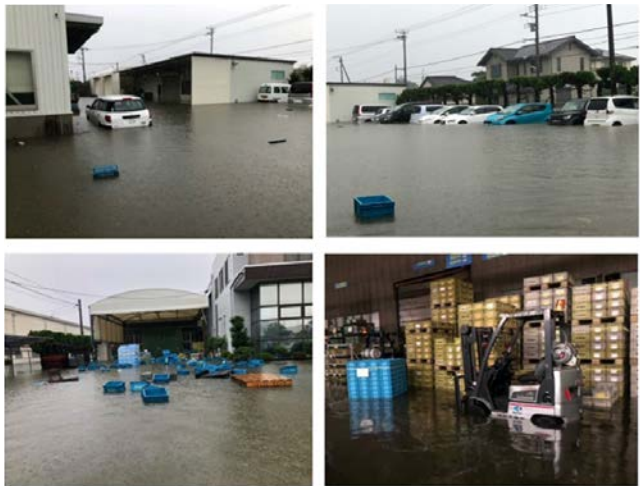

Fig. 1 Flooding caused by torrential rainfall in eastern Shizuoka prefecture (July 2021)

In addition to its regular activities for improving quality, reducing costs, etc., the department flexibly deals with various problems that occur irregularly. The following section describes examples of irregular efforts that that were undertaken in fiscal 2021.

3. Examples of irregular efforts

Japan is struck by natural disasters nearly every year, and some suppliers suffer damage from flooding and landslides caused by torrential rain. Another issue caused by the spread of COVID-19 infections in 2020 has been the difficulty of visiting suppliers' plants to carry out activities according to the "Sangen Principles" (i.e., actual place, actual object and actual condition).

Presented here are examples of BCM carried out to deal with flood damage suffered by suppliers and remote improvement activities under the pandemic situation.

3.1 Damage at a parts supplier due to flooding above the floor level

In July 2021, a stationary front that formed over the eastern part of Shizuoka prefecture caused a torrential downpour. The parking lot in JATCO's Head Office district was partially flooded and the factory of a parts supplier partner was also inundated with water above the floor level (Fig. 1).

Figure 2 outlines JATCO's supplier risk management scheme. The Purchasing Administration Department carries out supplier risk management activities through a cloud network like that shown in Fig. 3. During normal times, information on suppliers' recovery lead time is managed in

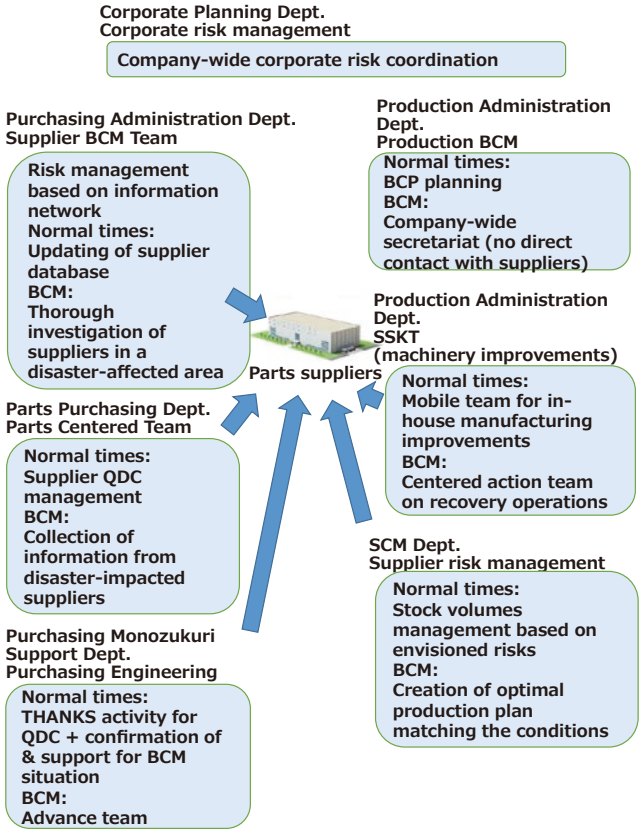

Fig. 2 Supplier BCM scheme

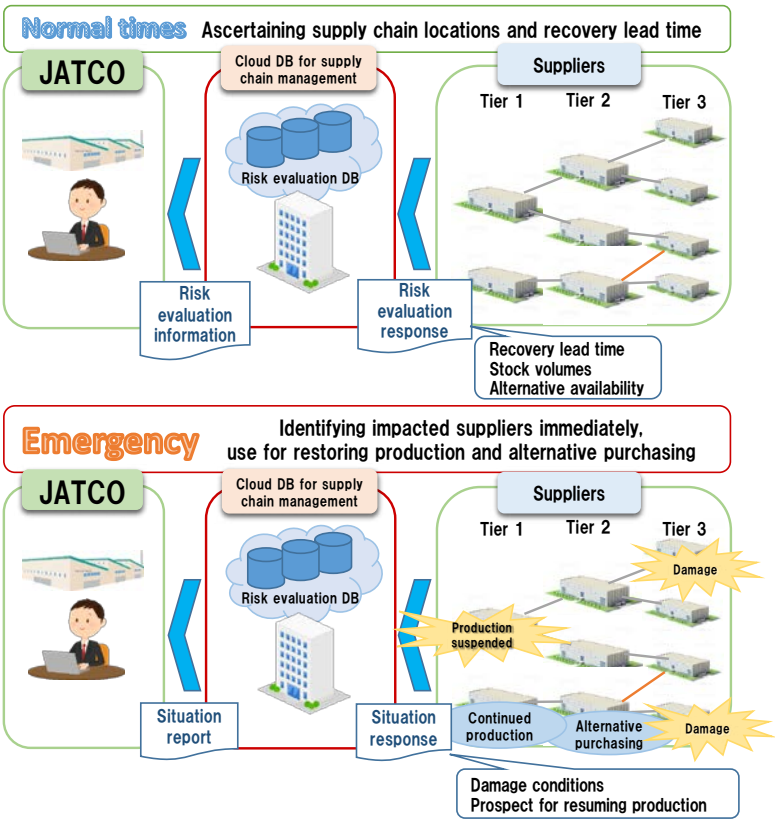

Fig. 3 Supply chain database management

a database, and a report on damage conditions following the occurrence of a disaster is requested through the system.

In the event a supplier needs recovery support, the Production Administration Department dispatches a mobile improvement team called SSKT. This team was active in the past following disasters, including torrential flooding in Saga, earthquake damage in Kumamoto and a factory fire in Ibaraki.

However, when damage has actually occurred, it sometimes takes time to judge whether or not to dispatch a working team on account of confused or delayed information from a supplier. Often it is necessary to start gathering information anew after arriving at the disaster site. In order to deal with this problem, the initial response system for emergencies was reviewed in fiscal 2021. If disaster information is available, an advance team from the Parts Purchasing Department and the Purchasing Monozukuri Support Department heads to the site before additional information is obtained from the supplier. Based on an action guide, they judge whether information needs to be gathered and whether support for the working team is needed, ascertain the scale of the damage, and determine what supplies and materials are required.

This recently created action guide was utilized following flood damage in the eastern part of Shizuoka prefecture. The advance team members reached the area in the morning on the first day of the recovery activities. After confirming the parts stock status and the extent of the damage, they requested the Production Administration Department via a hot line to dispatch the SSKT team and subsequently collaborated with the SCM Department and the supplier in drawing up a recovery plan. The SSKT recovery team also joined them in the afternoon on the first day and immediately initiated support activities. In this way, the flow of recovery efforts progressed smoothly.

Although some parts delivered to overseas had to be transported by air, the production schedule of JATCO's assembly line was not seriously affected. The recovery work was nearly completed within two weeks. The importance of obtaining accurate information in advance from suppliers on their parts stocks and plant facilities during normal times also became a point for reflection. Accordingly, an activity was launched to actually visit the plants of suppliers having a potential risk of damage from natural disasters and to confirm their production workplace conditions as well as to build a communications system focused on BCM as a key point.

3.2 Remote improvement activity with parts suppliers

THANKS is an acronym for Trusty and Harmonious Alliance Network Kaizen activity with Suppliers, which is a collaborative effort with suppliers for improving production lines. In this activity, JATCO personnel visit suppliers' plants, and suppliers and JATCO people share their wisdom for promoting improvements based on the "Sangen Principles." However, the impact of COVID-19 infections that expanded into a world-wide pandemic from the beginning of 2020 resulted in restrictions on overseas travel as well as requests for self-restraint regarding travel in Japan and face-to-face activities. Subsequently, online meeting applications became more familiar than before, but the following are examples of activities conducted with overseas suppliers around the autumn of 2020 at a time when some of them were not yet used to having remote meetings.

In conducting an online meeting about production workplace improvements, a manager at a supplier brought a PC connected to a Web camera to the shop floor. Observations were made of the workplace in accordance with methods for workplace improvements, and measures for improvements were proposed and implemented (Fig. 4).

This activity was carried out when both sides were unfamiliar with a remote meeting environment, and there were anxieties about how much could be accomplished. Yet, once we began to hold online meetings, various good aspects beyond our expectations became apparent.

First, many participants were able to focus on observing the same place of an operation simultaneously. Ordinarily, only around one or two observers can come close to the place of an operation on a narrow production line especially in assembly operations. However, using a live camera to transmit the scene remotely enabled many meeting participants to confirm the work operation with their own eyes (Figs. 5 & 6). Everyone from the employees in charge to the managers on both sides were able to confirm simultaneously an operation in a production workplace at an overseas plant. It became clear that this enabled the participants to notice things and actually propose more ideas for improvements. In this example, the manager, who normally does not go along on a plant visit, was able to participate remotely from home. He was able to point out differences from JATCO's in-house manufacturing methods, which enabled work procedures to be improved and eliminated the need for double checking.

Another benefit that can be cited is that meetings were held efficiently in terms of frequency and duration. Travel

time that has no added value was eliminated because meetings were attended without traveling, so short meetings could be scheduled frequently. For example, a 30-minute morning meeting was held to determine the details of a production trial that day, preparations were made, and the results were confirmed in a 30-minute evening meeting after the trial. Activities were carried out without any lost time. Naturally, confirmation of the production workplace based on the "Sangen Principles" is absolutely necessary, but it was found that skillfully combining the "Sangen" and remote meetings made it possible to speed up activities. As a result, more proposals for improvement were accumulated in this example than the fiscal year target without traveling overseas once.

Fig. 4 Remote improvement at an overseas plant

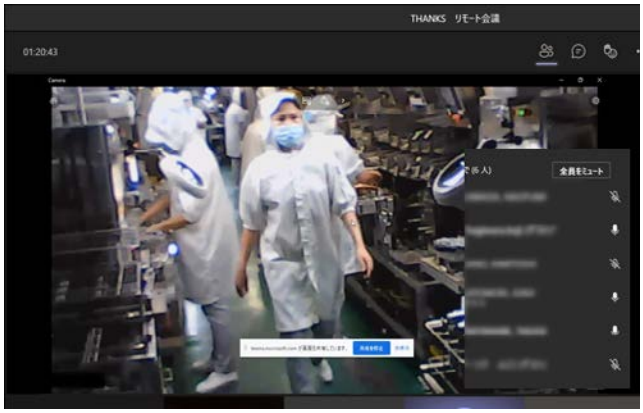

Fig. 5 Live online meeting via a Web application

Fig. 6 Work observation

4. Future issues

Accompanying the progress of hardware/software in the digital realm, we are also working to promote a digital transformation (DX) of our monozukuri activities. The procedures for emergency treatment of actual objects in workplaces and for promoting improvement activities will not change, but we believe that activities can be further quickened and efficiency enhanced by utilizing drones, smart glasses and other new devices.

The above-mentioned BCM example concerned flood damage, but dealing with earthquake risks is also necessary in Japan. When a production plant is damaged by an earthquake, we cannot enter the plant and check damage to the production equipment until the safety of the building is confirmed. Although this is still a proposal at the conceptual level, we are examining the possibility of using home-delivery drones to check the conditions inside the plant before the safety of the building is determined. Together with the Production Administration Department, we are now investigating drones, qualifications for operating them, applicable laws and regulations, training methods and other details.

Smartphones and PCs are currently the mainstream devices brought into production workplaces as communications tools, but trials are also being conducted on wearable devices with respect to safety and operability. Smart googles that support mixed reality (MR) and smart glasses for video communications have also been acquired and their usability, ease of operation and other aspects are being confirmed. MR devices superimpose a virtual model or a PC screen on a real-world view, enabling actual equipment and devices to be scanned, and the results are converted to data. However, smart googles have certain issues such as a heavy feeling when worn and requiring a large communications capacity (Fig. 7).

In contrast, smart glasses like those in Fig. 8 resemble a hands-free smartphone and represent devices that we want to adopt for the time being because of their convenience and ease of use.

Fig. 7 Smart googles for mixed reality

Fig. 8 Smart glasses

5. Conclusion

This article has described the activities of the Purchasing Monozukuri Support Department that provides a production engineering function. In the area of supplier BCM, the ability to take immediate action is essential in disasters. Our aim is to have the capability to identify process-like problems and the power to energize a network within and outside the company to implement solutions, even if we do not have specific support technologies. Toward that end, in addition to activities to improve the QDC competitiveness of our suppliers in normal times, we confirm the status of their BCM preparations and provide support. In this way, we confirm their production workplace conditions and build communications links with suppliers.

We are continuing to further strengthen supply chain resilience through these activities.

6. References

(1) Naofumi Kawada, THaNKS Activity through Cooperation with Suppliers, JATCO Technical Review No. 14, pp. 79-83.
(2) Kouichi Hasegawa and Tadashi Kaneko, Quality Health Check Aimed at Further Improving Suppliers' Product Quality, JATCO Technical Review No. 17, pp. 89-94.
(3) Tadashi Kaneko, Reduction of quality risks through quality checkups and improvement activities, JATCO Technical Review No. 18, pp. 85-90.

■ Author ■

Takayuki KURATA

Memo

Promotion of DX in the Human Resources Development & General Administration Department: Acquiring skills for digitalization

Michael DAWSON*

Summary

The Human Resources Development & General Administration Department digitalized peripheral operations of legacy core systems while making full use of the systems. That was done to respond flexibly to operating environment changes within and outside the company and to the changing needs of JATCO employees who are the Department's customers. The activities undertaken increased the number of team members capable of promoting digitalization themselves and led to a further advance in DX promotion throughout the entire Department.

1. Present situation

1.1 Background

The Human Resources Development & General Administration Department aims to provide more timely and higher quality services in order to respond flexibly to operating environment changes within and outside the company and to the evolving needs of the employees, referred to here as our customers.

However, employee data, forming the basis of such services, was being circulated mainly through legacy core systems that had been in place for a long time since launching (Fig. 1). When creating an employee list or other documents, much manual work had to be done every time such as adding and deleting information after downloading the data. Among the operations performed by the Department, creating and providing data for customers involved many man-hours and long lead time, so numerous improvements were necessary.

The Department previously formed an internal digital transformation (DX) promotion team and was making vigorous efforts to implement work process improvements from various perspectives. However, the way in which basic employee data was kept, among other things, stood out again as an issue preventing substantial efficiency improvements.

1.2 Digitalization policy

To deal with the issue above, it was decided to strive for business reforms (DX) using information and

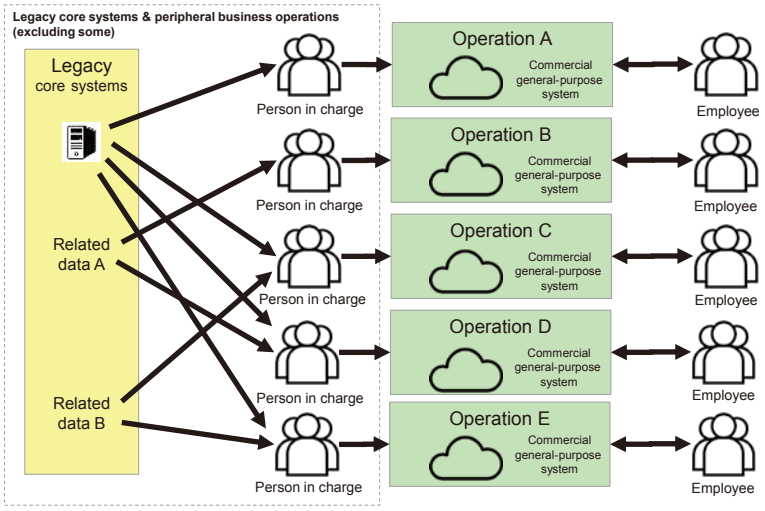

Fig. 1 Legacy core systems

* Human Resources Development & General Administration Department

communications technology (ICT) tools. Two major policy proposals were examined in this regard.

• Proposal 1: To implement a large-scale system

Implementation of a new system that would encompass the existing legacy core systems and all the peripheral business systems.

• Proposal 2: Collaboration based on multiple small-scale systems

Digitalization of peripheral operations while making use of the legacy core systems and implementation of commercial general-purpose systems for each specific purpose.

After examination, Proposal 2 was adopted for the following three reasons:

(1) Able to implement it ourselves
(2) Able to shorten lead time
(3) Able to respond to internal needs in an agile fashion

In trying to digitalize the peripheral operations handled by the legacy core systems, there were various things that could not be easily covered by one commercial general-purpose system because the types of operations involved were so numerous. Due to the ongoing implementation of commercial general-purpose systems in each business process, the volume of requests to the peripheral operations of the legacy core systems for data downloads and other tasks increased sharply. Therefore, it was decided to put priority on shortening lead time and being able to make improvements by ourselves, with the DX Promotion Teams in the Department playing a central role. The details of the improvements are described in the following section.

2. Improvements

2.1 Purposes

The improvements made this time had two main purposes:

• To make the work of producing data more efficient, and
• To shorten the lead time for providing data.

2.2 Approach

The approach taken consisted of three steps, based on QC story. First, efforts were made to thoroughly ascertain the current situation, visualize the current process and to eliminate all waste. After that, ICT tools for advancing digitalization were selected, and then digitalization was carried out.

1) Work process visualization and elimination of waste

The first things that were tackled were to visualize the current situation of work processes and to identify issues. The following activities were carried out with the representatives of each team in the Department.

A list was made of the frequency report preparation for customers and the outputs of peripheral operations of the legacy core systems were visualized. As an example, Employee Basic Data Report #1 was being created once a month.

Next, a list was made of the data and related information downloaded from the legacy core systems for creating the various outputs, and the inputs of each operation were visualized. For example, Employee Directory A and Employee Contact List B were needed to create Employee Basic Data Report #1.

A flow chart was then created and visualized to show the work steps involved in creating the outputs from the inputs. For example, in creating Employee Basic Data Report #1, Employee Directory A was downloaded and combined with Employee Contact List B. Unnecessary data fields were deleted, half-width and full-width characters were unified, and the results were saved for use by subsequent processes.

The final activity was to identify redundant tasks in the flow chart and to eliminate waste by applying the concept of eliminate–reduce–combine–simplify. For example, Employee Directory A was used for both Employee Basic Data Report #1 and Employee Basic Data Report #2 and was downloaded twice under the procedure used at that time. The number of downloads was reduced to one time and the Directory was shared with others.

The most difficult aspect here was to accurately ascertain the frequency of manual tasks and the number of hours required. Until the results were finalized, it was necessary to repeat the above-mentioned activities numerous times and to have lengthy discussions. In contrast, by thoroughly carrying out Step 1), the processes needing to be digitalized could be clarified.

2) Determination of digitalization items and selection of ICT tools

In determining the digitalization items, the same members as the step above carried out the following activities.

The optimized flow chart from which waste had been eliminated was re-evaluated, and the processes team member tasks required long lead times or many hours of work were analyzed to clarify the factors involved.

The functions and features of ICT tools were investigated by gathering information from inside and

outside the company. For example, one of the ICT tools investigated was robotic process automation (RPA), which records the PC operations performed by an employee in downloading data from a system. The operations are later reproduced making it possible to automate them.

With regard to each factor, each ICT tool was evaluated in terms of two criteria—effectiveness and practicality. The most effective tools were then selected. For example, RPA was rated as being highly effective for downloading data from legacy core systems, but its practicality was rated low because special skills are needed to actually use it.

The final activity was to summarize the factors and the tools adopted to digitalize them into "digitalization items." A diagram was then created to illustrate the items before and after digitalization.

Based on the investigations mentioned above, a total of five digitalization items were selected.

3) Implementation of digitalization items

One of the people responsible for promoting DX in the Department and the person in charge of the business operation pertaining to each item worked together as a pair in carrying out the following activities to implement digitalization.

The details of the target data of each item and the proper handling procedure in terms of data security were confirmed, and the process for proceeding with digitalization was determined. For example, Employee Basic Data Report #1 contains personal information that must be treated carefully. Accordingly, only designated members were allowed to access the data during the digitalization process.

Next, prototypes with 10% completion were developed for each digitalization item in around one week. Their feasibility was confirmed in relation to the diagram created in the previous step illustrating the items before and after digitalization. For example, several thousand rows of data must be processed when creating Employee Basic Data Report #1. At the prototype stage, however, the scope of the data was made more compact and a trial run was conducted to see if it could actually be processed as expected.

The next task was to arrange each of the digitalization items into a rough schedule outline, after which it was incorporated into a detailed work-based schedule, keeping the following two points in mind.

i. Assigning of time for acquiring skills.
ii. Determining the frequency of progress checks based on each item level of difficulty.

Time for acquiring the necessary skills for digitalization was assigned through both off-the-job training (Off-JT) and on-the-job training (OJT). Fundamental knowledge of ICT tools (10%) was acquired through the below two Off-JT methods, and practical skills (90%) were acquired in OJT based on communication with in-house experts.

- In-house training sessions.
- Watching online videos.

The frequency of progress checks was determined according to the level of item level of difficulty. For example, the progress checks for high difficulty items was handled by daily casual meetings lasting around 20 minutes; that of medium-level items was handled in once-a-week meetings of one hour as a general yardstick.

While personnel data in the legacy core systems served as the basis of the activities described above, peripheral operations that previously had to be done manually were digitalized (Fig. 2). As a result, a shared data platform was constructed through which necessary data can be obtained

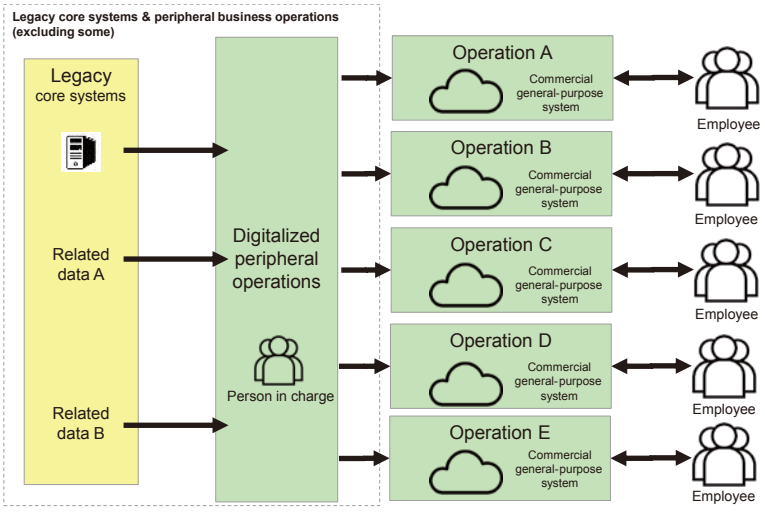

Fig. 2 Digitalization of peripheral business operations of legacy core systems

Table 1 Effects of improvements

Aim	Impact
① To make the work of producing data more efficient	Reduced man-hours by about 70%
② To shorten the lead time for providing data	Reduced response time by about 95%

according to needs at hand.

The benefits of these improvements are described in the following discussion.

2.3 Effects of improvements

Figure 2 illustrates the status of the legacy core systems after digitalization of the peripheral operations.

The effects of the improvements regarding the two main purposes of digitalization are shown in Table 1.

2.4 Secondary benefits

In addition to the effects noted in the table, the digitalization efforts mentioned here also provided an opportunity to obtain the following secondary benefits.

1) Employee development

One of the secondary benefits is that these activities led to further development of the Department's employees. The following benefits were confirmed in this regard.

A passive attitude toward using ICT tools was improved through the improvements made to our business operations. Many of the Department's employees gained their first experience with digitalization through the work of promoting the digitalization items. As a result, their anxiety about using unfamiliar ICT tools decreased after the activities compared with before undertaking them. A positive attitude now exists regarding consideration of implementing ICT tools in future efforts to improve business operations.

The activities led to the development of digitally capable employees, thereby increasing the number of Department employees able to promote digitalization. The digitalization items undertaken this time provided an opportunity for employees to improve their skills to the extent that approximately 70% of them are now able to develop related tools. It is likely that the horizontal deployment of such tools and further improvements can be completed within the Department in the future.

2) Synergies toward further digitalization

Another secondary benefit is that it heightened the motivation of other Department employees not directly involved. In the course of implementing the digitalization items, interest in the activities rose within the Department. Department employees and teams that had not been involved in the activities initially also joined in the efforts under way, which had the synergistic effect of employees motivating each other. That produced additional improvements which had not been originally planned.

2.5 Reflections and conclusions

The policy adopted this time was to utilize legacy core systems combined with the implementation of commercial general-purpose systems for different purposes. Under this policy, efforts were exerted to improve operational efficiency and to shorten response time by digitalizing peripheral operations of legacy core systems.

Digitalization was not something that was easy to accomplish, but the members of the Human Resources Development & General Administration Department undertook the challenge of doing it with a spirit of wanting to make improvements by themselves. They succeeded in improving both operational efficiency and customer response time. Considering that the activities also resulted in secondary benefits such as further development of Department personnel, it is conceivable that this 3-step approach could be one useful reference for others promoting workplace-initiated DX efforts in the future.

3. Going forward

The Human Resources Development & General Administration Department reduced manual operations and quickened customer response time though the digitalization items implemented this time. Going forward, we want to advance DX toward further service improvements by making skillful use of the time gained through improving efficiency together with the digitalization knowhow accumulated to date.

■ Author ■

Michael DAWSON

Introducing the Jatco CVT7 (JF015E) for the Dacia Sandero

The Jatco CVT7 (JF015E) is installed on the new Sandero released by Dacia, a Renault Group brand, in the European market in January 2021. Thanks to its auxiliary transmission, the JF015E features wide ratio coverage and low friction, in addition to a substantially updated control system. These features combine with the latest 1.0L 3-cylinder turbocharged engine to contribute to substantially improved fuel economy and driveability. The transmission is optimally tuned to match the concept of a hatchback, reflecting the needs of the European market. That feature achieves both excellent dynamic performance and quietness, which are highly praised by customers.

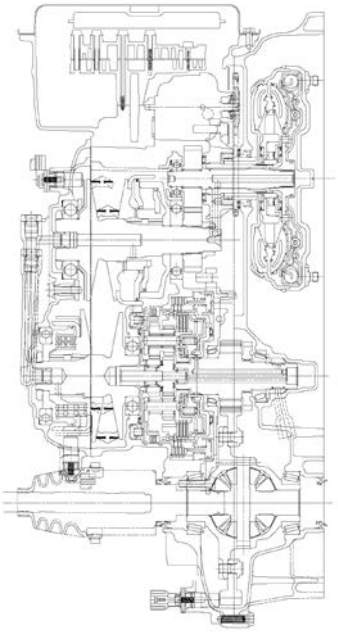

Fig. 1 Main cross-sectional view

Table 1 Specifications of JF015E

Torque capacity	142 Nm
Torque converter size	205 mm
Pulley ratios	2.200 - 0.550
Auxiliary transmission gear ratios	1st 1.821 2nd 1.000 Rev. 1.714
Ratio coverage	7.3
Final gear ratio	3.882
Selector positions	P, R, N, D, L
Overall length	334 mm
Weight (wet)	70.1 kg (2WD)

Dacia Sandero

Introducing the Jatco CVT8 (JF016E) for the Renault Duster

The Jatco CVT8 (JF016E) is installed on the new Duster that Renault launched in the Russian market in March 2021. The JF016E is distinguished by its superb shift response and markedly reduced friction, which combine with Renault's latest 1.3L 4-cylinder turbocharged engine to contribute to improved vehicle fuel economy and driveability. The JF016E is optimally tuned to match the concept of a 4WD SUV, thus reflecting the needs of the Russian market. That characteristic provides dynamic driving performance in the "4x4 Lock" mode that is highly regarded by customers.

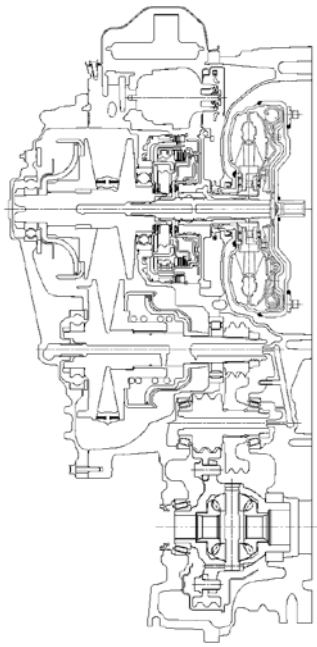

Fig. 1 Main cross-sectional view

Table 1 Specifications of JF016E

Torque capacity	250 Nm
Torque converter size	235 mm
Pulley ratios	2.631 - 0.378
Ratio coverage	7.0
Final gear ratio	5.694
Selector positions	P, R, N, D +7-step manual shift mode
Overall length	375.2 mm
Weight (wet)	95.2 kg (4WD)

Renault Duster

Introducing the Jatco CVT8 (JF016E) for the Mitsubishi Outlander

The Jatco CVT8 (JF016E) is installed on the new Outlander that Mitsubishi Motors Corporation launched in North America in April 2021. The new Outlander was developed in a collaborative project by the Renault-Nissan-Mitsubishi alliance. Developed for use on Mitsubishi Motors vehicles, the JF016E provides outstanding shift performance, thanks to its new control valve and shift-by-wire system adopted for the first time. It brings out the full performance of the new 2.5L engine, thereby contributing to the attainment of both high power output and excellent fuel economy, leading to high acclaim from our customers.

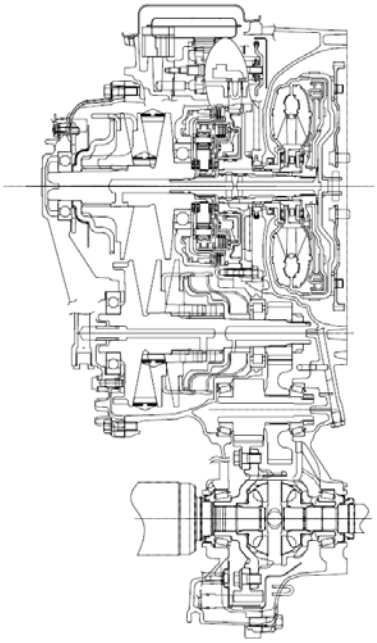

Fig. 1 Main cross-sectional view

Table 1 Specifications of JF016E

Torque capacity	250 Nm
Torque converter size	236 mm
Pulley ratios	2.631 - 0.378
Ratio coverage	7.0
Reverse gear ratio	0.745
Final gear ratio	5.694
Selector positions	R ← N ← H → N → D/M + P button
Overall length	362.3 mm
Weight (wet)	94.0 kg (2WD) / 94.8 kg (4WD)

Mitsubishi Outlander

Introducing the Jatco CVT7 W/R (JF020E) for the Nissan AD and NV200 Vanette

The Jatco CVT7 W/R (JF020E) with 2WD specifications is installed on the Nissan AD and the Nissan NV200 Vanette that Nissan Motor Co., Ltd. released specifically for the Japanese market in May and July 2021, respectively, following the implementation of minor model changes. The CVT7 W/R is distinguished by its wide ratio coverage and low friction. The effects of these features combine with the automatic stop-start system, newly added for the first time to the AD and the NV200 Vanette, to contribute to a significant improvement in vehicle fuel economy. This is the first application of the CVT7 W/R on Japanese commercial vehicles. The planetary gear set was further strengthened to ensure the durability needed for long-distance driving that characterizes commercial vehicles.

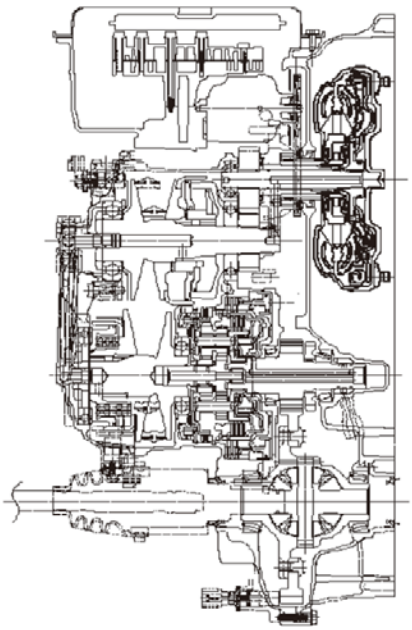

Fig. 1 Main cross-sectional view

Table 1 Specifications of JF020E

Torque capacity		147 Nm
Torque converter size		205 mm
Pulley ratios		2.200 - 0.458
Auxiliary transmission gear ratios	1st 2nd Rev.	1.821 1.000 1.714
Ratio coverage		8.7
Final gear ratio		4.055
Selector positions		P, R, N, D, L
Overall length		376.7 mm
Weight (wet)		73.4 kg

Nissan AD

Nissan NV200 Vanette

Introducing the JR710E 7-speed Automatic Transmission for the Nissan Caravan

The JR710E 7-speed automatic transmission (AT) for rear-wheel-drive vehicles is mounted on the Nissan Caravan, which is fitted with a 2L/2.5L gasoline engine and was released by Nissan Motor Co., Ltd. in Japan in October 2021. This is the first application of the JR710E on a cab-over vehicle. Compared with the 5-speed AT used heretofore on the Caravan, the 7-speed JR710E provides wider ratio coverage, increasing gear steps and also widens the lock-up operating region. As a result, it contributes significantly to improving the fuel economy, emissions performance, driving performance, quietness and driveability of the vehicle. Moreover, the added manual shift mode is also highly acclaimed by customers.

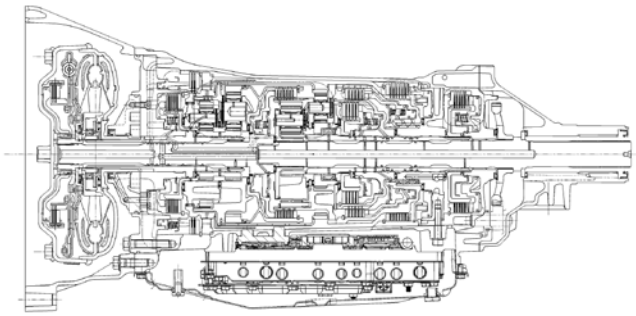

Fig. 1 Main cross-sectional view

Table 1 Specifications of JR710E

Torque capacity		178 Nm
Torque converter size		250 mm
Gear ratios	1st 2nd 3rd 4th 5th 6th 7th Rev.	4.783 3.102 1.984 1.371 1.000 0.870 0.775 3.858
Ratio coverage		6.31
Final gear ratio (reference)		3.700
Selector positions		P, R, N, D + M shift
Overall length		769.5 mm
Weight (wet)		92 kg

※ 2L 2WD

Nissan Caravan

Memo

Highlights of 2021

1. Participation in JSAE Annual Spring and Autumn Congresses

JATCO Group company employees presented a total of four technical papers at the Annual Spring and Autumn Congresses of the Society of Automotive Engineers of Japan, Inc. (JSAE).

The Spring Congress was held May 26-28, 2021. Because of the impact of the novel coronavirus (COVID-19), the Spring Congress was held online. A JATCO employee presented a paper entitled "Development of mass-production die-casting technology for heat-resistant, high-strength magnesium alloy." He talked about the mass-production die-casting technology developed for manufacturing the magnesium alloy case of JATCO's new 9-speed automatic transmission for rear-wheel-drive vehicles. A JATCO Korea Engineering Corp. employee presented a paper entitled "Development of a method for suppressing CVT chain noise." He described the method developed for mitigating noise, based on a clarification that the balance between chain stiffness and pulley clamping force correlates with chain noise.

The Autumn Congress was held October 13-15, 2021 and was also convened online like the Spring Congress. A JATCO employee presented a paper entitled "Clarification of the mechanism reducing torque capacity due to differences between the ideal and actual CVT chain path." He explained that deviation of the CVT chain from the ideal path was the mechanism causing torque capacity to decline. Another JATCO employee also presented a paper entitled "Stabilization of Gear Machining Accuracy by Controlling Gear Honing Machine Vibration." He explained that suitable control of honing machine vibration leads to suppression of ghost noise.

2. Participation in JFPS International Symposium on Fluid Power

The 11th JFPS International Symposium on Fluid Power was held online October 12-13, 2021. A JATCO employee presented a paper entitled "Clarification of Parameters and Development of a Method for Estimating Loading Forces Acting on The Spool Valve of a Hydraulically Controlled Automotive Transmission." He explained that the forces acting on the spool valve inside the control valve were calculated by a fluid analysis and their accuracy was verified experimentally.

3. Participation in the planning of JAMBE

Ten domestic vehicle manufacturers and parts makers, including JATCO, and the Japan Automobile Research Institute (JARI) agreed to establish the Japan Automobile Model-Based Engineering Center (JAMBE) to promote the nationwide diffusion of model-based development (MBD) in Japan's automotive industry. A briefing to explain JAMBE to the media was held on September 24, 2021 as an inaugural event. A JATCO company officer participated in the event online and talked about his thoughts and expectations of JAMBE as a member of the steering committee.

Source: JAMBE

4. Jatco CVT7-equipped vehicle named Compact SUV of the Year by a leading car magazine in India

The Nissan Magnite, equipped with the Jatco CVT7, was named Compact SUV of the Year by BBC TopGear India, one of that country's leading car magazines. The Jatco CVT7 contributes to the vehicle in the following three ways.

- D-step control(1) reduces the rubber-band feeling(2).
- The auxiliary transmission provides a wide gear ratio

range that delivers a feeling of powerful acceleration.

• Smooth, responsive shifting that distinguishes a CVT.

(1) Control procedure that provides AT-like shift performance.

(2) With accelerator-on, a condition where the engine speed flares first with vehicle acceleration catching up later.

5. Recipient of Superior Quality Award given by GMMC

GAC Mitsubishi Motors Co., Ltd. (GMMC) gave JATCO (Suzhou) Automatic Transmission Limited (JSZ) a Superior Quality Award on March 22, 2021. GMMC presented this award to just ten companies among the more than 300 suppliers it does business with. GMMC commented that, "JSZ's product quality was outstanding in FY 2020. JSZ always resolves quality issues promptly and efficiently and actively responds to our customers' requests. With its strong customer awareness, JSZ delivers outstanding products and at the same time it values the importance of providing high-quality service."

6. Certified as "Health and Productivity Management Organization 2021 (White 500)"

JATCO Ltd and JATCO Engineering Ltd (JE) were certified as a "Health and Productivity Organization 2021 (White 500)." This certification is given by the Ministry of Economy, Trade and Industry (METI) to commend enterprises that practice superior health and productivity management. JATCO and JE have been certified as "White

500" organizations for three consecutive years now, including 2019 and 2020.

JATCO and JE conduct nutrition education, health promotion activities such as walking and other events, along with in-house efforts to raise employees' health consciousness through wall posters and other means. Health is positioned as one of management's activities, and managerial-level people actively issue health messages both within and outside the company. The recognition of these activities resulted in the certification.

7. Certified as a "Sports Yell Company 2021" by the Japan Sports Agency

Companies that actively undertake sports activities to promote the health of their employees are certified by the Japan Sports Agency as a "Sports Yell Company." The purpose of this recognition is to encourage the installation of sports facilities for the prime working generation and to foster a social momentum towards sports. Four JATCO Group companies were certified this year as a "Sports Yell Company 2021": JATCO Ltd, JATCO Engineering Ltd, JATCO Tool Ltd and JATCO Plant Tec Ltd, out of a total of 623 certified organizations. The four companies were highly evaluated for undertaking activities to promote employees' health by providing opportunities for exercising

such as doing radio calisthenics before work, holding gymnastic and stretching events led by an instructor, and sponsoring walking events, among other things.

8. Recipient of the Silver Prize at the National Congress for Excellent Improvement Examples 2021

The National Congress for Excellent Improvement Examples 2021 was held online on October 28, 2021. At this event all the examples of outstanding improvements that were selected for Excellent Improvement Awards at the

district qualifying round held in June for the 2021 National Congress were presented at the same time. Twenty teams from across the country participated in this event. JATCO was the sole entrant in the National Congress from Nissan Group companies. Over 1,000 attendees watched the presentations and voted in the contest in which JATCO was awarded the Silver Prize.

9. Torque Rechecker Circle receives Area Head's Prize at Shizuoka Area QC Circle Satsuki Convention

JATCO Engineering's Torque Rechecker Circle participated in the Shizuoka Area QC Circle Satsuki Convention that was held on May 21, 2021 for the 6,311th time. They received the Area Head's Prize, securing the right to attend the Tokai Branch's Championship Conference held in September as the representative of the Shizuoka area. Their theme this time was "elimination of the breaking of the torque wrench tie band." This improvement example was put together by the vigorous efforts of a young female employee who served as the team leader for the first time in her second year with the company.

10. Cooperation with Fuji City's local vaccinations against the novel coronavirus

JATCO's medical staff cooperated with a local program undertaken by Fuji City to vaccinate senior citizens aged 65 or older. This cooperation contributed to the accomplishment of the government's goal to "complete vaccinations by end-July" in cooperation with the administration.

Memo

Patents

1. AIR VENT STRUCTURE OF OIL PUMP FOR AUTOMATIC TRANSMISSION, AND METHOD FOR ASSEMBLING AIR VENT STRUCTURE

(Fig. 1)

Application Number : 2018-507116
Application Date : 10.2.2017
Patent Number : 6559882
Registration Date : 26.7.2019
Title : AIR VENT STRUCTURE OF OIL PUMP FOR AUTOMATIC TRANSMISSION, AND METHOD FOR ASSEMBLING AIR VENT STRUCTURE
Inventors : Yuuki Tanaka

【SUMMARY OF THE INVENTION】

An automatic transmission has an oil pump driven by a travelling driving source. An air vent structure that expels air bubbles contained in automatic transmission fluid during pump operation has an air vent hole whose one end communicates with an outlet port of the oil pump and whose other end opens toward the oil pan. An air vent tube is connected to an opening end of the air vent hole. The air vent tube is extended up to a strainer lower side gap area located between a strainer and the oil pan, and a tube opening end of the air vent tube is placed in oil of the automatic transmission fluid.

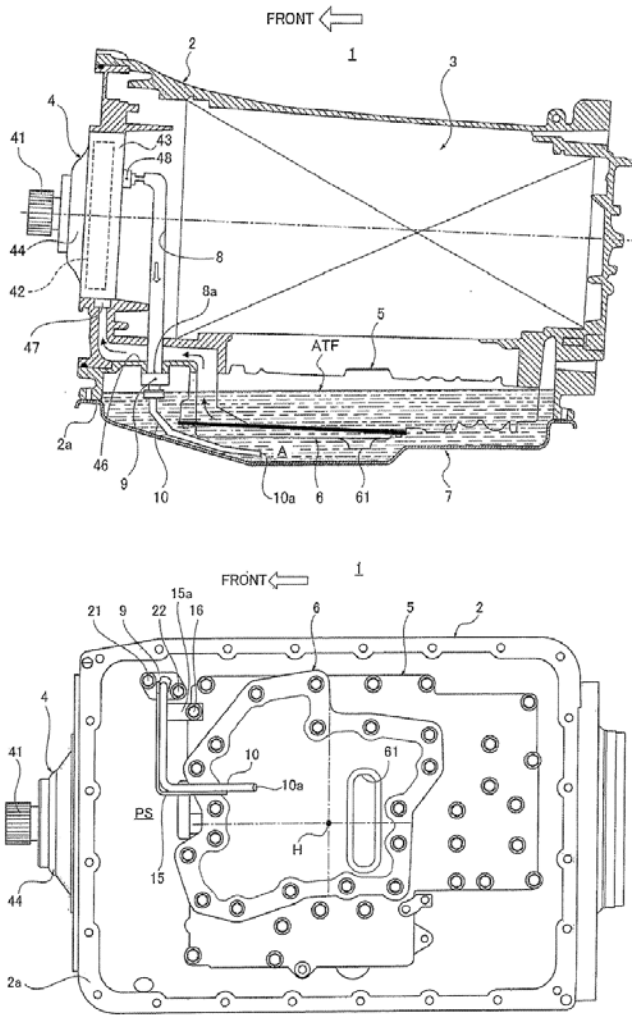

Fig. 1

2. Electric-vehicle control device and control method

(Fig. 2)

Application Number : 2015-230721
Application Date : 26.11.2015
Patent Number : 6653556
Registration Date : 30.1.2020
Title : Electric-vehicle control device and control method
Inventors : Tomoo Mochizuki, Kenichi Ooshima, Hiroshi Miyazaki, Yuji Torizawa, and three others

【SUMMARY OF THE INVENTION】

In a specific state where an electric vehicle is in a stop state and a creep torque is generate in an electric motor, when a shift range is switched from a traveling range to a non-traveling range, a motor control section performs a torque decrease control to stepwisely decrease the creep torque of the electric motor, and an automatic transmission control device performs a disengagement control to gradually disengage the frictional engagement element of the automatic transmission.

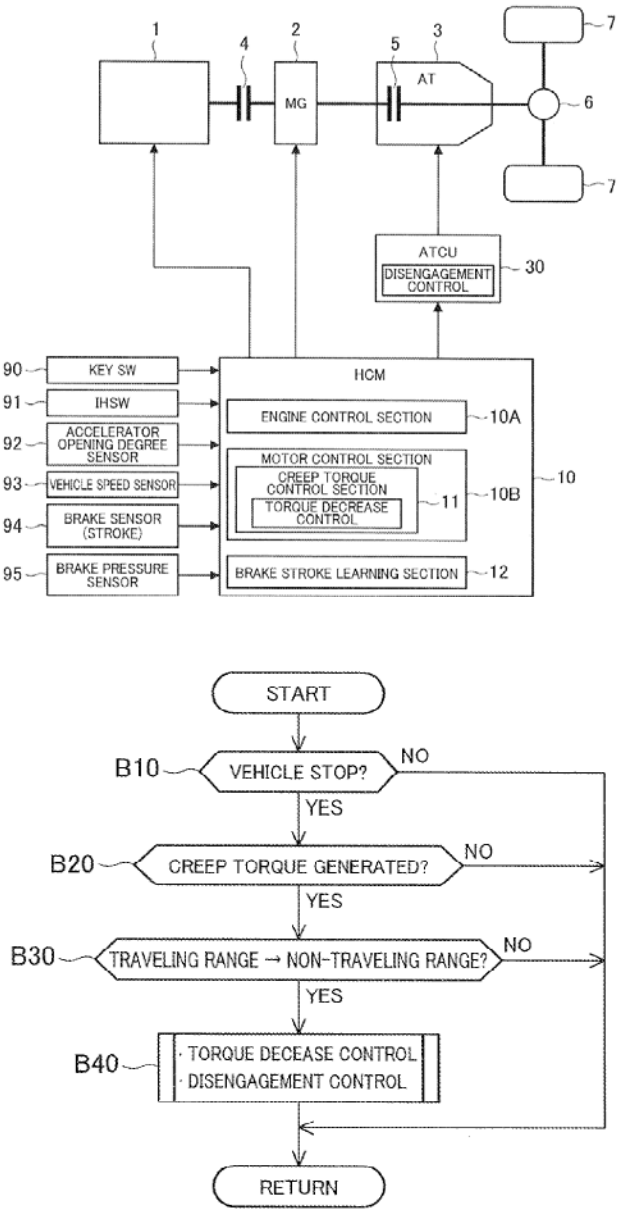

Fig. 2

ジヤトコ・テクニカル・レビュー　No.21

JATCO Technical Review No.21

発行　2022年3月

発行所　ジヤトコ株式会社
グローバル広報部
〒417-8585
静岡県富士市今泉700-1
TEL: 0545-51-0368
FAX: 0545-52-8286

印刷所　E−グラフィックス コミュニケーションズ株式会社
東京都三鷹市牟礼6丁目25番28号

March 2022

Distributor　Global Communications Department
JATCO Ltd
700-1 Imaizumi, Fuji City, Shizuoka
417-8585, Japan

JATCO Ltd

700-1, Imaizumi, Fuji City, Shizuoka 417-8585, Japan
TEL: +81-545-51-0368 FAX: +81-545-52-8286

www.jatco.co.jp/english